

# Nieuwklap bridge

## Prediction of the failure mode under collapse testing and seismic evaluation

Master of Science Thesis

Marios Tzortzinakis



Faculty of Civil Engineering and Geosciences  
Department of Structural and Building Engineering  
Concrete Structures

Challenge the future



# Nieuwklap Bridge

## Prediction of the Failure Mode under collapse testing and Seismic Evaluation

By

Marios Tzortzinakis

in partial fulfilment of the requirements for the degree of

**Master of Science**  
in Civil Engineering

at the Delft University of Technology,  
to be defended publicly on Tuesday October 30, 2018 at 15:30 PM.

Thesis committee:	Prof. dr. ir. D.A. Hordijk (Chair),	TU Delft
	Dr. ir. C. van der Veen,	TU Delft
	Dr. ir. M.A.N. Hendriks,	TU Delft
	Dr. ir. E.O.L Lantsoght,	TU Delft
	Ir. L.J.M. Houben,	TU Delft

An electronic version of this thesis is available at <http://repository.tudelft.nl/>



# Preface

This master thesis is submitted as a partial fulfilment of the requirements for the Master of Science degree in Structural Engineering, with a specialization in Concrete Structures at the Delft University of Technology. At this point, I would like to express my sincere gratitude to the people that contributed to the completion of this project.

At first, I would like to thank dr. ir. Cor van der Veen for his valuable guidance throughout this period and for entrusted me to carry out this challenging project. Moreover, I want to thank dr. ir. Eva Lantsoght for sharing her extensive knowledge and experience concerning this topic and for her useful comments and recommendations. Furthermore, I am thankful to the other members of my committee, prof. dr. ir. Dick Hordijk and dr. ir. Max Hendriks, for their valuable remarks and their professional guidance during this project.

Many thanks to my friends and my girlfriend, which supported and motivated me during these challenging years of my life making everything seem a lot easier.

Finally, I would like to thank my family for their sustained efforts, encouragement and support, without which this journey would not be possible.

*Marios Tzortzinakis  
Delft, October 2018*



# Abstract

The actual shear capacity of existing reinforced concrete solid slab bridges, constructed before 1960 in the Netherlands, is subject of an extensive research nowadays, since additional sources, increasing the total shear capacity of concrete slabs, have been ascertained to be present. In addition, the increasing occurrence of human-induced earthquakes in the province of Groningen due to gas extraction, arises uncertainties regarding the seismic behaviour and earthquake resistance of existing bridges in this area. The Nieuwklap bridge is a reinforced concrete solid slab bridge located in the Groningen province, combining both characteristics under investigation.

In the course of this research, the first two Levels of Assessment have been applied for the static analysis of the slab part of the deck of the Nieuwklap bridge, which was found to have sufficient shear and bending moment resistance under the application of the traffic loading defined by the current standards. The equivalent proof load tandems, that generate the same shear and bending moment stresses, for each load combination level have been found with both approaches, proving that localized phenomena at the area of load application are more intense when the field experiment takes place. Furthermore, by obtaining the equivalent tandem loading that leads to shear and flexural failure of the concrete slab, it has been concluded that flexural failure due to yielding of the reinforcement will occur first in case of exerting the collapse loading on the flexure-critical positions or on the shear-critical positions next to the end-supports. However, in case of applying the tandem loading on a shear-critical position next to a continuous support it is difficult to define which failure mode will precede.

Regarding the seismic evaluation of the Nieuwklap bridge, the simplified fundamental mode method and a modal response spectrum analysis have been used. The bridge deck has been found to have adequate resistance against the vertical component of the seismic excitation, which cannot be considered critical, generating nearly the half stresses compared to the traffic load (LM1) combination defined by Eurocode 2. The piers and the pendulums supporting the bridge deck have been also evaluated against the two horizontal components of the seismic excitation, for two different earthquake return periods, discovering that they are able to withstand the generated forces without additional measures. Finally, from the performed modal analysis it has been obtained that movement of the bridge on the longitudinal direction can be observed in lower frequencies compared to the vertical and the transverse direction and that more than 10 modes are necessary in order to describe accurately the bridge behaviour.

This Thesis describes the framework that can be used to prepare collapse tests at multiple Levels of Assessment, and for the seismic assessment of existing bridges in regions with recently initiated seismic activity.



# Nomenclature

## Abbreviations

AASHTO	American Association of State Highway and Transportation Officials
DIANA	Displacement Analyzer, Finite Element Software
EC2	Eurocode 2
EC8	Eurocode 8
EN	European Norm
FEA	Finite Element Analysis
FEM	Finite Element Method
fib	International Federation for Structural Concrete
FL	Failure Load
JCSS	Joint Committee on Structural Safety
KNMI	Koninklijk Nederlands Meteorologisch Instituut (Royal Netherlands Meteorological Institute)
LL	Live load
LM1	Load Model 1
LP	Loading Position
MBE	Manual of Bridge Evaluation
MCFT	Modified Compression-Field Theory
NEN	Nederlandse Norm (Dutch Norm)
NPR	Nederlandse Praktijkrichtlijn (Dutch Practical Guideline)
PGA	Peak Ground Acceleration
PL	Proof Load
QR22	Plain rebar with a yield strength of 220 MPa
Q12PL	Quadrilateral Plate bending elements with 12 degrees of freedom
RBK	Richtlijnen Beoordeling Kunstwerken (Dutch Guidelines for the Assessment of Existing Bridges)
SAP200	Structural Software for Analysis and Design
SD	Asphalt Load
SW	Self-Weight
TS	Tandem System
UC	Unity Check
UDL	Uniformly Distributed Load
ULS	Ultimate Limit State
VBC	Voorschriften Beton Commissie (Old Dutch Concrete Code)

## Greek symbols - Lower case

$\alpha$	factor related to the total number of earthquakes in a region
$\alpha_g$	design ground acceleration in the horizontal direction
$\alpha_{Qi}$	multiplication factors for TS of live load model 1
$\alpha_{qi}$	multiplication factors for UDL of live load model 1
$\alpha_{vg}$	design ground acceleration in the vertical direction
$\beta$	factor measures the relative number of large to small earthquakes
$\beta_1$	parameter that determines average compressive stress in concrete
$\beta_{ult}$	parameter that gives relation between height of rectangular compressive stress block and depth of the compression zone
$\gamma$	specific weight
$\gamma_{asph}$	specific weight of asphalt
$\gamma_c$	partial factor for concrete
$\gamma_G$	partial factor for dead loads
$\gamma_I$	Importance factor
$\gamma_Q$	partial factor for live loads
$\gamma_s$	partial factor for steel
$\varepsilon$	strain
$\varepsilon_0$	material parameter of the concrete
$\varepsilon_c$	strain in concrete fiber most in compression
$\varepsilon_{cr}$	strain at cracking of the concrete
$\varepsilon_{cu}$	strain at crushing of the concrete
$\varepsilon_{sy}$	strain at yielding of the steel
$\kappa_{cr}$	curvature at cracking of the concrete
$\kappa_{ult}$	curvature at crushing of the concrete
$\kappa_y$	curvature at yielding of the steel
$\nu$	Poisson's ratio
$\rho_l$	longitudinal reinforcement ratio
$\sigma$	stress
$\sigma_{xx}$	longitudinal normal stress
$\sigma_{xy}$	shear stress
$\sigma_{yy}$	transverse normal stress
$\tau_{combination}$	shear stress due to load combination
$\tau_{conc}$	shear stress due to concentrated loads
$\tau_{FL}$	shear stress due to failure load
$\tau_{line}$	shear stress due to distributed loads
$\tau_{LL}$	shear stress due to live load
$\tau_{PL}$	shear stress due to proof load
$\tau_{Rm}$	maximum allowable average shear stress
$\tau_{SD}$	shear stress due to asphalt loading
$\tau_{SW}$	shear stress due to self-weight
$\varphi_x$	rotation around x axis
$\varphi_y$	rotation around y axis
$\psi_{E,LL}$	combination coefficient for live loads, to be used when determining the effects of the design seismic action

## Latin symbols - Upper case

$A_c$	area of concrete
$A_s$	area of steel
$C_{R,c}$	calibration factor for the shear capacity
$C_{Rd,c}$	calibration factor for the design value of the shear capacity
$C_{Rm,c}$	calibration factor for the average value of the shear capacity
$E$	effect of seismic action
$E_c$	Young's modulus of concrete
$E_i$	response in mode $i$
$E_j$	response in mode $j$
$E_s$	Young's modulus of steel
$E_x$	seismic action effect in longitudinal direction
$E_{x,comb}$	combined seismic action effect in longitudinal direction
$E_y$	seismic action effect in transverse direction
$E_{y,comb}$	combined seismic action effect in transverse direction
$E_z$	seismic action effect in vertical direction
$E_{z,comb}$	combined seismic action effect in vertical direction
$F_c$	force at the concrete compression zone
$F_h$	equivalent static horizontal force
$F_s$	tensile force on steel
$F_v$	equivalent static vertical force
$F_x$	equivalent static longitudinal force
$F_y$	equivalent static transverse force
$F_{z,i}$	equivalent static vertical force on $i$ -th span
$H$	pier height
$I_{gross}$	moment of inertia of the gross (uncracked) section
$I_y$	moment of inertia of pier around $y$ axis
$K_{x,pier}$	pier stiffness in longitudinal direction
$K_{x,total}$	total stiffness in longitudinal direction
$K_{y,pendulum}$	pendulum stiffness in transverse direction
$K_{y,pier}$	pier stiffness in transverse direction
$K_{y,total}$	total stiffness in transverse direction
$K_{z,i}$	stiffness of the $i$ -th span
$L$	total length of the bridge
$L_{endspan}$	length of the end spans
$L_{midspan}$	length of the mid spans
$M$	mass of the bridge deck plus the mass of the upper half of the piers
$M_{cr}$	moment causing cracking of the cross section
$M_{crd}$	design moment causing cracking of the cross section
$M_{crm}$	average moment causing cracking of the cross section
$M_u$	moment causing crushing of the concrete in the cross section
$M_{ud}$	design moment causing crushing of the concrete in the cross section
$M_{um}$	average moment causing crushing of the concrete in the cross section
$M_y$	moment causing yielding of the steel in the cross section
$M_{yd}$	design moment causing yielding of the steel in the cross section
$M_{ym}$	average moment causing yielding of the steel in the cross section

$M_{Ed,span}$	acting bending moment at the mid-span
$M_{Ed,sup}$	acting bending moment at the supports
$M_{Ed,x}$	acting bending moment around x axis
$M_{Ed,x,pier}$	acting bending moment on the pier around x axis
$M_{Ed,x,pendulum}$	acting bending moment on a single pendulum around x axis
$M_{Ed,y}$	acting bending moment around y axis
$M_{Ed,y,pier}$	acting bending moment on the pier around y axis
$M_L$	earthquake magnitude in Richter scale
$N$	number of earthquakes with greater or equal magnitude
$P$	probability of exceedance of a specific earthquake magnitude
$P_{M,span}$	equivalent tandem load generating same bending moment at the mid-span as LM1
$P_{M,sup}$	equivalent tandem load generating same bending moment at the supports as LM1
$P_{Mcr,span}$	tandem load corresponding to moment causing cracking of the cross section at the mid-span
$P_{Mcr,sup}$	tandem load corresponding to moment causing cracking of the cross section at the supports
$P_{Mu,span}$	tandem load corresponding to moment at the ultimate limit state at the mid-span
$P_{Mu,sup}$	tandem load corresponding to moment at the ultimate limit state at the supports
$P_{My,span}$	tandem load corresponding to moment at yielding at the mid-span
$P_{My,sup}$	tandem load corresponding to moment at yielding at the supports
$P_{tot}$	total tandem load
$P_V$	equivalent tandem load generating same shear force as LM1
$P_{V,EC}$	expected maximum tandem load for shear failure according to EC2
$P_{V,EC,mean}$	average expected maximum tandem load for shear failure according to EC2
$P_{V,EC,para}$	expected maximum tandem load for shear failure according to EC2 and $b_{para}$
$P_{V,EC,skew}$	expected maximum tandem load for shear failure according to EC2 and $b_{skew}$
$P_{V,EC,str}$	expected maximum tandem load for shear failure according to EC2 and $b_{str}$
$P_{V,prop}$	expected maximum tandem load for shear failure according to proposed formula
$P_{V,prop,mean}$	average expected maximum tandem load for shear failure according to proposed formula
$P_{V,prop,para}$	expected maximum tandem load for shear failure according to proposed formula and $b_{para}$
$P_{V,prop,skew}$	expected maximum tandem load for shear failure according to proposed formula and $b_{skew}$
$P_{V,prop,str}$	expected maximum tandem load for shear failure according to proposed formula and $b_{str}$
$Q_i$	magnitude of an axle load on notional lane number $i$
$Q_{ik}$	magnitude of a characteristic axle load on notional lane number $i$
$R_{y,i}$	Reaction force in y direction on the $i$ -th pier
$S$	soil factor
$S_a(T)$	horizontal spectral acceleration according to the horizontal elastic response spectrum
$S_{av}(T)$	vertical spectral acceleration according to the vertical elastic response spectrum
$T$	pier thickness

$T_B$	numerical value of the lower limit of the vibration periods for which the spectral acceleration is constant
$T_C$	numerical value of the upper limit of the vibration periods for which the spectral acceleration is constant
$T_D$	period that indicates the start of the constant displacement response of the spectrum
$T_R$	earthquake return period
$T_x$	fundamental period of vibration in longitudinal direction
$T_y$	fundamental period of vibration in transverse direction
$T_{z,i}$	fundamental period of vibration of i-th span in vertical direction
$U$	combined action effect
$U_x$	combined seismic action effect in longitudinal direction with other actions
$U_y$	combined seismic action effect in transverse direction with other actions
$U_z$	combined seismic action effect in vertical direction with other actions
$V_{Ed}$	acting shear force
$V_{Ed,x}$	acting shear force in x direction
$V_{Ed,x,pier}$	acting shear force on the pier in x direction
$V_{Ed,y}$	acting shear force in y direction
$V_{Ed,y,pendulum}$	acting shear force on a pendulum in y direction
$V_{Ed,y,pier}$	acting shear force on the pier in y direction
$V_{FL}$	shear force due to failure load
$V_{LL}$	shear force due to live load
$V_{PL}$	shear force due to proof load
$V_{R,c}$	value of the shear capacity
$V_{R,c,prop}$	value of the shear capacity according to the proposed formula for concrete slabs subjected to concentrated loads close to supports
$V_{Rd,c}$	design value of the shear capacity
$V_{Rm,c}$	average value of the shear capacity
$V_{SD}$	shear force due to asphalt load
$V_{SW}$	shear force due to self-weight
$W$	pier width

## Latin symbols - Lower case

$b$	slab width
$b_{edge}$	distance of the tandem load to the edge of the slab
$b_{eff}$	effective width for shear
$b_{eff,1}$	effective width as used in Dutch practice
$b_{eff,2}$	effective width as used in French practice
$b_{para}$	effective width based on a load spreading parallel to the straight case
$b_{skew}$	effective width with horizontal load spreading under $45^\circ$ from the far side of the wheel print to the face of the support for a skew slab
$b_{str}$	effective width for a straight slab
$c_{cr}$	depth of the compression zone at onset of cracking
$c_{ult}$	depth of the compression zone at the ultimate limit state
$c_y$	depth of the compression zone at yielding of the tension steel
$d_l$	effective depth to the longitudinal reinforcement

$f_c$	cylinder compressive strength of concrete
$f_{cd}$	design cylinder compressive strength of concrete
$f_{cd,cube}$	design cube compressive strength of concrete
$f_{ck}$	characteristic cylinder compressive strength of concrete
$f_{ck,cube}$	characteristic cube compressive strength of concrete
$f_{cm}$	average cylinder compressive strength of concrete
$f_{cm,cube}$	average cube compressive strength of concrete
$f_{c,th}$	stress in the concrete using Thorenfeldt's stress–strain diagram at yielding of the steel
$f_{ctd}$	design tensile strength of concrete
$f_{ctk,min}$	minimum characteristic tensile strength of concrete
$f_{ctm}$	average tensile strength of concrete
$f_r$	rupture strength of concrete
$f_{td}$	design ultimate strength of steel
$f_{tm}$	average ultimate strength of steel
$f_y$	yield strength of steel
$f_{yd}$	design yield strength of steel
$f_{yk}$	characteristic yield strength of steel
$f_{ym}$	average yield strength of steel
$h$	pendulum height
$h_{slab}$	slab thickness
$k$	size effect factor
$k_2$	factor for the centroid of the concrete compressive stress distribution
$l_{bearings,i}$	length of the $i$ -th bearing along the support
$l_{sup}$	supported length
$m_i$	mass of $i$ -th span
$m_{xD}$	generalized combined longitudinal moment
$m_{xD,span}$	generalized combined longitudinal moment at the mid-span
$m_{xD,sup}$	generalized combined longitudinal moment at the supports
$m_{xx}$	generalized longitudinal bending moment
$m_{xy}$	generalized torsional moment
$m_{yD}$	generalized combined transverse moment
$m_{yy}$	generalized transverse bending moment
$n$	damping correction factor
$n_{bearings}$	number of bearings on support line
$n_{th}$	material parameter of concrete
$p$	ratio between the peak ground acceleration and the platform value of the elastic response spectrum
$q$	behaviour factor
$q_i$	magnitude of the vertical distributed load on notional lane number $i$
$q_{ik}$	magnitude of the characteristic vertical distributed load on notional lane number $i$
$q_r$	magnitude of the vertical distributed load on the remaining area
$q_{rk}$	magnitude of the characteristic vertical distributed load on the remaining area
$q_{xz}$	generalized longitudinal shear force
$q_y$	equivalent static transverse distributed force
$q_{yz}$	generalized transverse shear force

$r_{ij}$	correlation factor of modes
$r_x$	rotation around x axis
$r_y$	rotation around y axis
$r_z$	rotation around z axis
$t$	pendulum thickness
$t_{\text{asph}}$	asphalt thickness
$t_r$	period for exceedance of a specific earthquake magnitude
$u_x$	displacement in x direction
$u_y$	displacement in y direction
$u_z$	displacement in z direction
$u_{z,i}$	displacement in z direction of the i-th span
$V_{\text{min}}$	lower bound of the shear capacity
$V_{\text{Rd,c}}$	design value of the shear stress capacity
$V_{\text{Rm,c}}$	average value of the shear stress capacity
$V_{\text{s,30}}$	Average value of propagation velocity of S waves in the upper 30 m of the soil
$w$	pendulum width
$w_i$	width of notional lane number i
$w_r$	width the remaining area
$w_{\text{slab}}$	slab width

## Other symbols

$\emptyset$	reinforcement diameter
-------------	------------------------



# Table of Contents

1	Introduction .....	1
1.1.	Problem Definition.....	1
1.1.1.	Shear capacity of reinforced concrete bridges .....	1
1.1.2.	Human - induced earthquakes .....	3
1.2.	Research objectives.....	4
1.3.	Project approach - Methodology .....	5
1.3.1.	Literature study .....	5
1.3.2.	Static analysis - Analytical approach.....	6
1.3.3.	Static analysis - Numerical approach .....	6
1.3.4.	Seismic design - Fundamental mode method analysis.....	6
1.3.5.	Seismic design - Modal response spectrum analysis .....	6
1.4.	Thesis outline.....	7
2	Literature review .....	9
2.1.	Load testing on reinforced concrete solid slab bridges.....	9
2.2.	Shear capacity of reinforced concrete slabs.....	11
2.3.	Levels of approximation for the assessment of solid slab bridges .....	13
2.4.	Seismic evaluation of existing bridges.....	15
3	Case study description.....	17
3.1.	Location and background of the Nieuwklap Bridge .....	17
3.2.	Structural system .....	19
3.2.1.	Geometry.....	19
3.2.2.	Reinforcement layout.....	20
3.3.	Material properties .....	21
3.3.1.	Concrete.....	21
3.3.2.	Reinforcement steel.....	21
3.4.	Load test.....	22
4	Static analysis - Analytical approach.....	25
4.1.	Assumptions .....	25
4.1.1.	Analytical model.....	25
4.1.2.	Loading.....	26
4.1.3.	Capacity.....	31
4.2.	Results.....	36

4.2.1.	Eurocode loading .....	36
4.2.2.	Equivalent proof loading .....	38
4.2.3.	Failure field loading .....	39
4.3.	Discussion - Conclusions .....	41
5	Static analysis - Numerical approach .....	43
5.1.	Finite element model .....	43
5.1.1.	Geometry - Supports .....	43
5.1.2.	Finite element type - Mesh .....	44
5.1.3.	Loading - Analysis .....	46
5.2.	Results .....	48
5.2.1.	Eurocode loading .....	49
5.2.2.	Equivalent proof loading .....	51
5.2.3.	Eurocode and experimental loading comparison .....	52
5.2.4.	Failure field loading .....	54
5.3.	Discussion - Conclusions .....	55
5.4.	Comparison with Analytical approach .....	56
6	Seismic design .....	59
6.1.	General .....	59
6.1.1.	Earthquake data .....	59
6.1.2.	Response spectra .....	62
6.2.	Fundamental mode method .....	65
6.2.1.	Vertical component .....	65
6.2.2.	Horizontal components .....	68
6.3.	Modal response spectrum analysis .....	72
6.3.1.	Modal analysis .....	74
6.3.2.	Seismic action .....	75
6.4.	Discussion - Conclusions .....	78
7	Conclusions and Recommendations .....	81
7.1.	Conclusions .....	81
7.2.	Recommendations .....	82

# 1 Introduction

## 1.1. Problem Definition

### 1.1.1. Shear capacity of reinforced concrete bridges

During the decades of reconstruction after the Second World War a massive expansion of the Dutch road network took place. Simultaneously, a large amount of bridges were constructed in order to accommodate the increasing traffic flows. Therefore, the majority of the existing concrete bridges in the Netherlands was built during this era (*Figure 1.1*) [1], when the reinforced concrete solid slab bridges were a popular structural system, due to the requirements for small spans and ease of construction.

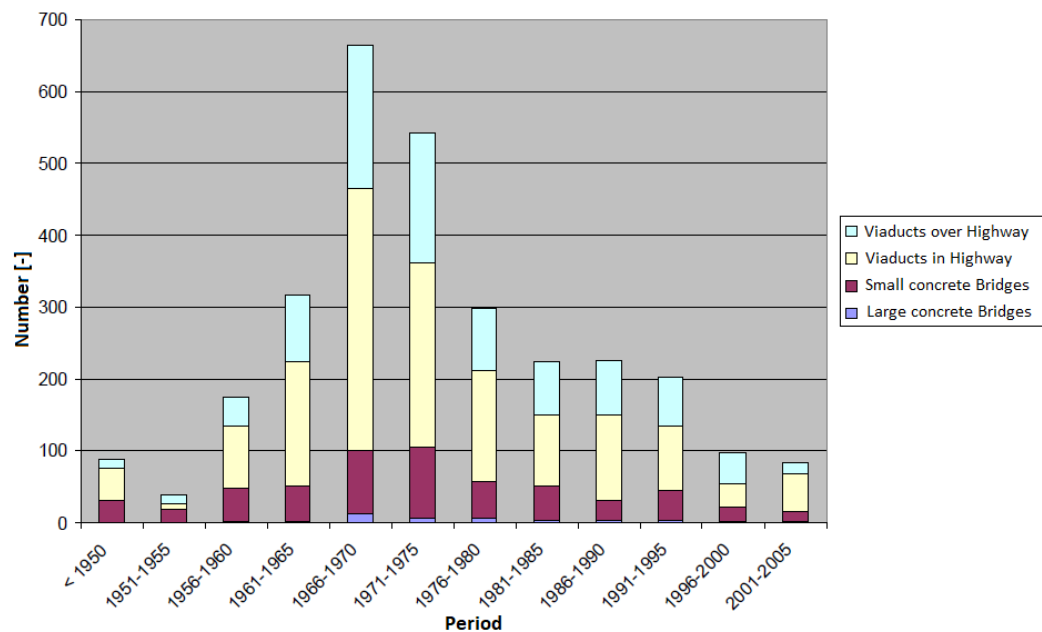


Figure 1.1: Building year of concrete viaducts and bridges in the Netherlands [1]

Nowadays these bridges are reaching the end of their originally devised service life and, since they were designed according to the regulations of that era, often rate insufficiently regarding their shear capacity when they are assessed with the current codes [2]. This lack of capacity results from the fact that the present design live load models according to NEN-EN 1991-2:2003 [3] are substantially heavier than the live loads of that era, reflecting the accretion of traffic loads and volumes, in combination with the lower shear capacities allowed by the current shear models, that

are defined by NEN-EN 1992-1-1:2005 [4], in comparison to the Dutch codes that were applied in the past, such as the VBC 1977 [5]. Surprisingly, a large number of reinforced concrete solid slab bridges that has been found after evaluation to not fulfil the requirements regarding their shear capacity, were observed to be fully functional upon inspection, with no indication of remarkable shear distress [6].

Taking into consideration these results, it can be concluded that, the fact that the majority of reinforced concrete solid slab bridges rates insufficiently according to the current provisions for shear, does not necessary entail that these bridges have to be demolished and replaced immediately. Contrariwise, it indicates that more suitable methods for evaluating the shear capacity of reinforced concrete slabs need to be developed in order to contribute to the making of informed decisions regarding the safety, function and remaining life of these structures.

It can be deduced that the actual shear capacity of the reinforced concrete solid slab bridges that were constructed during this period is larger than the capacity indicated by the code provisions. In order to identify the additional sources that contribute to the increase of the shear capacity of solid slab bridges research has been mainly limited to half scale slab specimens cast in the laboratory [7]. However, these models do not contain the complete details and the actual boundary conditions of a real bridge that has been in service for several decades. In order to describe the full structural behaviour and study the failure mechanism of reinforced concrete solid slab bridges, load testing to failure of actual bridges is essential. In the direction of contributing to this research field, Delft University of Technology has executed in the near past proof load tests on slab bridges as an assessment tool and a collapse test for the investigation of their ultimate capacity [8].

A reinforced concrete solid slab bridge is investigated by Delft University of Technology and in case that it is proven to be shear-critical, a full-scale load test to failure will be performed. The aforementioned bridge is located in the province of Groningen, it consists of 7 spans and was constructed in 1941. During this project it will be referred to as the Nieuwklap Bridge. The existing bridge is scheduled for demolition and replacement by a new one and for this reason arises the opportunity to carry out such a load test. In *Figure 1.2* [9] a view of the Nieuwklap bridge is depicted. More details about the structural system and the material properties of the investigated bridge will be elaborated in *Chapter 3*.



*Figure 1.2: View of the Nieuwklap Bridge [9]*

### 1.1.2. Human - induced earthquakes

Since the sixties the Netherlands has been extracting natural gas from the soil of the northern part of the country [10]. The gas extraction takes place at a depth of approximately 3 kilometers, absorbing the sandstone located in that area, resulting in pressure changes beneath the earth surface and finally leading to human-induced earthquakes. This gas extraction is responsible for virtually all earthquakes in this area, since there has been no history of significant seismic activity in the region before the onset of natural gas exploitation. These earthquakes take place in the immediate vicinity of the gas reservoirs, the largest of which is the Groningen gas field (*Figure 1.3*) [11]. The highest number of quakes with a magnitude greater than 1.5 was registered in 2013 according to Koninklijk Nederlands Meteorologisch Instituut (KNMI) [10], but the following years the incidents were considerably lower (*Figure 1.4*), as a result of the decision to reduce the production rate in the center of the gas field.

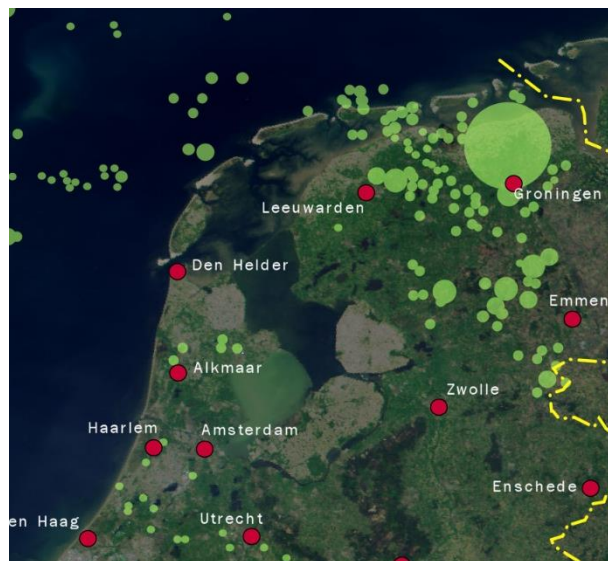


Figure 1.3: Location of the Groningen gas field [11]

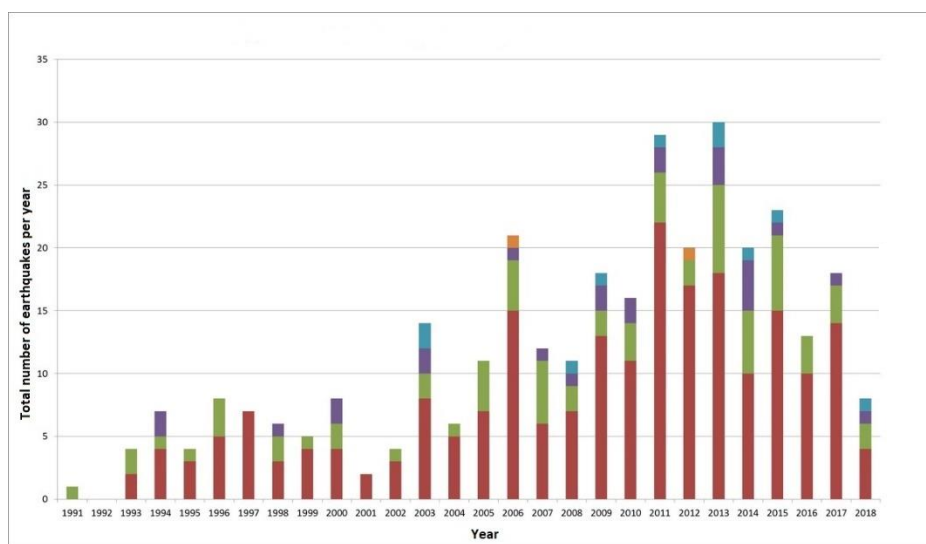


Figure 1.4: Annual number of earthquakes in the Groningen gas field with a magnitude ( $M_L$ ) higher than 1.5 [10]

Considering that the Netherlands was naturally an inactive seismic zone, the majority of the structures that were built in the past have not been designed for the present seismic activity. Therefore, uncertainties are arising regarding the earthquake resistance and the seismic behaviour of the engineering structures located in Groningen province, which are affected significantly from these phenomena. Taking that into account, the verification of the structural capacity and the earthquake resistance of a significant number of buildings and bridges is of great importance in order to guarantee the safety of these structures.

Consequently, the behaviour of the reinforced concrete solid slab bridges of the region is also uncertain under the seismic loading and there are no substantiated conclusions regarding its influence on their capacity and their service life, since the extent of the research that has been carried out investigating this subject is limited. In order to design structures subjected to earthquakes, the guidelines laid by the EN 1998-1:2004 [12] have to be followed and more specifically for bridge seismic design more details are included in EN 1998-2:2005 [13]. In 2015, the Nederlandse Praktijkrichtlijn (NPR) 9998 [14] was published by NEN for the design of earthquake-resistant new structures and the evaluation of existing structures in the north-east part of the Netherlands, which has been affected by the induced seismicity.

Due to its location, the Nieuwklap bridge is as well suitable for measurements of the effects of earthquakes in the province of Groningen. Their influence on the shear capacity of structures without shear reinforcement, considering also the vertical component of the seismic excitation can be investigated. Additionally, the piers and the supports of these type of bridges need to be assessed regarding their earthquake-resistance in order to validate their suitability for public use.

## 1.2. Research objectives

This project is subdivided into two main parts, with distinct main objectives for each part.

The main objective of the first part of the project is to accurately estimate the failure mode of the Nieuwklap Bridge by using the Levels of Approximation as these are recommended by the fib Model Code 2010 [15] and by RBK (Guidelines for the Assessment of Existing Bridges) [16], in order to analyze what kind of failure has to be expected during the preparation and execution of the loading test. Furthermore, it is of great significance to prove that even though the majority of existing reinforced concrete solid slab bridges is supposed to be inadequate regarding their shear capacity according to the current codes, they exhibit flexural failure in reality, because of the fact that shear failure is a brittle failure mode with no obvious signs of distress before collapse. Moreover, the specification of the required magnitude of the applied proof load is essential and it will be defined such that the same sectional shear and bending moment stresses as due to the live load models of the Eurocode [4] are generated. Finally, the equivalent field load that leads to shear and flexural failure of the bridge deck is important to be estimated, in order to define which failure mode will occur for a lower field load magnitude and to describe more accurately the structural behaviour of the bridge.

The main objective of the second part of the project is the evaluation of the Nieuwklap Bridge regarding its earthquake resistance and its seismic behaviour. The impact of the vertical component of the seismic action on the structural capacity of the bridge and more specifically the possibility of shear or flexural failure of its deck due to earthquake loading has to be investigated. Additionally, the ability of the bridge piers to withstand the horizontal components of the seismic

excitation and the combined seismic action has to be validated in order to guarantee the safety of the structure. At the end, the behaviour of the bridge under the dynamic seismic loading will be assessed in order to describe more accurately the effects of human-induced earthquakes on this type of bridges.

The research objectives can be formulated into two main research questions which are:

- ***“Which failure mode will occur in the Nieuwklap Bridge under a load test until failure?”***
- ***“Is the Nieuwklap Bridge able to withstand earthquake loading due to human-induced earthquakes and how does it behave under this seismic excitation?”***

At the same time the following additional questions arise:

- Are the current codes predicting accurately the actual shear capacity of the reinforced concrete solid slab bridges?
- Can the structure withstand the maximum required design loads?
- Which are the critical loading positions for a shear and a bending test?
- Which is the magnitude of the field loading that is representative for the live load models of the Eurocode?
- Which is the magnitude of the field loading that leads to shear and flexural failure of the bridge deck?
- Is it possible that the Nieuwklap Bridge will fail in shear?
- Can Linear Finite Element Models describe accurately the behaviour of the bridge and predict its failure mode?
- What are the differences between the response spectra defined by Eurocode 8 and NPR 9998?
- Is the vertical seismic load combination critical for the deck of reinforced concrete solid slab bridges?
- Are the piers and the supports of the bridge able to withstand the vertical seismic load combinations in transverse and longitudinal direction?
- Which are the fundamental natural periods of the structure and their corresponding modal shapes?

### 1.3. Project approach - Methodology

Accomplishing the final goal of the project, requires a specific approach to be defined with distinct parts. The methodology and the series of steps that will be followed during the research are presented.

#### 1.3.1. Literature study

In order to obtain more knowledge about load testing in reinforced concrete solid slab bridges, the shear behaviour of solid slabs, the assessment procedures that have been used in the past and the seismic evaluation of existing bridges, a detailed literature study is essential to be made to previous related researches and approaches concerning these subjects. The gained knowledge will be evaluated and can be used during the rest of the research.

### 1.3.2. Static analysis - Analytical approach

For the initial approach, in order to determine if the Nieuwklap bridge is able to resist the design loads, the characteristic and the mean values of the materials will be taken into account and Load Model 1 (LM1) according to NEN-EN 1991-2:2003 [3] will be applied on the bridge, on the most unfavorable positions for shear and flexure. Consequently, the shear and bending stresses will be calculated using the structural software SAP2000, while the shear and bending moment capacity of the bridge will be calculated according to NEN-EN 1992-1-1:2005 [4], for members without shear reinforcement not subjected to axial forces. An additional calculation for the shear capacity will be performed, by using a proposal for the extension of the Eurocode shear formula for concrete slabs under concentrated load close to supports, which is derived by the combination of experimental results and Monte Carlo simulations [17]. Recommendations derived from slab experiments, concerning the effective width at the supports of the bridge, will also be considered. The Quick Scan method will be used, resulting in a “Unity Check”, which is a ratio of the stresses caused by the applied loads to the corresponding capacity of the structure, identifying if the bridge can withstand the design loads. Afterwards, the equivalent proof load that generates the same stresses as LM1 and the maximum tandem loads, at which shear and flexural failure is expected in the load test, will be defined, determining which failure mode is expected at this level of assessment.

### 1.3.3. Static analysis - Numerical approach

A numerical approach, using DIANA FEA, will contribute to a better estimation of the actual capacity of the bridge. A 2D linear finite element model of the bridge will be constructed, using plate bending elements, and the Eurocode loading as well as the experimental loading will be applied, in order to obtain the corresponding shear and bending stresses at the critical cross-sections of the bridge and compare them with the previously estimated results. The differences between the Eurocode and the experimental loading will also be examined. Finally, the magnitude and position of the equivalent critical field loading will be determined again with this approach, providing a more accurate prediction of its failure mode under the performed load test.

### 1.3.4. Seismic design - Fundamental mode method analysis

Regarding the seismic design of the Nieuwklap bridge a linear static analysis will be performed initially by using the fundamental mode method. The representative response spectra will be obtained through NPR 9998 [14] for specific return periods. The equivalent static loads in each direction will be calculated considering the stiffness of the structure in the corresponding direction and its fundamental natural period. The equivalent static vertical force will be applied on the bridge deck in combination with the Eurocode live loading in order to examine if this combined action is critical and if it could possibly affect the failure mode. The equivalent static horizontal forces will also be applied in order to investigate the ability of the piers and the supports to withstand the seismic impact.

### 1.3.5. Seismic design - Modal response spectrum analysis

In order to describe more accurately the seismic behaviour of the Nieuwklap bridge a Modal response spectrum dynamic analysis will also be performed. A beam model will be constructed using the structural software SAP2000 and the corresponding vertical and horizontal response spectra will be applied. The bridge will be evaluated again for the seismic load combination and under the combined action of the three components of the seismic excitation the earthquake resistance of the bridge deck and the bridge piers will be checked. Additionally, more insight to

the seismic behaviour of the Nieuwklap bridge will be gained through the investigation of the eigenmodes and the corresponding natural periods that will be obtained through the Modal analysis.

## 1.4. Thesis outline

A short overview of the thesis is presented below, where the structure and the content of each chapter of this research is reported.

In *Chapter 1*, the problem definition has been described briefly and the main research objectives have been laid down by formulating the main research questions that need to be answered. Then, the project approach that will be followed and the methodology that will be applied in order to reach the specified goals have been analyzed.

In *Chapter 2*, a comprehensive background information about the examined topics relevant for this thesis will be obtained through a rigorous literature study.

A detailed description of the Nieuwklap bridge, which is the case study of the present thesis, takes place in *Chapter 3*.

In *Chapter 4*, the analytical approach that is applied for the prediction of the failure mode of the Nieuwklap bridge and the obtained results are presented, together with the assumptions that have been considered for the implemented analytical model.

The numerical approach regarding the evaluation of the Nieuwklap bridge and the prediction of its failure mode is displayed in *Chapter 5*, as well as the finite element model characteristics that was used for the linear elastic analysis.

In *Chapter 6*, the evaluation of the earthquake resistance and the description of the seismic behaviour of the structure is presented analytically, by using a simplified linear static method and a dynamic analysis.

Finally, in *Chapter 7*, the obtained conclusions of the thesis and the recommendations for future work are included.



## 2 Literature review

In order to gain more knowledge about crucial subjects related to load testing in reinforced concrete solid slab bridges, the shear behaviour of solid slabs and seismic evaluation, a rigorous literature study is essential to be made in this chapter. The emphasis of the literature study lies on specific topics that will be analyzed in detail.

### 2.1. Load testing on reinforced concrete solid slab bridges

AASHTO MBE (Manual of Bridge Evaluation) [18] distinguishes roughly two types of structural load tests that have been carried out predominantly over the past few decades, each with different procedure and purpose: diagnostic load tests and proof load tests.

Diagnostic load tests use low load levels and measurements in order to verify if the stiffness and behaviour of bridge structures are as expected by design calculations. These tests are widely performed on newly constructed bridges for the verification of their behavior and in several countries, such as Italy [19], Switzerland [20] and France [21], a diagnostic load test is required before the opening of a bridge. Additional diagnostic load tests can be performed during the lifespan of the bridge, monitoring the stiffness reduction as a result of material degradation. Furthermore, this type of load tests is used as a tool in order to update analytical models that are applied in the assessment of bridges. The structural response of the structure under loading is measured and the measurement result is compared with the analytically predicted response from a finite element model. Subsequently, the differences between the field test and the analytical model are minimized by calibrating the finite element model.

Proof load tests use higher load levels in order to verify a certain capacity or safety of a bridge. They are typically performed on existing bridges by application of a load equivalent to the factored live loads, verifying that the structure is able to carry this load without any indication of distress, fulfilling the code requirements. With this method are tested also structures for which there is lack of information, such as inaccurate structural plans or unknown effects of material degradation. In addition, the results of a proof load test can be used for a probabilistic analysis, because the reliability index will be updated by truncating the probability density function of the resistance (*Figure 2.1*) [22]. After the application of a proof load test further assessment is not necessary but due to the fact that high load-levels are required there is a risk of structural damage.

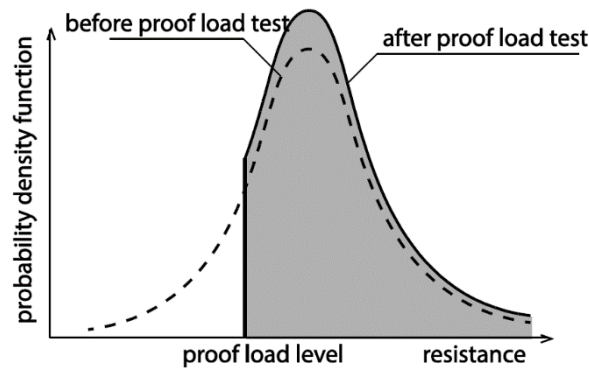


Figure 2.1: Truncation of probability density function of resistance after proof load test [22]

In fact, when a proof load test is performed some contradictory requirements are existent, on the one hand the load should be as high as possible in order to prove sufficient structural capacity and on the other hand the maximum load is limited in order to avoid irreversible structural damage of the bridge. For that purpose, there are available guidelines for proof load testing in the United Kingdom [23], in Ireland [24] and in France [21], where procedures for safe execution of proof load tests are described. There are also guidelines that indicate when a test needs to be abandoned, by specifying “stop criteria” and an appropriate cyclic loading protocol, for buildings in Germany [25] and the United States [26]. These stop criteria are related mainly to the limit state of flexure, measuring and checking deflections, strains, crack widths, the deviation from linearity index and the permanency ratio. On the other hand, for the limit state of shear, which is a brittle failure mode, stop criteria need to be developed and are subject of further scientific research. In order to evaluate the loading protocol and the stop criteria, which are defined from these guidelines, a research is carried out by Delft University of Technology and several laboratory tests have been performed [27, 28, 29]. Beams sawn from the Ruytenschildt Bridge were tested, by applying a cyclic loading protocol, and it was concluded that the specified stop criteria should be revised to become less conservative, since they were exceeded well before failure occurs as well as that for shear failure other criteria should be formulated [28]. In addition, a series of experiments on beams loaded with a cyclic or monotonic loading protocol were executed, assessing the guidelines and proposing other possible stop criteria, such as the deformation profiles and the stiffness reduction, considering the failure mode and the existence of cracking, while at the same time recommendations for a suitable loading protocol were made [29]. Moreover, data from tested beams in the laboratory were compared with the theoretical model of Monnier for the moment - curvature diagram and a satisfactory agreement was observed [27]. Also, the existing stop criteria from the literature were evaluated and it was realized that in order to increase their reliability further refinement is essential, due to the fact that large scatter was identified for many of them leading to uncertainties, as well as that these criteria cannot be directly applied in existing structures [27].

In addition to the abovementioned loading tests, collapse testing has been also introduced which is testing to failure of a bridge in the field. In the past, only a limited number of bridges have been tested to failure and it has to be emphasized that the majority of them were slab bridges and flexural failure was the dominating failure mode [30]. Also, a review of failure tests on concrete bridges of various types, prove that the theoretical calculations used traditionally for assessment and design are conservative estimations and that unexpected failure modes can possibly occur [31].

In the Netherlands, under a research carried out by Delft University of Technology, load tests have been performed on a number of existing reinforced concrete solid slab bridges over the past few years, and two bridges have been tested to failure, including bridges with and without material deterioration [8]. More specifically, diagnostic load tests have been performed on the viaduct Heidijk [32] and on the viaduct Medemblik [33] and proof load tests on the viaduct Vlijmen-Oost [34], on the Halvemaans Bridge [35], on the viaduct Zijlweg [36], on the viaduct De Beek [37] and on the Ruytenschildt Bridge [38]. The stop criteria for some of these executed tests were further analyzed and evaluated, concluding that some criteria prove to be valid. However, some others were rather conservative or should be ignored and other possible criteria were proposed [8].

Particularly interesting is the case of the Ruytenschildt Bridge. It is an integral reinforced concrete solid slab bridge, which was tested to failure in two spans during the summer of 2014 by Delft University of Technology, by applying the loading at the critical position for shear, at a specified distance from the supports [7, 16] and close to the obtuse angle [39]. It was ascertained that shear was not the governing failure mode, since in both tested spans flexural failure or flexural distress was observed, proving that current rating procedures for shear are rather conservative [30]. The bridge was further analyzed by using a linear elastic finite element model in order to determine the proof load level for flexure and an additional plastic analysis was performed [40]. The determination of the Unity Checks for flexure proved a sufficient bending moment capacity for the bridge and the conservativeness of the current rating procedures [40]. Moreover, since the stiffness and the support moments at the ends were unknown, a hinged support was assumed, resulting in an overestimation of the experimental moment [38].

The detailed analysis of the results that emerge from these load tests could contribute, alongside with additional research and experiments, to the formulation of the basis for a Dutch guideline on proof loading of bridges, describing accurately their preparation, execution and analysis [8]. More specifically, recommendations have been formulated for the determination of the position and magnitude of the proof load, as well as for a loading protocol, a set of stop criteria and a sensor plan [8, 22].

## 2.2. Shear capacity of reinforced concrete slabs

As highlighted in the introduction, the shear capacity of reinforced concrete solid slab bridges is nowadays a disputable subject in the Netherlands, because initial assessments according to the current design codes often prove that the requirements are not fulfilled [2], since in many cases the deterministic value of the moment capacity is larger than the deterministic value of the shear capacity. However, it is noteworthy to mention that several load-bearing mechanisms, that are activated in reinforced concrete slabs, are not taken into consideration in the empirical code equations due to simplifications. In addition, some of these mechanisms are neglected because in many cases, including the NEN-EN 1992-1-1:2005 [4], the shear capacity is derived based on beam shear experiments [41]. It can be concluded that in order to have an accurate estimation of the shear capacity of reinforced concrete slabs more suitable methods need to be developed.

Concerning this controversial topic, Delft University of Technology has researched extensively the past few years the behavior of reinforced concrete slabs. Experimental research has been carried out on slab specimens under concentrated loads close to supports and several parameters such as the size of the loading plate, the amount of transverse reinforcement, the concrete compressive strength, the position of the concentrated load and the effect of using ribbed

reinforcement bars versus plain reinforcement bars were studied, proposing a code extension based on statistical analysis, that takes these factors into account [7, 42, 43, 44]. Through the combination of experimental research and Monte Carlo simulations even formulas, which allow greater shear stresses for concrete slabs under concentrated loads close to supports have been proposed for the extension of the shear provisions of the Eurocode [17]. Regarding the effect of skewness, it has been found to be negative on the shear capacity due to stress concentrations in the obtuse corner [45] and in the Netherlands a set of skew factors is used raising the load effects [46], but until more experimental results are available its impact cannot be predicted accurately. Furthermore, beams sawn out of the Ruytenschildt Bridge have been tested in the laboratory, resulting in a deeper understanding of shear and flexural capacity of existing structures, proving that shear failure has to be taken into account also for elements with plain reinforcement, since it was not observed an increase in the shear capacity compared to elements with deformed reinforcement bars [30].

The main conclusion of this research was that there is a significant difference with regard to the shear capacity and behaviour between concrete slabs and beams. The explanation for this conclusion is that slabs are three-dimensional elements and when concentrated loads are exerted on them, an additional shear capacity occurs because of their ability to redistribute stresses in the transverse direction resulting in a higher shear strength [7, 47].

In the direction of a more detailed description and a deeper understanding of the shear behaviour of concrete, several theories and models have been developed and still are continuously evolving, such as Yang's Critical Shear Displacement theory [48], the Extended Strip Model [7, 49], which is a suitable method for the assessment of slabs subjected to concentrated loads close to supports, and the Modified Compression-Field Theory (MCFT) [50], where cracked concrete is considered as a "new" material with its own characteristics. In addition, the use of probabilistic analyses and non-linear finite element analyses is introduced for advanced shear analysis of concrete slabs [51] and also the Critical Shear Crack Theory [52], which takes into account the asymmetric nature of the problem.

Moreover, in the lower Levels of Assessment the additional shear capacity of concrete slabs is considered by defining an effective width in shear at the slab support [47], which can be determined theoretically from a horizontal load spreading method, such that the total shear stress over the support equals the maximum shear stress over this effective width. Practically the horizontal load spreading differs according to the local regulations. For example, in the Netherlands a horizontal load spreading under a 45° angle from the center of the load towards the support is assumed and in France under a 45° angle from the far corners of the loading plate towards the support (*Figure 2.2*). This procedure is even more complicated when a skew slab is under investigation, due to the fact that a direct application of the recommendations for straight slabs is not valid and other possible interpretations for the calculation of the effective width should be used [30, 40]. In order to have a better estimation of the effective width of the supports also linear elastic finite element analyses have been used, deducing that the boundary conditions have a major influence on the results [53].

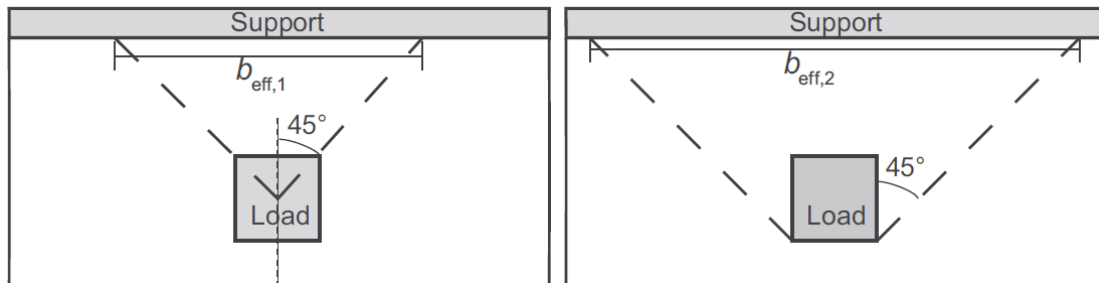


Figure 2.2: Determination of the effective width according to Dutch practice (left) and to French practice (right) [47]

However, these laboratory tests are a simplification of an actual bridge, since the tested specimens were half-scale models of slab bridges and important details regarding the serviceability and the supporting conditions of actual reinforced concrete slab bridges were neglected. Therefore, field testing to failure of solid slab bridges that are going to be demolished or replaced is of great importance, offering useful information about their ultimate capacity and their failure mode and creating a link between field and laboratory testing.

### 2.3. Levels of approximation for the assessment of solid slab bridges

The concept of Levels of Approximation is introduced by the fib Model Code 2010 [15]. Increasing the Level of Approximation is more complicated and increases the computational time and effort, but on the other hand results in a closer estimation of the actual capacity of the tested member under consideration. An approach that is based on Levels of Approximation for the shear capacity and the punching shear capacity is applied by the fib Model Code. For a preliminary design the lowest Level of Approximation is adequate but for optimization purposes higher levels are necessary. This concept is also used currently in the Netherlands for the assessment of existing concrete structures, and in particular for the shear assessment of solid slab bridges [54], leading to the following so-called Levels of Assessment.

The first Level of Assessment is the “Quick Scan” method [55], a conservative spreadsheet-based method that takes into account recommendations derived from experiments. The sectional shear stress is determined based on a method comparable to hand calculations, the shear capacity is determined according to NEN-EN 1992-1-1:2005 [4], and a “Unity Check” is performed, which is a ratio between the generated stresses and the calculated capacity. For the second Level of Assessment, a linear elastic finite element model is used for the determination of the shear stress distribution over the width of the support. Then, the peak shear stress is averaged over a distance of  $4d_l$  (where  $d_l$  is the effective depth to the longitudinal reinforcement) and is defined as the governing shear stress [56], and finally is compared to the shear capacity calculated according to NEN-EN 1992-1-1:2005 [4] (First Level of Assessment). The third Level of Assessment deploys non-linear finite element models in order to determine the behaviour of the structure under the assigned live load model [57]. Furthermore, probabilistic methods are also used during this Level of Assessment, since reliability analysis is a useful assessment tool for the identification of the failure mode and also for the preparation and execution of proof load experiments, specifying

which kind of failure should be expected [58]. The fourth and final Level of Assessment is the execution of proof loading on the structure under investigation [59].

For each Level of Assessment, a “Unity Check” is performed and if the result is larger than 1 it should not be concluded immediately that the structure does not have sufficient capacity, but that a higher Level of Assessment has to be used and the analysis has to be repeated. Due to the fact that more sophisticated Levels of Assessment are more time and labor consuming, it is preferred that sufficient accuracy is able to be reached at the lower Levels of Assessment (*Figure 2.3*).

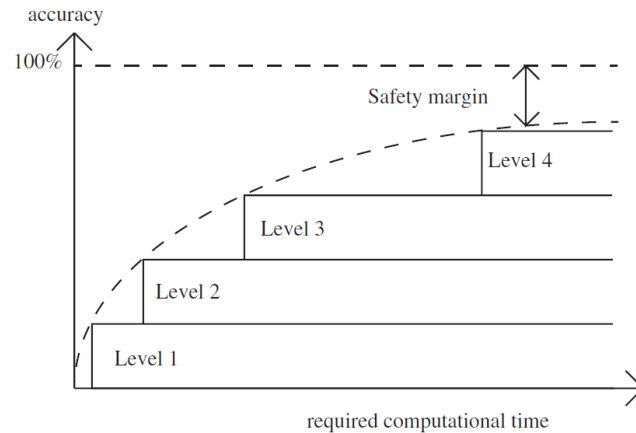


*Figure 2.3: Principle of Levels of Approximation according to Fib Model Code [15]*

Methods based on reliability have been currently considered of great importance for the assessment of reinforced concrete solid slab bridges, resulting in an improvement of the current bridge rating practices [60]. The Probabilistic Model Code, developed by the Joint Committee on Structural Safety (JCSS) [61], specifies the recommended probability density functions of the applied loads, the resistance models and the material models, that should be prescribed in order to determine the probability failure. Due to the aforementioned transverse load distribution that takes place in solid slab bridges, different probability density functions of the resistance model from beams have to be used [7], which can be conservatively approximated based on a lognormal distribution [58].

In the Netherlands, the Dutch Guidelines for the Assessment of Existing Bridges (RBK) [16] are developed according to the philosophy of the Eurocodes, adopting the reliability levels of NEN-EN 1990:2003 [62] and NEN 8700:2011 [63] and allowing more reliability levels. Different safety levels for assessment are defined in these codes with different load factors based on different reliability indices and reference periods. For existing solid slab bridges values for Consequences Class 3 have been considered under the regulations for construction before 2003, because for newer structures there is requirement for higher reliability levels. Reliability indices can also be specified in conformance with the AASHTO Manual of Bridge Evaluation (MBE) [18], which are considerably lower than the corresponding Dutch codes [16].

Moreover, for the evaluation of shear and bending moment capacity in existing bridges, more advanced and detailed probabilistic analyses, including also full probabilistic nonlinear analysis, have been developed in Switzerland [64], in the United States [65] and in Germany [66]. Regarding the safety philosophy for the assessment of solid slab bridges it is important to be

emphasized that, despite the fact that generally three sources of uncertainty are classified, and more specifically the material (mechanical and chemical properties), the fabrication (geometrical properties), and the analysis (approximate method of analysis) [67], in the Netherlands only the material and analysis uncertainties are taken into consideration since the geometric properties of the existing structures are accounted as specified [68].

In particular, in order to determine the probability of shear failure in comparison with the probability of flexural failure, for the load testing of the Ruytenschildt Bridge [69], the concrete compressive strength and the calibration factors of the capacity models were considered as random variables, following a lognormal distribution [58]. It was also observed that the variability on the moment capacity is significantly lower than the variability on the shear capacity and for that reason the use of a Monte Carlo simulation was considered to be vital in order to investigate the probability of a certain failure mode. A limit state function, derived from Unity Checks of the predicted and the experimental capacities, was used for the simulations and after the inclusion of the material and the capacity model uncertainties the probability of failure in bending moment was found to be considerably higher, accurately predicting the actual failure mode of the bridge [40, 30]. After verification of this method with a correct prediction of the failure mode of four additional slab shear experiments, it can be concluded that it can be safely used for future experiments [69].

## 2.4. Seismic evaluation of existing bridges

The amount of research studies regarding the seismic evaluation of concrete bridges in the Netherlands is rather limited. Generally, the main guidelines for the design, detail and retrofitting of structures subjected to earthquakes are laid down in EN 1998-1:2004 [12] and in NPR 9998 [14], where four different methods for the structural analysis are proposed, considering the structural characteristics of the building under investigation (*Figure 2.4*).

The lateral force method of analysis is a linear static analysis, suitable for structures whose response in each principal direction is affected significantly only by its fundamental mode. The modal response spectrum analysis is a linear dynamic method of analysis, which can be performed for all type of structures, when the response of all the modes of vibration contributing significantly to the global response have to be considered, by using the appropriate response spectra as defined in NPR 9998:2017 [14]. In some cases, such as non-base-isolated load bearing structures, the use of nonlinear structural analysis is also justified because it may be proven less conservative. Non-linear static (pushover) analysis, by monotonically increasing the applied loads, can be used in order to assess the structural performance of existing buildings and to verify newly designed structures. Non-linear time-history (dynamic) analysis, where the time-dependent response of the structure is obtained through direct numerical integration of its differential equations of motion, can also be performed in order to evaluate existing structures. In particular for bridges under seismic excitation more details are included in EN 1998-2:2005 [13], where the lateral force method of analysis is subdivided into three approaches, depending on the particular characteristics of the bridge:

1. The rigid deck model, which may only be applied when the deformation of the deck within a horizontal plane is negligible compared to the horizontal displacements of the pier tops.
2. The flexible deck model, which is applied when the abovementioned condition is not satisfied.
3. The individual pier model, which is implemented in cases of seismic action resisted mainly by the piers, with insignificant interaction between adjacent piers of the bridge.

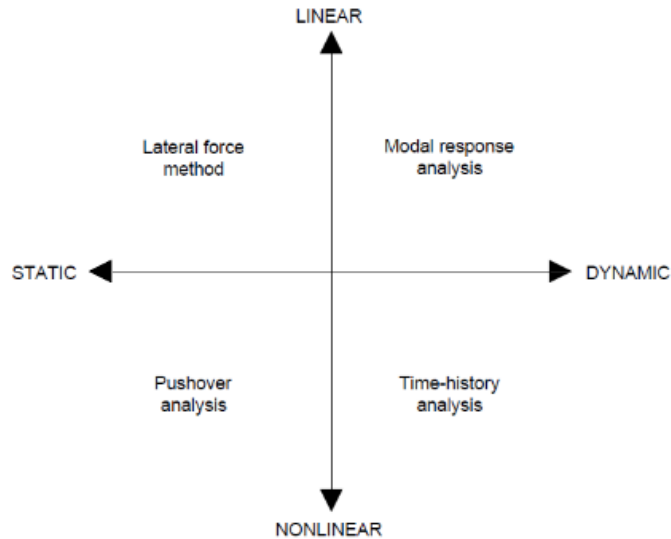


Figure 2.4: Schematization of different methods of structural analysis

Furthermore, researches about the evaluation of existing bridges have been carried out throughout the world. Analytical models were developed in both horizontal directions in order to evaluate eight reinforced concrete bridges located in Ottawa region, in Canada, that were built between 1957 and 1973. They were investigated by using representative seismic excitations (response spectrum analysis and time-history analysis) and their seismic performance was evaluated based on maximum ductility demand, shear demand/capacity ratios and lateral drifts. These results were compared with the performance of newly built reinforced concrete bridge, which had been constructed according to the appropriate specifications for earthquake resistance, and it was concluded that the seismic behaviour of the old bridges was satisfactory [70]. Moreover, seismic evaluation was performed on 14 selected highway bridges in Western Kentucky by using a non-linear time-history response spectrum of an earthquake with a return period of 250 years. Also, a capacity/demand ratio method was used in order to evaluate the main bridge components, such as bearings and piers providing decent results [71]. A non-linear static push-over analysis was used also for the evaluation of an existing 11-span reinforced concrete bridge in Karnataka, India. Additionally, time-history analysis was performed in order to compare the behaviour of an integral and an isolated bridge, concluding that base isolation is an efficient way of reducing the effect of seismic forces on bridges [72].

# 3 Case study description

In this chapter a detailed description of the case study is included. At first, some information about the location of the Nieuwklap bridge and its background are mentioned. Furthermore, the structural plans of the bridge are closely examined in order to define the structural system and the reinforcement layout. The properties of the materials that were used during the bridge construction and then are adopted along this project are also outlined. Finally, a comprehensive description of the collapse load test is performed, in order to understand the usefulness of such a large-scale experiment.

## 3.1. Location and background of the Nieuwklap Bridge

The Nieuwklap bridge is located on the national road N355, the Friesestraatweg, in the province of Groningen, which connects the cities of Groningen and Leeuwarden and more specifically it lies over a canal, the Aduarderdiep, in Nieuwklap. Below the bridge and alongside the canal lies the Nieuwbrugsterweg. The map with the exact location of the bridge (*Figure 3.1*), as well as the location specified by the given drawings (*Figure 3.2*), are depicted on the following figures. Due to its location, in the region of the Groningen gas field, the Nieuwklap bridge is subjected to earthquakes that are caused from the natural gas extraction.

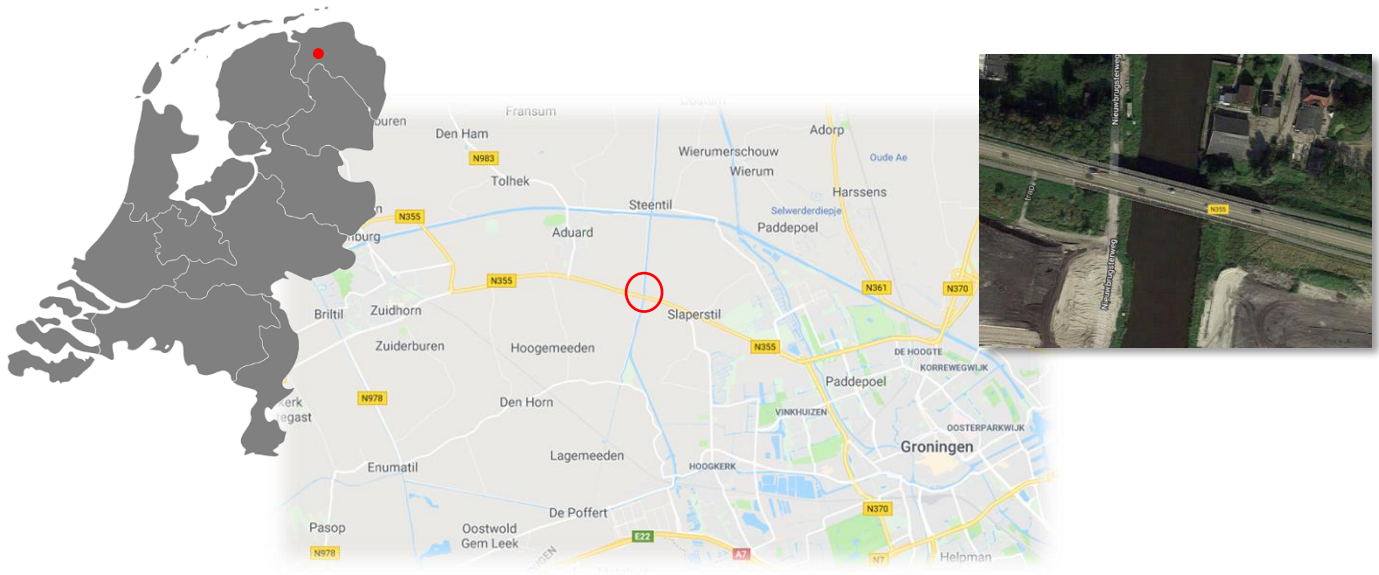


*Figure 3.1: Location of the Nieuwklap bridge*

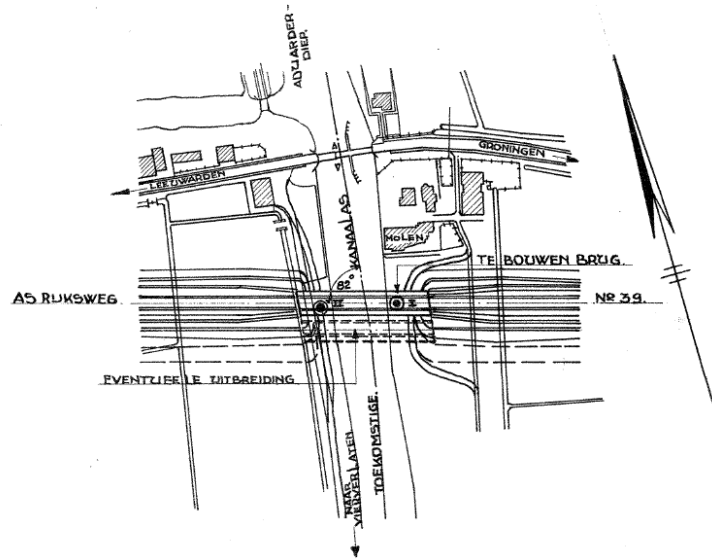


Figure 3.2: Bridge construction location

The bridge was designed in 1937 and was constructed in 1941, in order to replace a swing bridge that was previously used to cross the Aduarderdiep [73]. The initial structural plans depict a five-span bridge, but because of the poor soil conditions it was decided to add two more spans in order to shift the abutments further away from the Aduarderdiep and to achieve better stabilization of the soil. Therefore, a seven-span bridge was finally constructed and its present form can be seen in *Figure 3.3*.



Figure 3.3: South view of the Nieuwklap Bridge

Nowadays the bridge is scheduled for demolition and replacement by a new one, which has been constructed just south of it. In *Figure 3.4* a view of the new bridge under construction alongside the Nieuwklap bridge can be seen.



Figure 3.4: New bridge under construction

## 3.2. Structural system

### 3.2.1. Geometry

According to the structural plans (*Appendix A*), the Nieuwklap Bridge is a reinforced concrete solid slab bridge with a total length of approximately 100.70 m. It consists of seven spans which have a length of 11.20 m and 14.14 m for the end-spans and the mid-spans respectively (*Figure 3.5*). The bridge has a skew angle of  $82^\circ$  and an overview where the spans and the supports are labelled is illustrated below (*Figure 3.6*). The total width of the bridge deck is 14.31 m, consisting of two traffic lanes and two bike lanes. The carriageway, which is also the slab part of the bridge cross-section has approximately 65 cm thickness and has a width of 8.25 m (*Figure 3.7*).

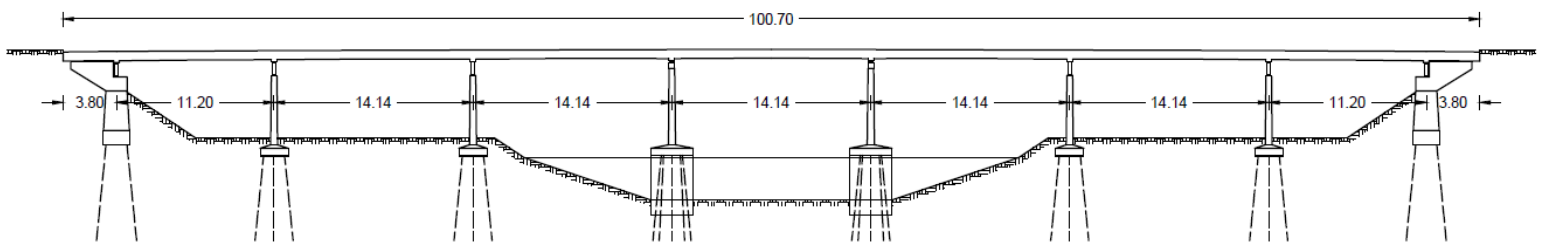


Figure 3.5: Sideview of the Nieuwklap bridge with dimensions (m)

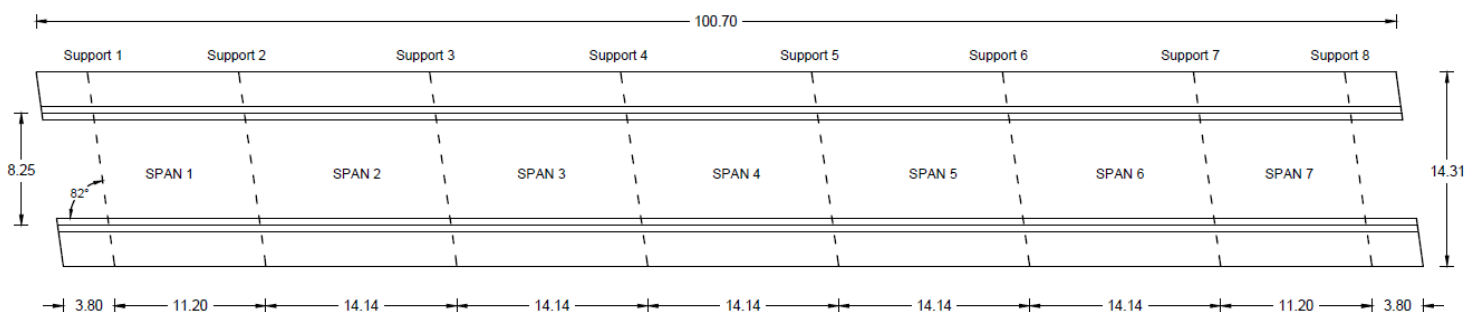


Figure 3.6: Overview of the Nieuwklap bridge with dimensions (m)

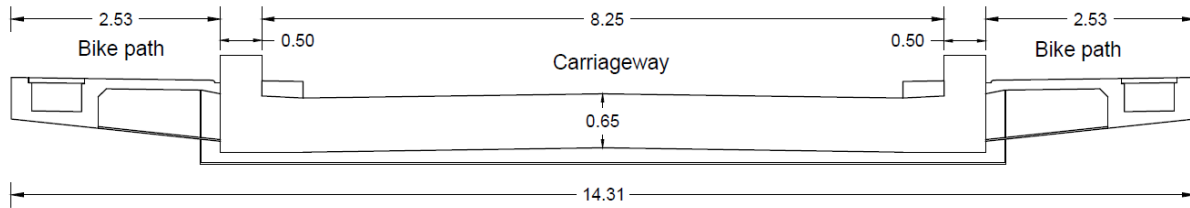


Figure 3.7: Cross-section of the Nieuwklap bridge close to supports with dimensions (m)

The bridge deck is continuous and simply supported to the piers, which are reinforced shear walls (Figure 3.3). More specifically, it is directly rested on piers located at supports 4 and 5 with a formation which allows only rotational movement. Regarding all the other supports, there are seven concrete pendulums of 1 m height between the deck and each of the piers, which can accommodate also horizontal movements, due to expansion or contraction of the bridge deck.

### 3.2.2. Reinforcement layout

The information about the reinforcement layout of the Nieuwklap bridge can only be extracted through the given structural plans (Appendix A), where the reinforcement drawings for the five-span variant are only available. The longitudinal and the transverse reinforcement layout of the deck is available and it was remarked that bent-up bars were used in the longitudinal direction close to supports. Stirrups and curved rods were used in addition for the construction of the bike path and for the longitudinal beam which is present next to the carriageway. The reinforcement layout of the piers and the piles, which were used for the foundation, is also available and all the corresponding drawings are placed in the Appendix A.

Reinforcement layout								
Position		No	Reinforcement	Amount	$\emptyset$ (mm)	Spacing (mm)	$A_s$ (mm <sup>2</sup> /m)	$\rho_l$ (%)
Span 1	Top	21	34 $\emptyset$ 25/240	34	25	240		
		<b>TOTAL</b>	34 $\emptyset$ 25/240	34	25	240	2045	0.32
	Bottom	11	30 $\emptyset$ 25/240	30	25	240		
		12	32 $\emptyset$ 25	32	25	-		
		13	16 $\emptyset$ 25	16	25	-		
14		14 $\emptyset$ 25	14	25	-			
<b>TOTAL</b>	92 $\emptyset$ 25	92	25	80	6136	0.97		
Span 2	Top	21	34 $\emptyset$ 25/240	34	25	240		
		<b>TOTAL</b>	34 $\emptyset$ 25/240	34	25	240	2045	0.33
	Bottom	11	30 $\emptyset$ 25/240	30	25	240		
		15	32 $\emptyset$ 25	32	25	-		
		16	30 $\emptyset$ 25	30	25	-		
<b>TOTAL</b>		92 $\emptyset$ 25	92	25	80	6136	0.99	
Supports	Bottom	11	30 $\emptyset$ 25/240	30	25	240		
		<b>TOTAL</b>	30 $\emptyset$ 25/240	30	25	240	2045	0.31
	Top	21	34 $\emptyset$ 25/240	34	25	240		
		19	30 $\emptyset$ 25/240	30	25	240		
		22	34 $\emptyset$ 25	34	25	-		
23		36 $\emptyset$ 25	36	25	-			
<b>TOTAL</b>	134 $\emptyset$ 25	134	25	65	7552	1.16		

Table 3.1: Longitudinal reinforcement layout for Span 1, Span 2 and over the Supports

The layout of the longitudinal reinforcement of the Spans 1 and 2 and over the supports is examined carefully, since it will be used for the static analysis. In *Table 3.1* the label, the amount of the reinforcement bars and their diameter are depicted according to the structural plans. Furthermore, the total reinforcement steel area per meter as well as the reinforcement percentage is included for the three abovementioned positions for the top and bottom of the concrete slab.

### 3.3. Material properties

#### 3.3.1. Concrete

According to the given concrete composition, initially it has been supposed that concrete with strength class B45 had been used [73]. In order to accurately determine the compressive and the tensile strength of the concrete that was used for the construction of the Nieuwklap bridge, cores have been drilled from the concrete deck and were tested in the laboratory.

The average concrete compressive strength was found to be approximately 80 MPa and the corresponding cylinder compressive strength is then around 70 MPa. Thus, the characteristic value based on the drilled cores can be estimated at 60 MPa. Additionally, considering the ratio between the compressive and the tensile strength it can be expected a mean tensile strength of 4.36 MPa [73].

Accounting the abovementioned results and the recommendations from Rijkswaterstaat [57] regarding the material properties of concrete, the adopted values that are used in the present project are detailed in *Table 3.2*.

Concrete		
Characteristic compressive strength	$f_{ck,cube}$ (MPa)	60
	$f_{ck}$ (MPa)	50
Mean compressive strength	$f_{cm,cube}$ (MPa)	80
	$f_{cm}$ (MPa)	70
Design compressive strength	$f_{cd,cube}$ (MPa)	40
	$f_{cd}$ (MPa)	33.33
Mean tensile strength	$f_{ctm}$ (MPa)	4.36
Min. characteristic tensile strength	$f_{ctk,min}$ (MPa)	3.05
Design tensile strength	$f_{ctd}$ (MPa)	2.035
Young's Modulus	$E_c$ (MPa)	31570
Partial factor	$\gamma_c$ (-)	1.5
Specific weight	$\gamma$ (kN/m <sup>3</sup> )	25
Poisson's ratio	$\nu$ (-)	0.15

*Table 3.2: Material properties of concrete*

#### 3.3.2. Reinforcement steel

Samples from the Nieuwklap bridge regarding the reinforcement were not available at the beginning of this project, for that reason its properties had been assumed and estimated from samples that were measured from similar structures that were built the same period [30]. It is supposed that for the reinforcement, plain bars of QR22 steel grade had been used during

construction and the corresponding value for the yield strength is used for the calculations. In order to find the average value of the yield strength, the characteristic value can be multiplied by 1.1 [73]. Eventually, the assumed mean yielding strength of the reinforcement was confirmed by laboratory tests. The material properties of the reinforcement are summarized in *Table 3.3*.

Reinforcement steel (QR22)		
Characteristic yielding strength	$f_{yk}$ (MPa)	220
Mean yielding strength	$f_{ym}$ (MPa)	242
Design yielding strength	$f_{yd}$ (MPa)	191
Mean ultimate strength	$f_{tm}$ (MPa)	330
Design ultimate strength	$f_{td}$ (MPa)	287
Young's Modulus	$E_s$ (MPa)	200000
Partial factor	$\gamma_s$ (-)	1.15
Specific weight	$\gamma$ (kN/m <sup>3</sup> )	78.5
Poisson's ratio	$\nu$ (-)	0.3

*Table 3.3: Material properties of reinforcement steel*

### 3.4. Load test

Since the Nieuwklap bridge is planned to be replaced, the opportunity arises to carry out a collapse load test. In case that the bridge is found to be shear-critical during the preparation, this test will provide us information in order to determine the actual capacity and the failure mode of the Nieuwklap bridge as well as of similar reinforced concrete slab bridges, which constitute a significant percentage of the existing bridges in the Netherlands.

In order to achieve the abovementioned goals a load testing until the bridge collapses is required. For that reason, the load test should be performed on the critical positions for bending moment failure, by yielding of the reinforcement, and for shear failure. The tests should be performed on both spans 1 and 2, in order to consider also the effect of the bending moment over a continuous support [73]. Furthermore, due to the presence of reinforced concrete beams along the bridge, between the carriageway and the cantilever parts, the shear capacity is expected to be significantly larger, since the beams contain shear reinforcement and the compressive zone is additionally increased. In order to eliminate the additional shear contribution of these side-beams and to be able to achieve failure of the bridge, before the execution of the experiment, a saw cut has to be made in a longitudinal way in the one side of the deck, so that only the shear capacity and the behaviour of the slab part will be studied as depicted in *Figure 3.8*.



*Figure 3.8: Cross-section of the bridge with the position of the saw cut*

In case that, after these modifications, the Nieuwklap bridge does not collapse in shear, even when it is loaded on a shear critical position, it may become possible to formulate a statement

about the failure mode of reinforced concrete solid slab bridges with plain reinforcement, which are found to be shear-critical according to the current standards but their actual shear capacity can be greater thanks to additional transfer mechanisms, that the present codes do not take into account.

Moreover, by performing this load test, the proposed stop criteria and the field load method used for this type of bridges can be reevaluated. Suitable measurements during the application of the failure loading can be analyzed and validate the proposed proof load methods and stop criteria, since their safety margin can be inspected by using several load levels in the load protocol. In this way, the margin will be easily determined by comparing the applied load at which a stop criterion is exceeded and the maximum load that failure occurs.



# 4 Static analysis - Analytical approach

In this Chapter, a detailed description of the analytical approach that is applied for the static analysis at the Nieuwklap bridge, will take place.

Initially, the assumptions that have been considered for the construction of the analytical model are listed. Then, the loading cases are displayed, by an extensive description of the Eurocode loading specified for bridges [3] and the field loading that will be applied during the experimental procedure. The loading combinations according to RBK [16] and the investigated loading positions are also presented, along with the shear force spreading considerations for concentrated loads, that have to be taken into account.

Afterwards, the bending moment capacity of the bridge deck at several limit states (cracking, yielding, ULS) and the shear capacity at the ultimate limit state, by using two approaches, for the characteristic and the mean values of the material properties are calculated.

Consequently, the shear and bending moment stresses generated by Eurocode loading are obtained and a “Unity Check” is performed, in order to evaluate the resistance of the Nieuwklap bridge on the most critical positions for shear and flexure. By comparing the obtained values, a first prediction about the bridge failure mode can be substantiated.

The equivalent magnitude of the proof load tandems that generate the same stresses as the current standards are calculated next, in order to examine the structure for several load combination levels.

Finally, the maximum field load tandems that lead to shear and flexural failure are determined, by including also the magnitudes that required for crack formation of concrete and yielding of the reinforcement. This process will provide us with a better understanding of the bridge behaviour under field loading and a legitimate statement regarding the expected failure mode can be made.

## 4.1. Assumptions

### 4.1.1. Analytical model

A structural model always constitutes an approximation of reality. For that reason, the assumptions that have been adopted for the present analytical model should be mentioned and justified thoroughly. These simplifications are essential in order to reduce the computational time without altering significantly the nature of the real problem.

In the present analytical model, it is assumed that the deck of the Nieuwklap bridge can be represented as a continuous beam, since the total length of the structure is larger than the other two dimensions. The width of the beam assumed to be identical to the width of the carriageway part of the deck (*Figure 3.7*), in order to include only the reinforced concrete solid slab element, and the height is considered constant over the whole length of the bridge equal to 650 mm.

Regarding the supports of the analytical model, an idealization is assumed to be really important. As it was described in the previous chapter, the supports 4 and 5 can be regarded as hinges, since only rotational movement is permitted and at all the other locations sliding supports are placed, because of the presence of concrete pendulums which allow horizontal movement in longitudinal direction. Due to the fact that the loading that will be applied is non-symmetrical it is not possible to make further simplifications by applying symmetry conditions. A schematization of the analytical model is illustrated in *Figure 4.1*.



*Figure 4.1: Simplified mechanical scheme of the Nieuwklap bridge*

The characteristic and the mean material properties that are used for the analytical calculations have been specified through experimental testing on drilled cores and according to the recommendations from Rijkswaterstaat [57], and they have been already defined in Chapter 3 (*Table 3.2, Table 3.3*).

Furthermore, some constitutive conventions that are important in association with the simplified beam model and according to NEN-EN 1992-2:2005 [74] should be mentioned at this point. The cross-section of the beam model remains plane during bending and the strain is linearly distributed over its height. The strain of the bonded reinforcement is always the same as the of the concrete at the same level. The compressive strength of the reinforcement is ignored and its stresses, as well as the stresses of concrete, are given by stress-strain relationships. Finally, the properties of the beam are assumed to be constant and not influenced by the possible presence of weak spots on the real structure, due to material deterioration.

#### 4.1.2. Loading

For the analytical approach two types of loading have been applied on the beam model on the most unfavorable positions for shear and flexural failure. Both of these loading types and the way that they have been are described extensively in this paragraph.

At first, in order to determine if the Nieuwklap bridge is able to resist the design loads according to NEN-EN 1991-2:2003 [3], traffic loading (LL) as described by Load Model 1 (*Figure 4.2*) has been used, which is suitable for general and local verifications, simultaneously with the dead load, due to the self-weight (SW) of the bridge and the present asphalt loading (SD).

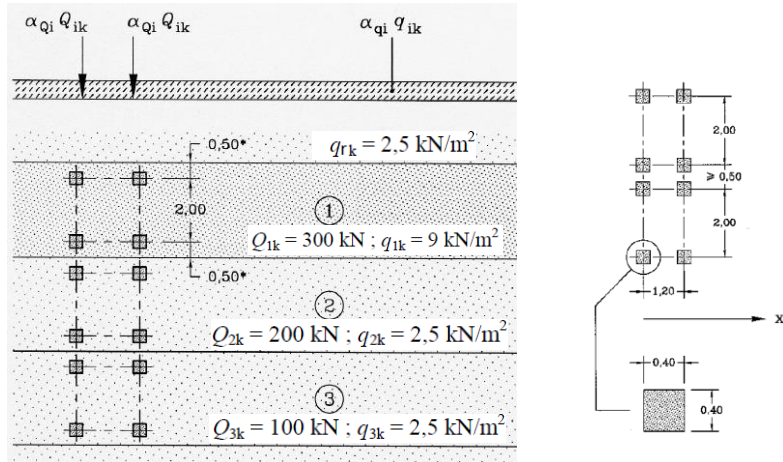


Figure 4.2: Load Model 1 for normal traffic loading [3]

The Load Model 1 consists of two partial systems, the double-axle concentrated loads, which are called tandem system (TS), and the uniformly distributed loads (UDL) on each notional lane and the remaining area. The notional lanes have been defined again according to the Eurocode and it has occurred that the deck consists of two notional lanes of 3 m width and a remaining area of  $w_r = 1.25$  m width. The adjustment factors for the abovementioned systems are taken equal to 1, since the number of heavy lorries is not specified for the project and the carriageway consists of two notional lanes [3].

The loading is applied by representing the loads that are acting on the deck surface as distributed loads and the tandem system of LM1 is represented as point loads. For the asphalt loading it was assumed an asphalt layer of 12 cm thickness and with specific weight  $\gamma_{asph} = 23$  kN/m<sup>3</sup>. The acting loads on the beam model according to the standards can easily be defined by the procedure described below and the results are listed in Table 4.1.

$$\begin{aligned}
 SW &= A_c \cdot \gamma_c \text{ [kN/m]} \\
 SD &= w_{slab} \cdot t_{asph} \cdot \gamma_{asph} \text{ [kN/m]} \\
 UDL &= w_1 \cdot q_1 + w_2 \cdot q_2 + w_r \cdot q_r \text{ [kN/m]} \\
 TS &= 2 \cdot (Q_1 + Q_2) \text{ [kN]}
 \end{aligned}
 \tag{4.1}$$

Loads		
Selfweight	SW (kN/m)	134
Asphalt	SD (kN/m)	20
Traffic loading	UDL (kN/m)	37.625
	TS (kN)	2 · 500

Table 4.1: Acting loads on beam model

These load cases have been combined and the load combinations that will be investigated are defined in accordance with the RBK [16].

- Design:  $U = 1.25 \cdot SW + 1.25 \cdot SD + 1.50 \cdot LL$
- Reconstruction:  $U = 1.15 \cdot SW + 1.15 \cdot SD + 1.30 \cdot LL$
- Usage:  $U = 1.15 \cdot SW + 1.15 \cdot SD + 1.25 \cdot LL$
- Disapproval:  $U = 1.10 \cdot SW + 1.10 \cdot SD + 1.25 \cdot LL$

Then, in the interest of describing the field loading that will be exerted on the bridge during the experimental procedure, a load combination that replicates satisfactory the proof load test has been employed. In this case, the loads that have been applied on the model consist of the self-weight (SW) of the bridge, the asphalt loading (SD) and the four concentrated loads of the proof loading experiment (PL).

The main difference that has been adopted, is that the factors for this loading type have been taken equal to 1, since the unknown factors that cause uncertainties have not be considered. For that reason, there is one load combination for this case.

Proof load combination:  $U = SW + SD + PL$

Nevertheless, since the equivalent proof load tandems, which generate the same stresses as the Eurocode loading, needs to be specified, the magnitude of proof loading required in order to test every load combination level has to defined.

- Design:  $PL = 0.25 \cdot SW + 0.25 \cdot SD + 1.50 \cdot LL$
- Reconstruction:  $PL = 0.15 \cdot SW + 0.15 \cdot SD + 1.30 \cdot LL$
- Usage:  $PL = 0.15 \cdot SW + 0.15 \cdot SD + 1.25 \cdot LL$
- Disapproval:  $PL = 0.10 \cdot SW + 0.10 \cdot SD + 1.25 \cdot LL$

Finally, due to the fact that the capacity of the Nieuwklap bridge has to be examined during the execution of the collapse load test, the equivalent failure load tandems (FL) have to be defined by considering the mean material properties. For this loading type the factors have been taken again equal to 1.

Failure load combination:  $\text{Mean Capacity} = SW + SD + FL$

All the above-mentioned load combinations include concentrated loads, acting on the bridge deck, which have to be placed on the most unfavorable positions for shear and flexure in order to check the resistance of the Nieuwklap bridge. Regarding the bending moment, the most critical position of the concentrated loads can be found by shifting the loads across the spans until they generate the maximum bending moment. For concrete slabs bridges with constant height and without variation of the reinforcement the critical position for shear force is at a distance  $2.5d_1$  from the edge of the supports [73]. At this point is important to be repeated that in the Nieuwklap bridge bent-up bars close to supports had been used during construction, which means that the shear critical position could be further away from the support and closer to the mid-span, however in favor of the research purpose of the present project their influence will be omitted.

The loading has been applied on both spans 1 and 2, in order to consider also the effect of the bending moment over a continuous support. The 6 discrete loading positions (LP) that were chosen are depicted with labels in *Figure 4.3*. In detail, LP1 and LP2 are the critical positions for flexure for Span 1 and Span 2 respectively, placed on a specific distance from the supports, expressed in span length, and are defined as stated above where the maximum bending moment occurs by shifting the concentrated loads across the spans. LP3 and LP4 are the shear critical positions for Span 1, at a distance  $2.5d_i$  from Support 1 and 2 respectively. At last, LP5 and LP6 are the shear critical positions for Span 2, at a distance  $2.5d_i$  from Support 2 and 3 respectively. All the possible variants for these two spans can be examined for shear and bending moment resistance.

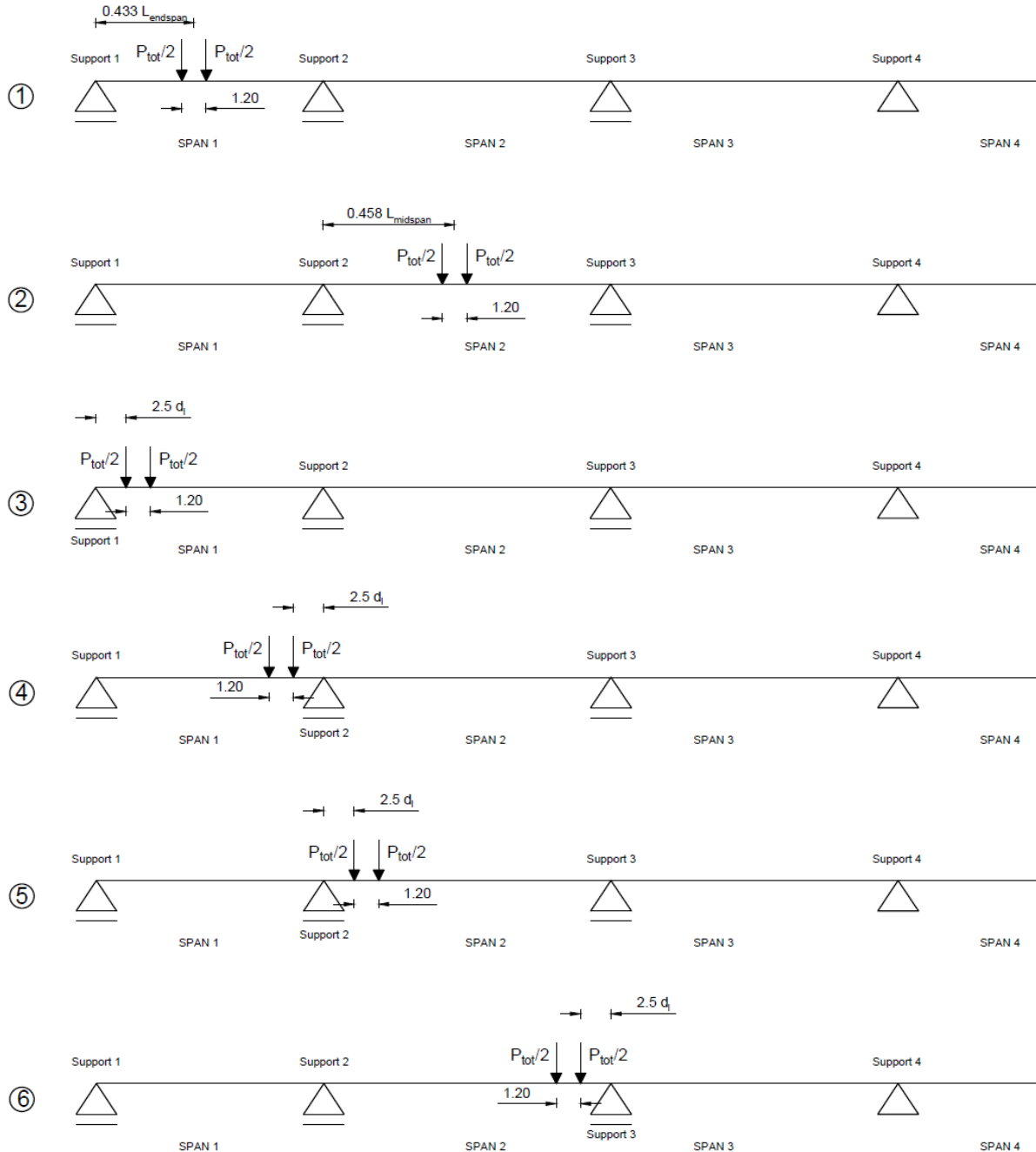


Figure 4.3: Loading positions of the concentrated loads

As mentioned before in this paragraph, all the loading types include concentrated loads, which means that the effective width of these loads over the supports needs to be defined. For the determination of these effective width the French approach was adopted, which considers a horizontal load spreading under a 45° angle from the far corners of the loading plates towards the support. However, since the Nieuwklap bridge has a skew angle of 82°, three different approaches were implemented in order to specify the effective width and the obtained values are depicted in *Figure 4.4*. The first approach is similar to the one performed for straight slabs, the second one applies the same principle of a 45° horizontal load spreading from the far corners of the loading plates, but for a skewed slab, and the third one defines the effective width based on a load spreading parallel to the straight case.

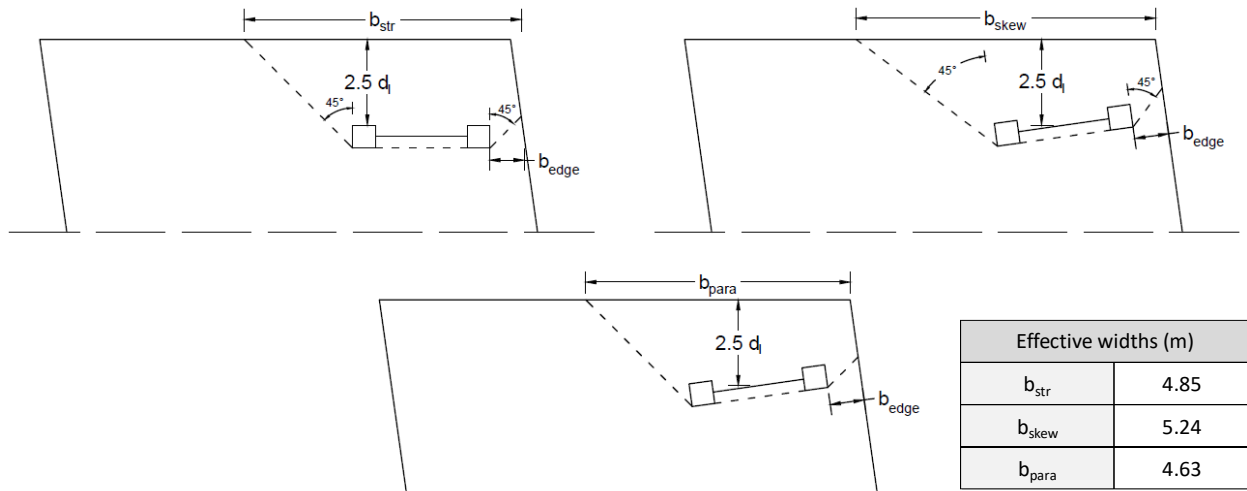


Figure 4.4: Different approaches for the determination and values of the effective width for skewed slabs

More specifically, for the Eurocode loading, the total width of the concrete deck has been considered as effective width, due to the fact that the deck has limited wideness and with all the above-mentioned approaches nearly its whole width found to be effective (*Figure 4.5*). For the estimation of the equivalent proof loading only the second approach has been practiced, but for the determination of the failure load all the three approaches have been considered, assuming that the second axle has the same effective width as the first one.

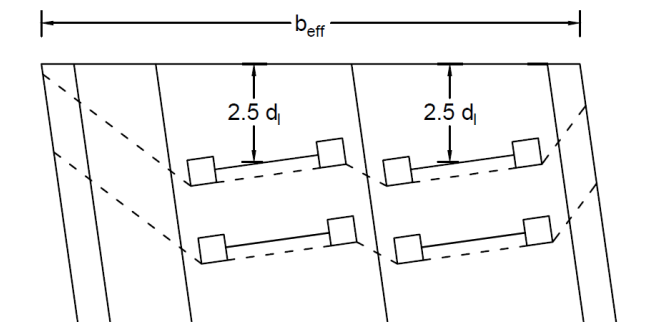


Figure 4.5: Effective width of the Tandem system of LM1

Finally, it is of great significance to explain how the concentrated loads contribute to the generation of stresses on a concrete slab. A safe assumption that can be made is that these stresses, caused by a concentrated load and are distributed over a certain effective width can be

added to the generated stresses caused by a distributed load using the principle of superposition [7] (Figure 4.6).

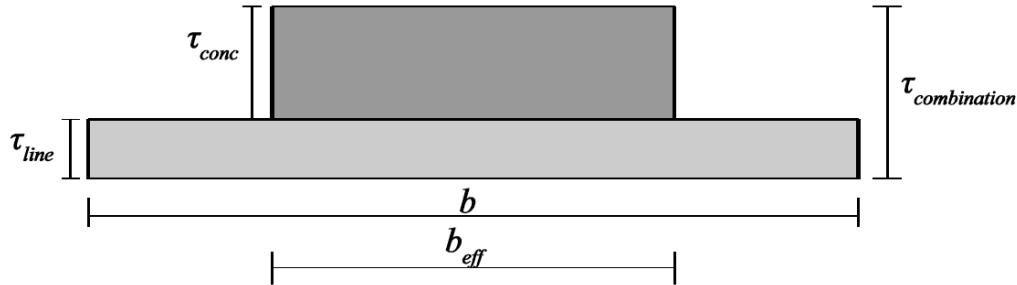


Figure 4.6: Superposition of shear stress due to a concentrated load over the effective width with the distributed load over the full slab width

### 4.1.3. Capacity

For the specification of the capacity of the Nieuwklap bridge the bending moment and resistance of the concrete slab cross-section at various limit states and the shear resistance at the ultimate limit state (ULS) need to be derived. The capacities are defined per meter width, since the stresses caused by the acting load combinations have been considered in the same manner.

Regarding the bending moment capacity, in order to develop a moment-curvature diagram, a subdivision into the moment at cracking, yielding of the longitudinal reinforcement and the ultimate bending moment at ULS are calculated [73], based on traditional beam analysis for both the characteristic and the mean values of the materials (Table 3.2, Table 3.3) and by taking into account the assumptions mentioned previously in this chapter. The procedure carried out for Span 1, Span 2 and over the supports, since the effective depth of the longitudinal reinforcement is different for each occasion.

The cracking moment capacity has been determined as:

$$M_{cr} = f_r \cdot \frac{I_{gross}}{(h_{slab} - c_{cr}) \cdot b} \text{ [kNm/m]} \quad (4.2)$$

where,

$$f_r = \frac{7.5}{12} \cdot \sqrt{f_c} \text{ [MPa]} \quad (4.3)$$

And the corresponding curvature is:

$$\kappa_{cr} = \frac{\varepsilon_{cr}}{h_{slab} - c_{cr}} \text{ [1/mm]} \quad (4.4)$$

The moment capacity at yielding, is based on the stress-strain diagram for concrete as specified by Thorenfeldt's parabola (Figure 4.7).

$$M_y = \beta_1 \cdot f_{c,th} \cdot c_y \cdot (d_l - k_2 \cdot c_y) \text{ [kNm/m]} \quad (4.5)$$

The formulas for the calculations of the parameters defined by Thorenfeldt, which were used during this procedure are presented analytically:

$$k_2 = 1 - 2 \cdot \frac{\varepsilon_c/\varepsilon_0 - \arctan(\varepsilon_c/\varepsilon_0)}{(\varepsilon_c/\varepsilon_0)^2 \cdot \beta_1} \quad (4.6)$$

$$\beta_1 = \frac{\ln[1 + (\varepsilon_c/\varepsilon_0)^2]}{\varepsilon_c/\varepsilon_0} \quad (4.7)$$

$$\varepsilon_0 = \frac{f_c}{E_c} \cdot \left( \frac{n_{th}}{n_{th} - 1} \right) \quad (4.8)$$

$$n_{th} = 0.8 + \frac{f_c}{17} \quad (4.9)$$

Thus, the concrete stress according to Thorenfeldt's parabola is:

$$f_{c,th} = \frac{0.9 \cdot f_c \cdot n_{th} \cdot \varepsilon_c/\varepsilon_0}{n_{th} - 1 + (\varepsilon_c/\varepsilon_0)^{n_{th}}} \text{ [MPa]} \quad (4.10)$$

And the corresponding curvature:

$$\kappa_y = \frac{\varepsilon_{sy}}{d_l - c_y} \text{ [1/mm]} \quad (4.11)$$

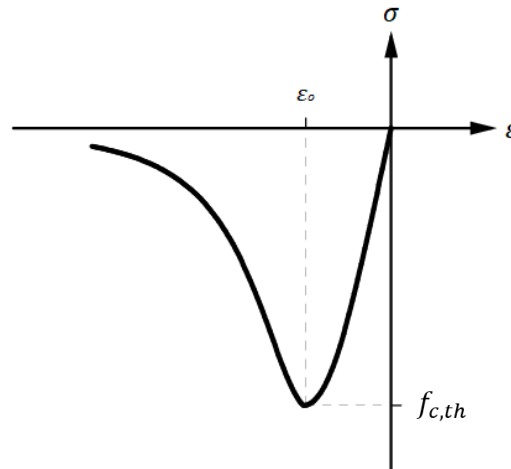


Figure 4.7: Thorenfeldt's stress-strain parabola

The ultimate bending moment is calculated based on a rectangular stress block diagram (Figure 4.8) without taking into account the compressive strength of the reinforcement.

$$M_u = 0.85 \cdot f_c \cdot \beta_{ult} \cdot c_{ult} \cdot \left( d_l - \frac{\beta_{ult} \cdot c_{ult}}{2} \right) \text{ [kNm/m]} \quad (4.12)$$

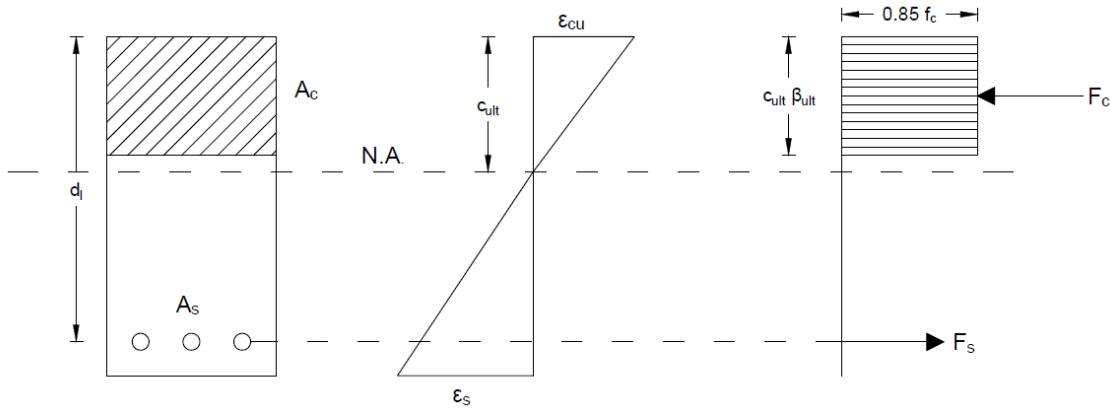


Figure 4.8: Simplified concrete stress block

The corresponding curvature is calculated also:

$$\kappa_{ult} = \frac{\epsilon_{cu}}{c_{ult}} [1/mm], \text{ where } \epsilon_{cu} = 0.003 \tag{4.13}$$

The results obtained from the previously displayed procedure are summarized in *Table 4.2* for both the characteristic and the mean material properties (*Table 3.2, Table 3.3*) and for all the positions that will be examined, including also the different parameters that used for each position. Moreover, the moment-curvature diagrams are presented in *Figure 4.9*.

Bending Moment Capacity				
Input				
Parameters		Span 1	Span 2	Supports
Total slab height	$h_{slab}$ (mm)	631	620	650
Effective depth	$d_l$ (mm)	586	575	605
Reinforcement area	$A_s$ (mm <sup>2</sup> /m)	6136	6136	7552
Characteristic material properties				
Position		Span 1	Span 2	Supports
Cracking moment capacity	$M_{crd}$ (kNm/m)	244.67	236.27	257.98
Yielding moment capacity	$M_{yd}$ (kNm/m)	599.39	587.54	755.68
Ultimate moment capacity	$M_{ud}$ (kNm/m)	663.55	650.64	837.22
Mean material properties				
Position		Span 1	Span 2	Supports
Cracking moment capacity	$M_{crm}$ (kNm/m)	354.56	342.39	373.85
Yielding moment capacity	$M_{ym}$ (kNm/m)	752.42	737.57	949.70
Ultimate moment capacity	$M_{um}$ (kNm/m)	851.62	835.29	1077.61

Table 4.2: Bending moment capacity

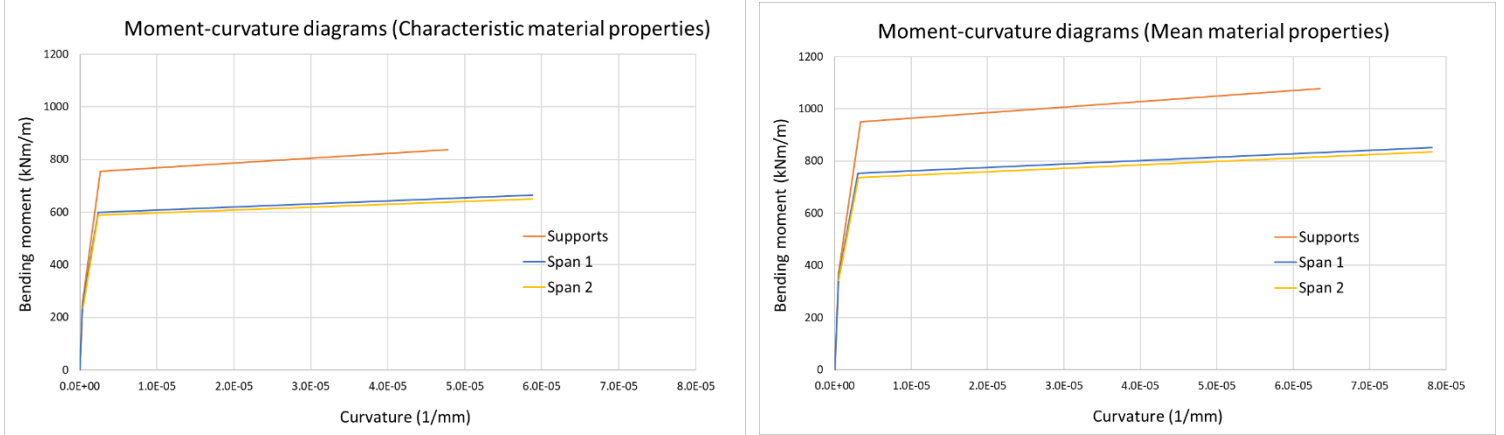


Figure 4.9: Moment-curvature ( $M$ - $\kappa$ ) diagrams for characteristic and mean material properties

The shear capacity of the Nieuwklap bridge at ULS is calculated according to NEN-EN 1992-1-1:2005 [4], for members without shear reinforcement not subjected to axial force, for the shear critical position and, likewise the flexural resistance, for the characteristic and the mean values of the material properties. The default value of the calibration factor according to Eurocode procedures is  $C_{Rd,c} = 0.18/\gamma_c$  and for the calculation with the mean material properties it can be taken as  $C_{Rm,c} = 0.15$  [38].

Therefore, the shear capacity of the concrete slab is obtained:

$$V_{R,c} = C_{R,c} \cdot k \cdot (100 \cdot \rho_l \cdot f_c)^{1/3} \cdot d_l \geq v_{min} \cdot d_l \quad [kN/m] \quad (4.14)$$

where,

$$v_{min} = 1.08 \cdot k^{3/2} \cdot \left(\frac{f_c}{f_y}\right)^{1/2} \quad [MPa] \quad (4.15)$$

and

$$k = 1 + \sqrt{d_l/200} \leq 2.0 \quad (4.16)$$

As it can be noticed, for the determination of the lower bound of the shear capacity, at which flexural failure will start to govern, a different formula is used, because it includes also the steel strength of the reinforcement which is omitted in Eurocode 2, because it assumes a yield strength of approximately 500 MPa. In our occasion, it is of great importance, since the reinforcement that had been used for the Nieuwklap bridge has significantly lower strength than the steel grades that are used nowadays to consider also this parameter in the calculations.

Furthermore, in order to consider the effect of parameters, that are omitted in the empirical code equations due to simplifications, but are activated in reinforced concrete slabs, the shear capacity is recalculated. For this procedure, a shear formula which has been proposed for the extension of the Eurocode, for concrete slabs under concentrated loads close to supports will be used [17]. For the determination of this formula, a series of experiments on concrete slabs have been carried out and by using Monte Carlo simulations, an effort for the quantification of the increase of the shear capacity, that has been observed due to transverse load redistribution, has been made. An enhancement factor was found, as a result of the comparison of the code formula and the

experiments, considering the concrete compressive strength and the ratio between the experimental and the predicted capacity as random variables. The proposed formula, that allows greater shear stresses in concrete slabs is:

$$V_{R,c,prop} = C_{R,c} \cdot k \cdot (100 \cdot \rho_l \cdot f_c)^{\frac{1}{3}} \cdot \left(1.9 - \frac{f_c}{225}\right) \cdot 0.5 \cdot \left(\frac{l_{sup}}{b} + 1\right) \cdot d_l \geq v_{min} \cdot d_l [kN/m] \quad (4.17)$$

where, the supported length is considered:

$$l_{sup} = \sum_{i=1}^{n_{bearings}} l_{bearings,i} \quad (4.18)$$

The summarized results, that have been obtained from the calculation of the shear capacity with both the abovementioned formulas are included in *Table 4.3*, including the corresponding parameters. It can be observed that, regardless the use of either the characteristic or the mean values for the material properties (*Table 3.2*, *Table 3.3*), when the shear formula instructed by the Eurocode 2 is used, the value of the lower bound of the shear capacity is decisive due to low yield strength of the reinforcement. On the other hand, when the proposed formula for concrete slabs under concentrated loads is applied, the reinforcement yield strength is no longer the determinant factor.

Shear Capacity			
Parameters		Eurocode 2 (4.14)	Proposal for slabs (4.17)
Effective depth	$d_l$ (mm)	605	605
Reinforcement ratio	$\rho_l$ (%)	1.16	1.16
Supported length	$l_{sup}$ (mm)	-	7 · 700
Characteristic material properties			
Formula		Eurocode 2 (4.14)	Proposal for slabs (4.17)
Design shear stress capacity	$v_{Rd,c}$ (MPa)	0.793	1.060
Minimum shear stress capacity	$v_{min}$ (MPa)	1.018	1.018
Design shear capacity	$V_{Rd,c}$ (kN/m)	615.68	641.38
Mean material properties			
Formula		Eurocode 2 (4.14)	Proposal for slabs (4.17)
Average shear stress capacity	$v_{Rm,c}$ (MPa)	1.109	1.404
Minimum shear stress capacity	$v_{min}$ (MPa)	1.148	1.148
Average shear capacity	$V_{Rm,c}$ (kN/m)	694.58	849.37

Table 4.3: Shear capacity

## 4.2. Results

In order to facilitate the calculations of the sectional forces and moments for the continuous beam model the use of the structural software SAP2000 was considered essential. The model was constructed according to the specifications and assumptions mentioned in *Paragraph 4.1.1*.

### 4.2.1. Eurocode loading

The resulted sectional forces and moments, from Eurocode loading application have been averaged along the whole width of the concrete slab, even for the Tandem system (*Figure 4.5*), considering that the whole bridge deck is effective under this type of loading, since the tandems have been placed next to each other. The results for shear ( $V_{Ed}$ ), hogging ( $M_{Ed,sup}$ ) and sagging bending moment ( $M_{Ed,span}$ ) are summarized in *Table 4.4* for all the examined loading positions and load combinations described in *Paragraph 4.1.2*.

EUROCODE LOADING						
LOADING POSITION	1	2	3	4	5	6
	FLEXURE CRITICAL			SHEAR CRITICAL		
<b>DESIGN</b>						
<b>LOAD = 1.25*SW + 1.25*SD + 1.50*(UDL + TS)</b>						
$M_{Ed,span}$ (kNm/m)	634.56	641.03	497.48	361.89	352.02	351.61
$M_{Ed,sup}$ (kNm/m)	-658.12	-708.69	-576.01	-619.71	-636.75	-647.56
$V_{Ed}$ (kN/m)	306.58	-312.99	-265.34	372.14	-373.20	374.91
<b>RECONSTRUCTION</b>						
<b>LOAD = 1.15*SW + 1.15*SD + 1.30*(UDL + TS)</b>						
$M_{Ed,span}$ (kNm/m)	560.70	566.16	440.59	323.89	315.32	315.15
$M_{Ed,sup}$ (kNm/m)	-590.53	-634.36	-519.37	-557.24	-572.02	-582.11
$V_{Ed}$ (kN/m)	274.47	-280.01	-235.13	331.30	-332.19	333.78
<b>USAGE</b>						
<b>LOAD = 1.15*SW + 1.15*SD + 1.25*(UDL + TS)</b>						
$M_{Ed,span}$ (kNm/m)	546.27	551.41	429.90	318.31	309.99	309.94
$M_{Ed,sup}$ (kNm/m)	-581.20	-623.34	-512.77	-549.19	-563.39	-573.59
$V_{Ed}$ (kN/m)	269.74	-275.04	-229.52	324.37	-325.22	326.81
<b>DISAPPROVAL</b>						
<b>LOAD = 1.10*SW + 1.10*SD + 1.25*(UDL + TS)</b>						
$M_{Ed,span}$ (kNm/m)	538.21	543.47	422.82	310.55	302.31	302.13
$M_{Ed,sup}$ (kNm/m)	-566.08	-608.22	-497.65	-534.07	-548.27	-557.92
$V_{Ed}$ (kN/m)	263.16	-268.48	-225.64	317.79	-318.65	320.17

*Table 4.4: Sectional forces and moments - Eurocode loading - Analytical approach*

It can be observed that, as expected, for the flexure critical loading positions the generated bending moments are larger and the shear forces are smaller than the corresponding ones that occur for the shear-critical loading positions. This observation is valid for all cases except for LP3, which is a shear-critical position, but is located next to the end-support of the beam. For this case the shear forces are quite smaller even from the flexure critical positions and the sagging bending moment is much higher in comparison to the other three shear critical positions, which are placed next to a continuous support.

Afterwards, a “Unity Check” has been performed, which is a ratio of the stresses caused by the applied loads to the corresponding capacity of the structure, identifying if the bridge can withstand the design loads (*Table 4.5*).

UNITY CHECKS						
LOADING POSITION	1	2	3	4	5	6
	FLEXURE CRITICAL			SHEAR CRITICAL		
<b>DESIGN</b>						
<b>UNITY CHECK (LOAD/DESIGN CAPACITY)</b>						
$UC_{M,span}$	0.96	0.99	0.75	0.55	0.54	0.54
$UC_{M,sup}$	0.79	0.85	0.69	0.74	0.76	0.77
$UC_{V,EC}$	0.50	0.51	0.43	0.60	0.61	0.61
$UC_{V,prop}$	0.48	0.49	0.41	0.58	0.58	0.58
<b>RECONSTRUCTION</b>						
<b>UNITY CHECK (LOAD/DESIGN CAPACITY)</b>						
$UC_{M,span}$	0.85	0.87	0.66	0.49	0.48	0.48
$UC_{M,sup}$	0.71	0.76	0.62	0.67	0.68	0.70
$UC_{V,EC}$	0.45	0.45	0.38	0.54	0.54	0.54
$UC_{V,prop}$	0.43	0.44	0.37	0.52	0.52	0.52
<b>USAGE</b>						
<b>UNITY CHECK (LOAD/DESIGN CAPACITY)</b>						
$UC_{M,span}$	0.82	0.85	0.65	0.48	0.48	0.48
$UC_{M,sup}$	0.69	0.74	0.61	0.66	0.67	0.69
$UC_{V,EC}$	0.44	0.45	0.37	0.53	0.53	0.53
$UC_{V,prop}$	0.42	0.43	0.36	0.51	0.51	0.51
<b>DISAPPROVAL</b>						
<b>UNITY CHECK (LOAD/DESIGN CAPACITY)</b>						
$UC_{M,span}$	0.81	0.84	0.64	0.47	0.46	0.46
$UC_{M,sup}$	0.68	0.73	0.59	0.64	0.65	0.67
$UC_{V,EC}$	0.43	0.44	0.37	0.52	0.52	0.52
$UC_{V,prop}$	0.41	0.42	0.35	0.50	0.50	0.50

*Table 4.5: Unity Check - Eurocode loading - Analytical approach*

The “Unity Check” has been carried out for the design of the Nieuwklap bridge and for both approaches, regarding the shear capacity. It can be noticed that the value of the “Unity Check” never exceeds 1, which means that the Nieuwklap bridge has sufficient shear and bending moment capacity to withstand Eurocode loading. However, considering the design load combination of the slab, the bending resistance of the bridge is borderline sufficient for the flexure-critical positions.

In addition, for LP1, LP2 and LP3 the “Unity Check” for sagging moment is considerably higher than the corresponding “Unity Check” for shear. On the other hand, for LP4, LP5 and LP6 the reverse result is observed when the Eurocode formula for the calculation of the shear capacity is applied. This is not the case if the shear capacity is calculated according to the proposal for slabs under concentrated loads, when the “Unity Checks” for shear and bending moment are close.

### 4.2.2. Equivalent proof loading

The magnitude of proof loading required during the execution of the experiment, in order to evaluate the structure for every load combination level, is important to be defined. Therefore, the equivalent proof load tandem, which generates the same stresses as the Eurocode loading, for the loading combinations defined in *Paragraph 4.1.2*, needs to be determined.

For the specification procedure, the effective width is considered with a horizontal load spreading under a 45° angle from the far side of the concentrated experimental loads, taking into account the skew angle of the concrete deck ( $b_{skew} = 5.24$  m), as illustrated in *Figure 4.4*. The principle of superposition is also used in order to add the occurring stresses. In order to determine the shear force that has to be generated from the proof loading for the beam model, an equivalency has been assumed between the shear stresses due to Eurocode loading and field loading, as described below (*Figure 4.10*).

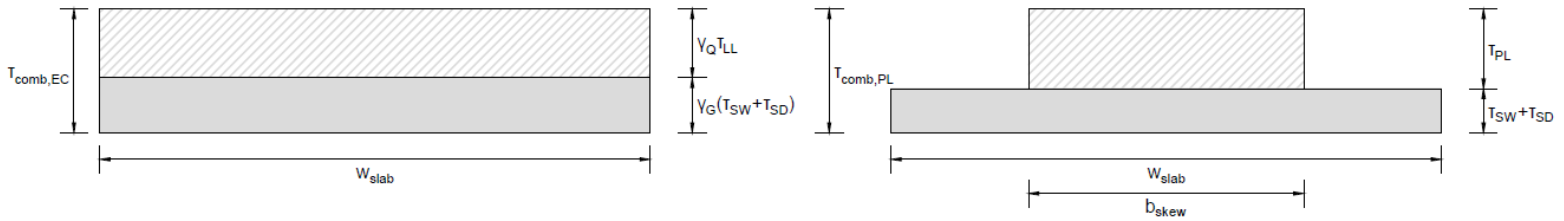


Figure 4.10: Stresses generated by EC loading (left) and proof loading (right)

$$\begin{aligned}
 \tau_{comb,EC} = \tau_{comb,PL} &\rightarrow \gamma_G \cdot (\tau_{SW} + \tau_{SD}) + \gamma_Q \cdot \tau_{LL} = \tau_{SW} + \tau_{SD} + \tau_{PL} \\
 &\rightarrow \tau_{PL} = (\gamma_G - 1) \cdot (\tau_{SW} + \tau_{SD}) + \gamma_Q \cdot \tau_{LL} \quad (4.19) \\
 &\rightarrow V_{PL} = [(\gamma_G - 1) \cdot (V_{SW} + V_{SD}) + \gamma_Q \cdot V_{LL}] \cdot \frac{b_{skew}}{W_{slab}}
 \end{aligned}$$

It is of great significance to repeat that the whole slab width has been considered effective regarding the Tandem system of the LM1 (*Figure 4.5*). The resulted values for the proof load tandems, that cause the same shear force ( $P_V$ ), sagging bending moment ( $P_{M,span}$ ) and hogging bending moment ( $P_{M,sup}$ ) are listed in *Table 4.6*.

EQUIVALENT PROOF LOAD						
LOADING POSITION	1	2	3	4	5	6
	FLEXURE CRITICAL		SHEAR CRITICAL			
<b>DESIGN</b>						
<b>EQUIVALENT PROOF LOAD = <math>0.25*SW + 0.25*SD + 1.50*(UDL + TS)</math></b>						
$P_{M,span}$ (kN)	1896	1884	1302	1448	1478	1464
$P_{M,sup}$ (kN)	3150	2770	4706	2308	2154	2260
$P_V$ (kN)	2798	2704	1278	1438	1430	1440
<b>RECONSTRUCTION</b>						
<b>EQUIVALENT PROOF LOAD = <math>0.15*SW + 0.15*SD + 1.30*(UDL + TS)</math></b>						
$P_{M,span}$ (kN)	1600	1590	1090	1200	1224	1214
$P_{M,sup}$ (kN)	2552	2264	3734	1856	1738	1816
$P_V$ (kN)	2286	2212	1072	1194	1188	1196
<b>USAGE</b>						
<b>EQUIVALENT PROOF LOAD = <math>0.15*SW + 0.15*SD + 1.25*(UDL + TS)</math></b>						
$P_{M,span}$ (kN)	1542	1532	1052	1158	1182	1172
$P_{M,sup}$ (kN)	2470	2188	3620	1798	1680	1760
$P_V$ (kN)	2204	2140	1034	1152	1148	1154
<b>DISAPPROVAL</b>						
<b>EQUIVALENT PROOF LOAD = <math>0.10*SW + 0.10*SD + 1.25*(UDL + TS)</math></b>						
$P_{M,span}$ (kN)	1510	1502	1024	1118	1140	1130
$P_{M,sup}$ (kN)	2336	2086	3356	1688	1582	1650
$P_V$ (kN)	2106	2042	1008	1112	1108	1114

Table 4.6: Equivalent proof load - Analytical approach

It can be remarked that, for all the examined loading positions, the required experimental loading for the hogging bending moment has the greatest magnitude. Moreover, the obtained values for shear force are much higher than sagging bending moment for the flexure-critical positions (LP1, LP2), but are almost identical for the shear critical scenarios.

#### 4.2.3. Failure field loading

For the purpose of an accurate estimation of the failure mode during the implementation of the experimental field loading on the Nieuwklap bridge, the maximum tandem loads, at which shear and flexural failure is expected, will be defined for this level of assessment.

The ultimate bending moment capacity and additionally the bending moment capacity for cracking and yielding of the reinforcement for the mean material properties have been used. In addition, the mean shear capacity calculated with both approaches mentioned in *Paragraph 4.1.3* has been considered.

In order to make a more accurate prediction of the failure loading as possible, for the determination of the effective shear width, all the three approaches for skewed slabs have been considered (*Figure 4.4*), and the shear failure loading has been calculated for all these cases. Such as the proof loading shear specification for the beam model, the shear force that has to be caused from the failure loading in order to reach the ultimate shear resistance for the mean material properties can be determined.

$$\begin{aligned}\tau_{Rm} &= \tau_{comb,FL} \rightarrow \tau_{Rm} = \tau_{SW} + \tau_{SD} + \tau_{FL} \\ \rightarrow V_{FL} &= [V_{Rm} - (V_{SW} + V_{SD})] \cdot \frac{b_{eff}}{w_{slab}}\end{aligned}\quad (4.20)$$

Thus, the predicted field loading that leads to cracking of concrete ( $P_{Mcr}$ ), yielding of the reinforcement ( $P_{My}$ ) and ultimate bending failure ( $P_{Mu}$ ), by crushing of the compression zone, can be specified, as well as the total load for which shear failure occurs according to the present standards ( $P_{V,EC}$ ) and the proposal for concrete slabs under concentrated loads ( $P_{V,prop}$ ). The corresponding results are presented in *Table 4.7*. For flexure-critical positions, since the effective width for shear is the total width of the deck, only one magnitude is specified for shear failure and since they do not meet the criterion for concentrated loading close to supports, the proposed formula is excluded.

FAILURE LOAD						
LOADING POSITION	1	2	3	4	5	6
	FLEXURE CRITICAL		SHEAR CRITICAL			
PREDICTED MAXIMUM FIELD LOAD: MEAN CAPACITY = SW + SD + FL						
$P_{Mcr,span}$ (kN)	776	716	688	972	984	958
$P_{My,span}$ (kN)	2372	2262	2098	2962	3100	3018
$P_{Mu,span}$ (kN)	2768	2644	2450	3460	3624	3528
$P_{Mcr,sup}$ (kN)	630	478	786	518	460	408
$P_{My,sup}$ (kN)	5724	4416	7070	4710	4168	4300
$P_{Mu,sup}$ (kN)	6864	5286	8466	5642	4992	5168
$P_{V,EC,str}$ (kN)	8998	8380	3886	3114	3086	3090
$P_{V,EC,skew}$ (kN)			4200	3366	3334	3340
$P_{V,EC,para}$ (kN)			3710	2972	2944	2950
$P_{V,prop,str}$ (kN)	-		4862	3968	3930	3944
$P_{V,prop,skew}$ (kN)			5254	4290	4248	4260
$P_{V,prop,para}$ (kN)			4642	3786	3752	3764

*Table 4.7: Failure load - Analytical approach*

From the results depicted above, it can be observed that the magnitude that leads to cracking of concrete at midspan is the lowest for all loading scenarios. In addition, as expected, the bigger the prediction for the effective width the larger the load required in order to cause shear failure. Furthermore, the values for span flexural failure are higher for LP4, LP5 and LP6 compared to the other loading positions and especially LP3 case for which the lowest magnitude is required. Apropos, the values of tandem loading for shear failure, these are considerably higher for LP1 and LP2, which are the flexure critical positions. Flexural failure over the support for LP3 occurs for really large field loading, due to the fact that is placed next to an end-support.

More importantly, for LP1, LP2 and LP3 the required proof load tandem that leads to yielding of the reinforcement at the mid-span is significantly lower than the one that causes shear failure and even ultimate bending failure loading has a lower value than shear failure loading for these loading positions. Contrariwise, for LP4, LP5 and LP6 there are no major differences between the field loading magnitude for reinforcement yielding at span position and shear failure according to the Eurocode shear provisions. Notwithstanding, when the extension proposal formula for concrete

slabs is applied, the magnitude of the shear failure loading becomes higher than the one required for flexural failure due to yielding of the longitudinal reinforcement. Substantially large values are observed for this loading positions, regarding flexural failure over the supports.

### 4.3. Discussion - Conclusions

In the previous chapter, an analytical approach was adopted for the evaluation of the Nieuwklap bridge. The procedure that carried out with this level of approximation is not time consuming, since a simplified beam model is assumed and several additional assumptions have been considered in favor of simplification.

It can be deduced, by analyzing the obtained results, that the Nieuwklap bridge has sufficient capacity to withstand the Eurocode load combinations, even the one that is defined for new structures. This statement can be safely made since all the performed “Unity Checks” for Eurocode loading, applied on the most critical positions for shear and flexure, never dissatisfy the unity check.

It is also observed that, for the occurring stresses, not only the loading position has a significant role but also the supporting conditions are of great importance. Therefore, on the one hand, for the flexure critical loading scenarios larger bending moments and smaller shear forces are generated comparing to the shear critical loading positions, but on the other hand the shear critical position which is located close to an end-support exhibits really different results that the ones located close to continuous supports, since the shear forces are considerably smaller and the sagging bending moment is much higher.

Moreover, comparing the “Unity Checks” for each loading scenario, it can be noted that for flexure-critical positions and for the shear-critical position next to the end-support the “Unity Check” for sagging moment is much higher than the corresponding “Unity Check” for shear, which means that for these cases a first estimation of bending moment failure can be made. For the remaining shear critical positions, a difference is displayed, depending on the approach that has been adopted for the calculation of the shear capacity. According to the Eurocode shear provisions, shear failure is more likely to occur first for these scenarios, since the corresponding “Unity Checks” are larger than the “Unity Checks” for sagging bending moment, but when the extension proposed formula is applied, it is unclear which failure mode is critical since the “Unity Checks” have not a significant difference.

Furthermore, from the calculation of the field load magnitude that leads to flexural and shear failure, the way that the Nieuwklap bridge will collapse under field loading can be estimated. In order to have an overview of the results, the required load that leads to bending moment failure due to yielding of the reinforcement and the average value, of the three different approaches for the shear effective width determination, of the field load that causes shear failure according to Eurocode and to the proposed formula for slabs are listed in *Table 4.8*.

FAILURE LOAD						
LOADING POSITION	1	2	3	4	5	6
	FLEXURE CRITICAL			SHEAR CRITICAL		
PREDICTED FAILURE MODE						
$P_{M_y,span}$ (kN)	2372	2262	2098	2962	3100	3018
$P_{V,EC,mean}$ (kN)	8998	8380	3932	3151	3121	3127
<b>FAILURE MODE</b>	Bending	Bending	Bending	Shear/Bending	Shear/Bending	Shear/Bending
$P_{M_y,span}$ (kN)	2372	2262	2098	2962	3100	3018
$P_{V,prop,mean}$ (kN)	-	-	4919	4015	3977	3989
<b>FAILURE MODE</b>	Bending	Bending	Bending	Bending	Bending	Bending

Table 4.8: Predicted failure mode - Analytical approach

Finally, according to this level of approximation, it can be concluded that for the flexure-critical loading positions and for the shear-critical position located next to an end-support, yielding of the reinforcement will occur definitely first, because the required magnitude of the corresponding field load considerably smaller than the one that leads to shear failure. For the shear-critical positions located next to continuous supports, according to the Eurocode is uncertain which failure mode is the dominant one, but when the shear resistance is estimated according to the approach for slabs under concentrated loads close to supports, flexural failure seems to dominate also these loading scenarios.

# 5 Static analysis - Numerical approach

In this chapter, the numerical approach that was followed for the structural analysis of the Nieuwklap bridge will be described extensively.

At first, a comprehensive description of the constructed finite element model takes place, reporting the initial assumptions, its geometry, the finite element type and the application of loading.

Afterwards, the averaged shear forces and bending moments, corresponding to the Eurocode loading, are obtained. In order to evaluate the Nieuwklap bridge against the design loads, a “Unity Check” is performed for the flexure and shear critical loading positions. The equivalent experimental loading, generating the same averaged forces and moments is also determined and the differences between the Eurocode and the applied field loading are analyzed.

The expected failure mode of the bridge under the application of the experimental loading is predicted later, by estimating the magnitude of the field load that leads to shear and flexural failure of the bridge.

Finally, the results obtained from the analytical model and the outcome of the numerical approach will be compared.

## 5.1. Finite element model

### 5.1.1. Geometry - Supports

For this level of assessment, a linear elastic finite element model of the Nieuwklap bridge has been constructed, by using the finite element software, DIANA FEA. As mentioned also in the previous chapter for the analytical model, the assumptions and simplifications that have been considered for the realization of the present finite element model need to be introduced.

At first, it is important to notice that a two-dimensional solution is considered to be highly accurate since the thickness of the concrete deck is much smaller than its other two dimensions. Providing that only the slab part of the bridge deck is examined for the purpose of this project and in order to reduce computational time as well, a simplified 2D plate model is adopted, with a constant thickness of 650 mm and a total width of 8.25 m. The whole bridge has been modelled, since symmetry cannot be used due to the nature of the applied loading. Moreover, the skew angle of 8° according to the structural plans has been also included in the model, in order to examine its influence on the flow of stresses.

Apropos the replication of the bridge supporting conditions, the same assumptions as for the analytical model have been considered, assuming hinges at Supports 4 and 5 and sliding connections for all the other supports. In order to apply these conditions to the finite element model, the vertical ( $u_z$ ) and the longitudinal ( $u_x$ ) displacements have been constrained along the lines representing the two middle piers and along the other supports only the vertical displacement ( $u_z$ ) has been restricted. In addition, regarding the lateral displacement ( $u_y$ ) of the model, it has been constrained only at the nodes at the one end of the line supports in order to take into account the Poisson's ratio effect. A global view of the finite element model, illustrating the supports, is presented in *Figure 5.1*.

Due to the fact that linear elastic analysis is planned to be performed, for the determination of the material properties a linear elastic isotropic material is considered. The values for the Young's modulus and the Poisson's ratio are specified according to the concrete properties listed in *Table 3.2* and the stiffness effects of the reinforcement steel have been ignored.

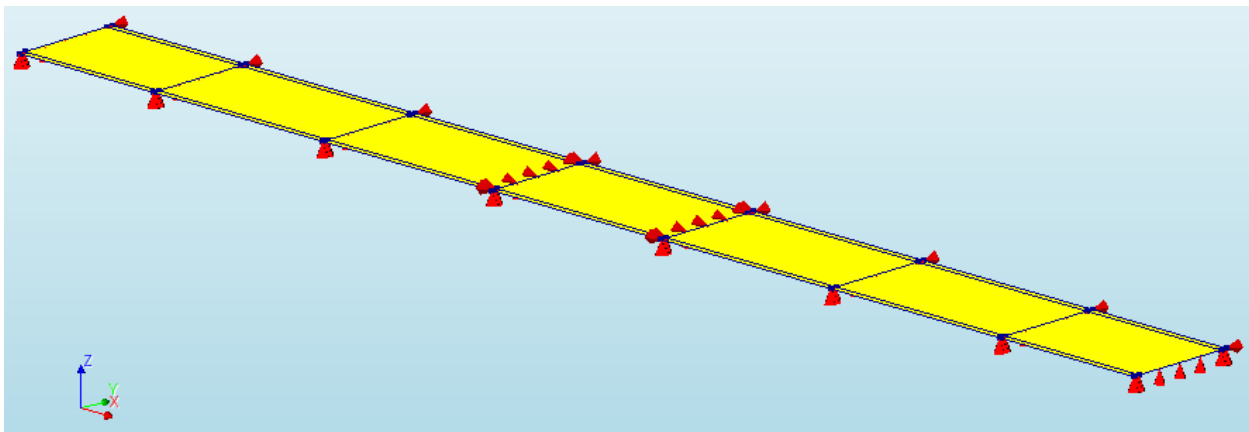


*Figure 5.1: Global view of the Finite element model with the supports*

### 5.1.2. Finite element type - Mesh

Plate bending elements have been used for the finite element model, with a size of 200 mm. After the generation of the mesh, the model consists of 19614 elements of this type and 20538 nodes. A detail of the top view of the mesh discretization that has been applied for the FEM is depicted in *Figure 5.2*.

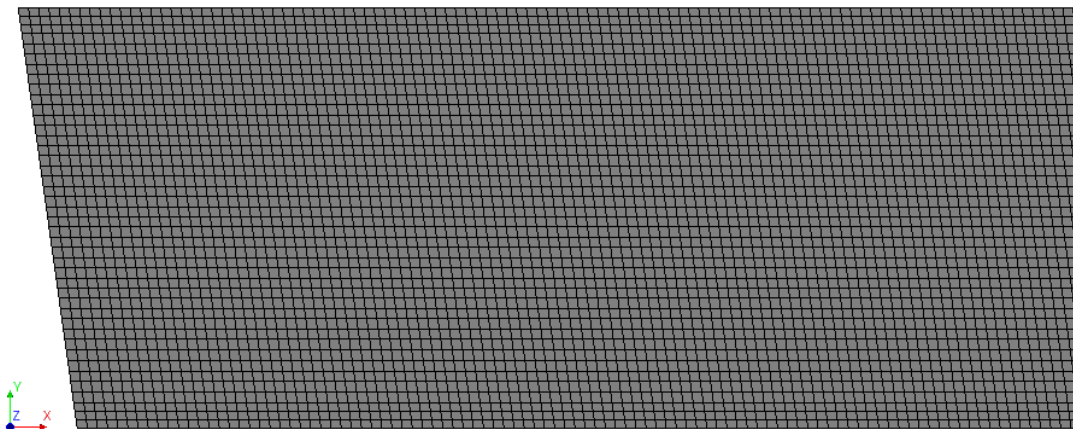


*Figure 5.2: Mesh discretization - Top view detail*

Specific conditions have to be fulfilled in order to justify the use of plate bending elements. At first, the coordinates of the nodes have to be in one flat plane, the thickness must be small in comparison to the other dimensions of the element, forces must act perpendicular to the element plane and bending moments have to act around an axis which is in the element plane [75]. As it is obvious, all these conditions are met by the presented model and can describe the nature of the actual problem. In addition, the stress component perpendicular to the element face is equal to zero, satisfying the plane stress condition, and the element plane remains straight after the occurrence of deformation.

More specifically, Q12PL elements have been used, which are four-node quadrilateral isoparametric elements (Figure 5.3), with three degrees of freedom per node, one displacement and two rotations, based on the Mindlin-Reissner theory [75]. According to this theory, the transverse displacements and rotations of the mid-surface of the element are independent and obtained through interpolation from the translations and the rotations in the nodes, including transverse shear deformation. Therefore, they are quite sensitive regarding shear locking which can lead to an excessively stiff behaviour. Moreover, it is significant to mention that they are based on linear interpolation and their only possible integration scheme is 2x2, meaning that there are 4 integration points for each element.

Important characteristics of the finite element model and of the elements that have been used are summarized in the following table (Table 5.1).

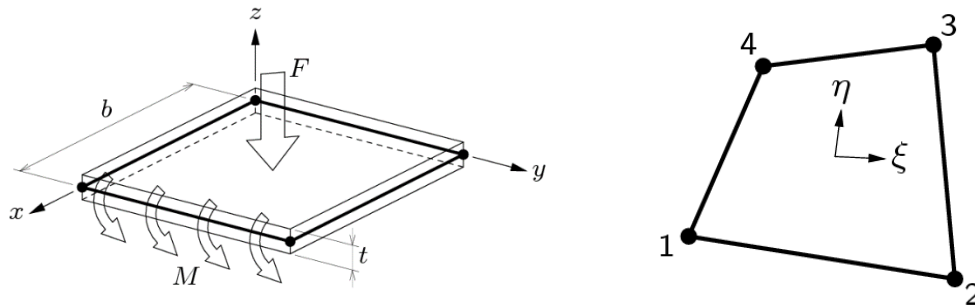


Figure 5.3: Characteristic plate bending element (left) and Q12PL element (right) [75]

Finite Element model	
Finite element type	Plate bending elements (Q12PL - 4 nodes)
Element size	200 x 200 (mm)
Degrees of freedom	12 (1 displacement and 2 rotations per node)
Interpolation scheme	$u_z$ - linear $\varphi_x$ and $\varphi_y$ - linear
Topological and shape dimension	2D
Stress components	Plane stress state ( $\sigma_{xx}, \sigma_{yy}, \sigma_{xy} = \sigma_{yx}$ )
Generalized forces and moments components	Plane stress state ( $q_{xz}, q_{yz}, m_{xx}, m_{yy}, m_{xy} = m_{yx}$ )
Integration scheme	2 x 2
Number of elements	19614
Number of nodes	20538

Table 5.1: Finite element type characteristics

### 5.1.3. Loading - Analysis

For the numerical approach the two types of loading that were applied during the analytical approach have been considered as well. A rigorous description of the Eurocode loading, the field loading and the load combinations that have been considered can be found in *Paragraph 4.1.2*.

The acting loads on the structure are applied by representing the surface loads as specified and the concentrated loads of the tandem systems of LM1 as surface loads distributed over the wheel print, which is 0.4 m x 0.4 m according to NEN-EN 1991-2:2003 [3] (*Figure 4.2*). The acting loads on the FEM model can be easily obtained by the procedure described below and the results are listed in.

$$\begin{aligned}
 SW &= h_{slab} \cdot \gamma_c \text{ [kN/m}^2\text{]} \\
 SD &= t_{asph} \cdot \gamma_{asph} \text{ [kN/m}^2\text{]} \\
 UDL_i &= q_i \text{ [kN/m}^2\text{]} \\
 TS_i &= 2 \cdot \frac{Q_i}{0.4^2} \text{ [kN/m}^2\text{]}
 \end{aligned}
 \tag{5.1}$$

Loads		
Selfweight	SW (kN/m <sup>2</sup> )	16.25
Asphalt	SD (kN/m <sup>2</sup> )	2.76
Traffic loading	UDL <sub>1</sub> (kN/m <sup>2</sup> )	9
	UDL <sub>2</sub> (kN/m <sup>2</sup> )	2.5
	UDL <sub>r</sub> (kN/m <sup>2</sup> )	2.5
	TS <sub>1</sub> (kN/m <sup>2</sup> )	2 · 1875
	TS <sub>2</sub> (kN/m <sup>2</sup> )	2 · 1250

Table 5.2: Acting loads FEM

Six different loading scenarios have been examined similar to the ones depicted in *Figure 4.3*. The concentrated loads have been placed on the most shear and flexure critical positions. One significant difference is the way of specification of these unfavorable positions, because, notwithstanding that for the flexure-critical cases a similar procedure, by shifting the loads across the spans, as for the analytical approach has been applied, for the shear-critical cases a more complicated process has to take place. The tandem system of the first notional lane is placed at distance  $2.5d_1$  from the edge of the support to the closer axle, and as close as possible to the obtuse angle of the bridge deck. The position of the second tandem is determined so that the rear side of the second axle just contributes to the shear force in the obtuse angle when a load spreading under  $45^\circ$  is assumed [73]. The described arrangement for the tandem system for the LP3 case as an example is illustrated in *Figure 5.4*.

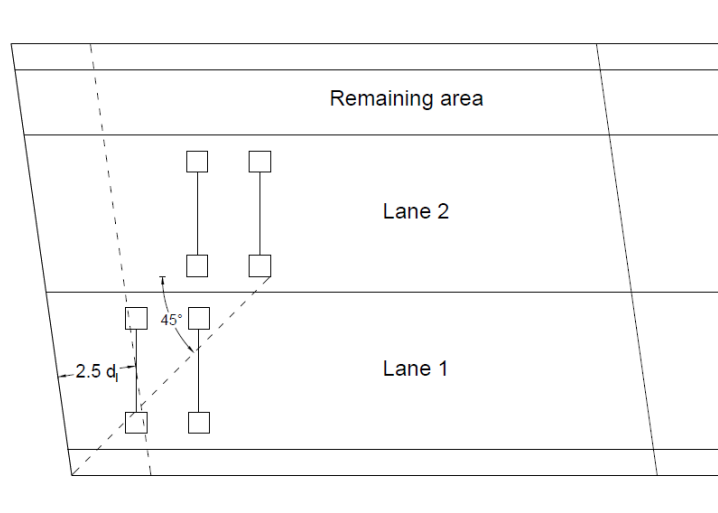


Figure 5.4: Shear critical layout of the Tandem system (LP3)

Finally, a plan view of the finite element model with the division in notional lanes and the wheel print areas for the application of the tandem system according to LM1 is depicted in *Figure 5.5*, and a global view of the model with the applied loads in *Figure 5.6*. The load case scenario LP4 has been used as an example.

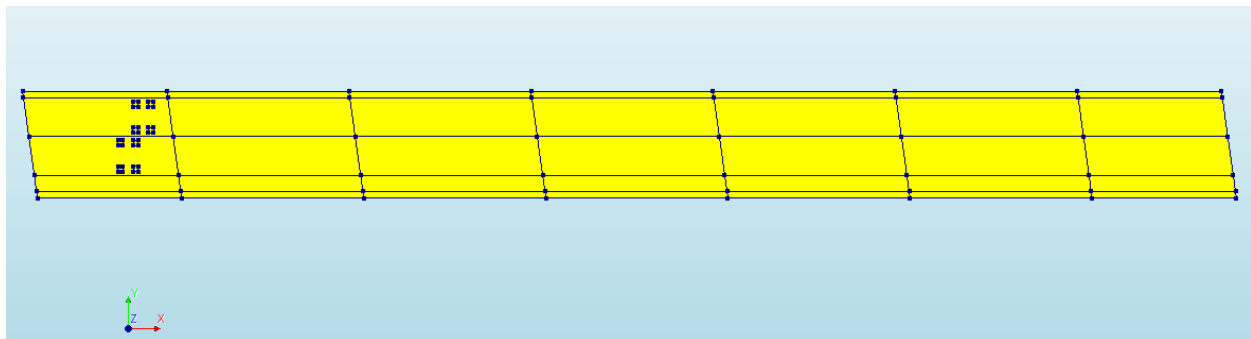


Figure 5.5: FEM plan view with notional lanes and wheel prints (LP4)

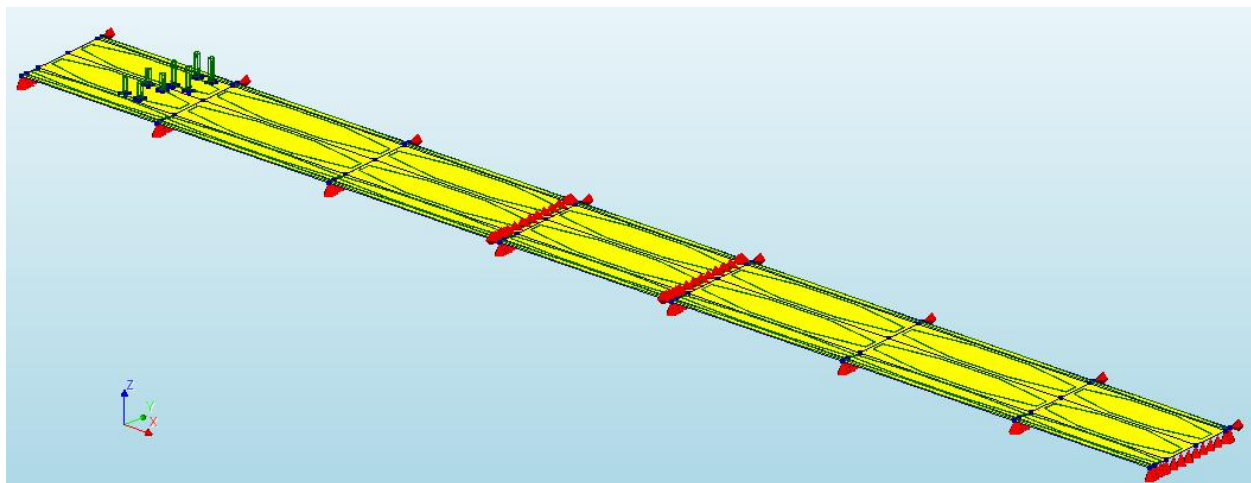


Figure 5.6: FEM global view with applied loads according to Eurocode 2 (LP4)

The constructed finite element model is examined by performing linear elastic analysis for all the considered loading scenarios.

At this level of assessment, the shear stress distribution over the width of the support is determined by averaging the peak shear stress over a distance of  $4d_l$  in the width direction. The bending moment stresses are also averaged over a specific width, which for this project is selected to be 3 m.

Finally, the reinforced concrete slab of the Nieuwklap bridge will be evaluated, by comparing the obtained averaged stresses to its design and mean capacity in bending and shear, that has been already specified analytically in *Paragraph 4.1.3*.

## 5.2. Results

In order to investigate the stress distribution on the bridge deck, the generalized bending moments ( $m_{xx}$ ) and forces ( $q_{xz}$ ) along specified cross-sections have been obtained by using the capability of DIANA FEA to create probe curves. The results have been chosen to be determined at the integration points of the elements, increasing the outcome accuracy.

The influence of the torsional moment ( $m_{xy}$ ), has been taken also into account for the determination of the design moment ( $m_{xD}$ ) of the structure, based on the following calculations:

$$\begin{aligned} m_{xx} > m_{yy} \text{ and } m_{yy} \geq -|m_{xy}| &\rightarrow m_{xD^+} = m_{xx} + |m_{xy}| \\ m_{xx} < m_{yy} \text{ and } m_{yy} \leq |m_{xy}| &\rightarrow m_{xD^-} = -m_{xx} + |m_{xy}| \end{aligned} \quad (5.2)$$

In *Figure 5.7*, the generalized bending moment with and without the inclusion of torsion is illustrated for LP1 at the mid-span position of Span 1. It can be observed that the obtained results are considerably affected by the presence of torsion, therefore it will be considered in the course of this project for the evaluation of the Nieuwklap bridge.

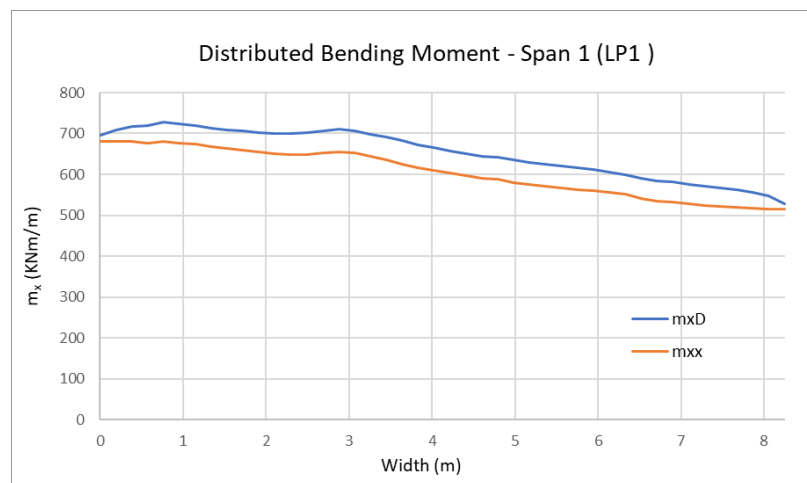


*Figure 5.7: Distributed bending moment for Span 1 with ( $m_{xD}$ ) and without ( $m_{xx}$ ) torsion inclusion (LP1)*

### 5.2.1. Eurocode loading

The obtained generalized moments and forces from DIANA FEA, after the application of Eurocode loading, have been averaged over a distance of 3 m for bending moments and over a distance of  $4d_i$  for shear forces in the width direction. This procedure is depicted in the following figures (Figure 5.8) and diagrams (Figure 5.9), for the loading case scenario LP6 as an example, for the distributed shear force over Support 3 and for distributed design bending moment in Span 2.

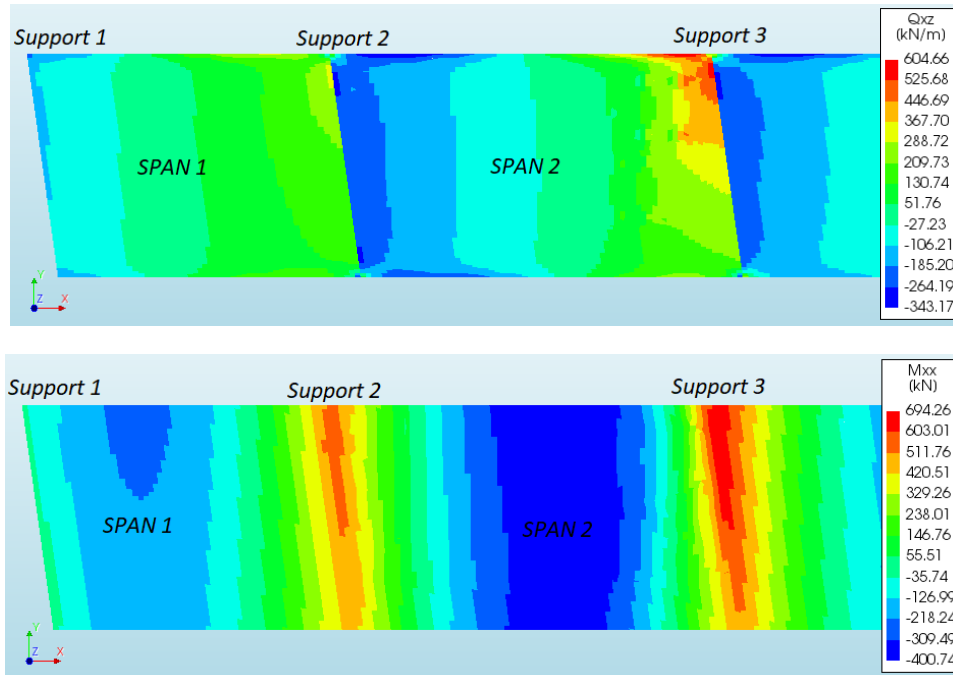


Figure 5.8: Generalized shear forces (top) and bending moments (bottom) (LP6)

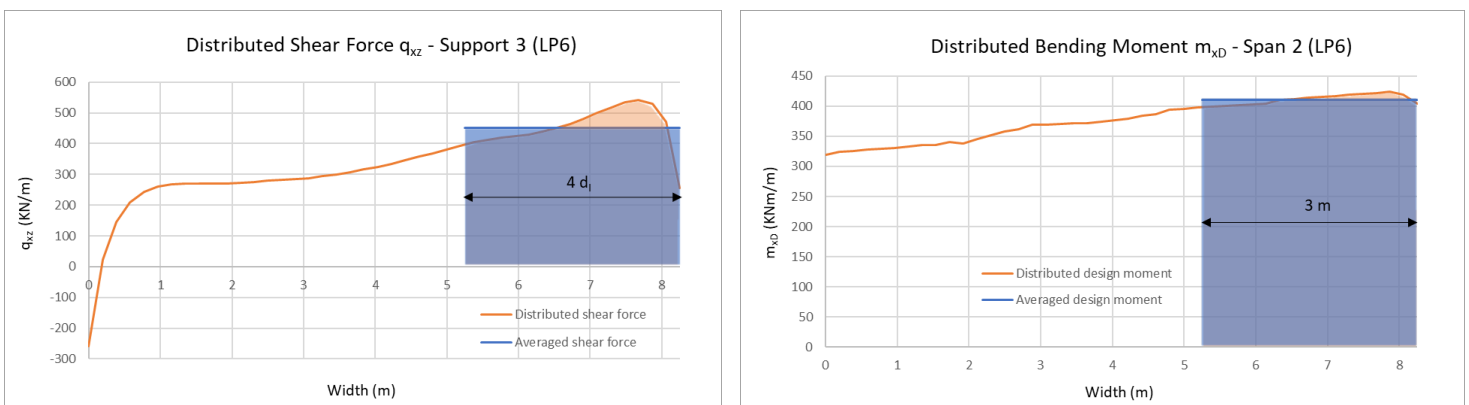


Figure 5.9: Averaged shear forces (left) and averaged design bending moments (right) (LP6)

The averaged shear forces ( $q_{xz}$ ), design hogging bending moments ( $m_{xD,sup}$ ) and design sagging bending moments ( $m_{xD,span}$ ) that have been obtained for all the investigated loading positions and load combinations are summarized in Table 5.3.

EUROCODE LOADING						
LOADING POSITION	1	2	3	4	5	6
	FLEXURE CRITICAL		SHEAR CRITICAL			
<b>DESIGN</b>						
<b>LOAD = 1.25*SW + 1.25*SD + 1.50*(UDL + TS)</b>						
$m_{x_D,span}$ (kNm/m)	709.70	711.35	601.21	434.10	414.46	410.89
$m_{x_D,sup}$ (kNm/m)	-680.84	-715.44	-584.99	-668.99	-677.11	-659.99
$q_{xz}$ (kN/m)	319.52	-378.22	-318.99	460.23	-455.79	451.08
<b>RECONSTRUCTION</b>						
<b>LOAD = 1.15*SW + 1.15*SD + 1.30*(UDL + TS)</b>						
$m_{x_D,span}$ (kNm/m)	625.17	626.70	530.94	384.79	367.45	364.35
$m_{x_D,sup}$ (kNm/m)	-608.12	-637.35	-525.26	-598.58	-605.01	-590.85
$q_{xz}$ (kN/m)	284.85	-336.61	-281.52	407.50	-403.83	399.20
<b>USAGE</b>						
<b>LOAD = 1.15*SW + 1.15*SD + 1.25*(UDL + TS)</b>						
$m_{x_D,span}$ (kNm/m)	607.82	609.37	517.08	375.68	358.80	355.81
$m_{x_D,sup}$ (kNm/m)	-596.71	-624.38	-517.18	-588.02	-593.80	-580.63
$q_{xz}$ (kN/m)	279.16	-329.51	-274.06	397.56	-394.14	389.33
<b>DISAPPROVAL</b>						
<b>LOAD = 1.10*SW + 1.10*SD + 1.25*(UDL + TS)</b>						
$m_{x_D,span}$ (kNm/m)	600.25	601.72	509.66	369.25	352.61	349.63
$m_{x_D,sup}$ (kNm/m)	-583.17	-611.34	-503.48	-573.93	-580.17	-566.49
$q_{xz}$ (kN/m)	273.21	-322.90	-270.26	391.08	-387.53	383.13

Table 5.3: Averaged forces and moments - Eurocode loading - Numerical approach

It becomes obvious through the results that, for the unfavorable for flexure cases (LP1, LP2) the averaged design bending moments are greater than the other loading scenarios and that, for the unfavorable for shear cases, except from LP3, the generated shear forces are considerably larger than the flexure critical positions.

Consequently, the evaluation of the Nieuwklap bridge took place with a “Unity Check”, a ratio between the obtained averaged results and the corresponding capacity of the concrete slab in order to specify the capability of the structure against the Eurocode loading (Table 5.4). For the presented “Unity Check”, the shear capacity has been considered again with both approaches described in Paragraph 4.1.3.

It can be concluded that the Nieuwklap bridge has sufficient shear capacity against Eurocode loading since the “Unity Check” is for all the loading cases below 1. On the contrary, if the design load combination is considered, it arises that the bridge has not sufficient bending resistance, when the loading is exerted on the flexure critical positions (LP1, LP2). However, it is not true to be ascertained that the bridge will collapse under this loading combination, since it meets the criteria for usage and reconstruction.

Furthermore, by comparing the “Unity Check” for shear and sagging bending for each loading position separately, it can be remarked that for LP1, LP2 and LP3 the bending moment “Unity Check” is considerably higher. For the scenarios LP4, LP5 and LP6 it depends on the shear capacity approach, whether the shear “Unity Check” is the higher (Eurocode formula) or whether both of them are quite similar (Proposed formula for slabs).

UNITY CHECKS						
LOADING POSITION	1	2	3	4	5	6
	FLEXURE CRITICAL		SHEAR CRITICAL			
<b>DESIGN</b>						
<b>UNITY CHECK (LOAD/DESIGN CAPACITY)</b>						
UC <sub>mxD,span</sub>	1.07	1.09	0.91	0.65	0.64	0.63
UC <sub>mxD,sup</sub>	0.81	0.85	0.70	0.80	0.81	0.79
UC <sub>qz,EC</sub>	0.52	0.61	0.52	0.75	0.74	0.73
UC <sub>qz,prop</sub>	0.50	0.59	0.50	0.72	0.71	0.70
<b>RECONSTRUCTION</b>						
<b>UNITY CHECK (LOAD/DESIGN CAPACITY)</b>						
UC <sub>mxD,span</sub>	0.94	0.96	0.80	0.58	0.56	0.56
UC <sub>mxD,sup</sub>	0.73	0.76	0.63	0.71	0.72	0.71
UC <sub>qz,EC</sub>	0.46	0.55	0.46	0.66	0.66	0.65
UC <sub>qz,prop</sub>	0.44	0.52	0.44	0.64	0.63	0.62
<b>USAGE</b>						
<b>UNITY CHECK (LOAD/DESIGN CAPACITY)</b>						
UC <sub>mxD,span</sub>	0.92	0.94	0.78	0.57	0.55	0.55
UC <sub>mxD,sup</sub>	0.71	0.75	0.62	0.70	0.71	0.69
UC <sub>qz,EC</sub>	0.45	0.54	0.45	0.65	0.64	0.63
UC <sub>qz,prop</sub>	0.44	0.51	0.43	0.62	0.61	0.61
<b>DISAPPROVAL</b>						
<b>UNITY CHECK (LOAD/DESIGN CAPACITY)</b>						
UC <sub>mxD,span</sub>	0.90	0.92	0.77	0.56	0.54	0.54
UC <sub>mxD,sup</sub>	0.70	0.73	0.60	0.69	0.69	0.68
UC <sub>qz,EC</sub>	0.44	0.52	0.44	0.64	0.63	0.62
UC <sub>qz,prop</sub>	0.43	0.50	0.42	0.61	0.60	0.60

Table 5.4: Unity Check - Eurocode loading - Numerical approach

### 5.2.2. Equivalent proof loading

By using the constructed finite element model, a better estimation of the proof load magnitude, which generates the same cross section forces and moments as the Eurocode loading, has been pursued. Every combination level has been examined again, providing valuable information for the real field experiment. The same procedure as for the Eurocode loading is carried out in order to get the values for the equivalent proof loads that generate the same average shear forces and design bending moments.

The magnitudes for the equivalent proof load tandems, that cause the same average shear force ( $P_V$ ), design sagging bending moment ( $P_{M,span}$ ) and design hogging bending moment ( $P_{M,sup}$ ) are presented in Table 5.5.

EQUIVALENT PROOF LOAD						
LOADING POSITION	1	2	3	4	5	6
	FLEXURE CRITICAL		SHEAR CRITICAL			
<b>DESIGN</b>						
<b>EQUIVALENT PROOF LOAD = <math>0.25*SW + 0.25*SD + 1.50*(UDL + TS)</math></b>						
$P_{M,span}$ (kN)	1552	1584	1632	1936	1936	1936
$P_{M,sup}$ (kN)	2272	1984	3712	2576	2512	2432
$P_V$ (kN)	2304	2016	1504	1600	1584	1568
<b>RECONSTRUCTION</b>						
<b>EQUIVALENT PROOF LOAD = <math>0.15*SW + 0.15*SD + 1.30*(UDL + TS)</math></b>						
$P_{M,span}$ (kN)	1312	1344	1392	1696	1712	1712
$P_{M,sup}$ (kN)	1856	1648	2976	2144	2080	1984
$P_V$ (kN)	1904	1696	1280	1344	1344	1312
<b>USAGE</b>						
<b>EQUIVALENT PROOF LOAD = <math>0.15*SW + 0.15*SD + 1.25*(UDL + TS)</math></b>						
$P_{M,span}$ (kN)	1264	1296	1344	1648	1680	1680
$P_{M,sup}$ (kN)	1792	1600	2912	2080	2016	1920
$P_V$ (kN)	1840	1632	1232	1296	1296	1264
<b>DISAPPROVAL</b>						
<b>EQUIVALENT PROOF LOAD = <math>0.10*SW + 0.10*SD + 1.25*(UDL + TS)</math></b>						
$P_{M,span}$ (kN)	1248	1280	1312	1616	1648	1648
$P_{M,sup}$ (kN)	1728	1536	2736	1984	1936	1856
$P_V$ (kN)	1776	1600	1200	1264	1264	1248

Table 5.5: Equivalent proof load - Numerical approach

It can be noticed that higher tandem values are required for bending for loading scenarios LP4, LP5 and LP6 than cases LP1 and LP2 and the opposite results are observed for shear. Despite the fact that LP3 is a shear critical loading position, the obtained values are notably different than the other shear critical cases, since the equivalent proof load for the design sagging bending moment is much smaller, almost equal to the flexure critical cases.

### 5.2.3. Eurocode and experimental loading comparison

The acquired output from the Eurocode and the experimental loading is of great significance to be compared, in order to understand the differences in the behaviour of the bridge deck under the application of these distinct loading types and to be sufficiently prepared during the execution of the field loading. It is important to be reminded that the experimental loading consists of four concentrated loads in contrast with LM1 of the Eurocode, which includes eight concentrated loads (Tandem system) and a uniformly distributed load.

Loading scenario LP5 has been selected in order to depict the differences obtained between the Eurocode loading, regarding this shear critical case, and the experimental loading that causes the same averaged shear forces ( $q_{xz}$ ) along a width of  $4d_1$  over the supports and the same averaged design bending moments ( $m_{x,b}$ ) along a width of 3 m. The distributed generalized forces and design moments in specified cross-sections, for both examined loading types are illustrated in *Figure 5.10*.

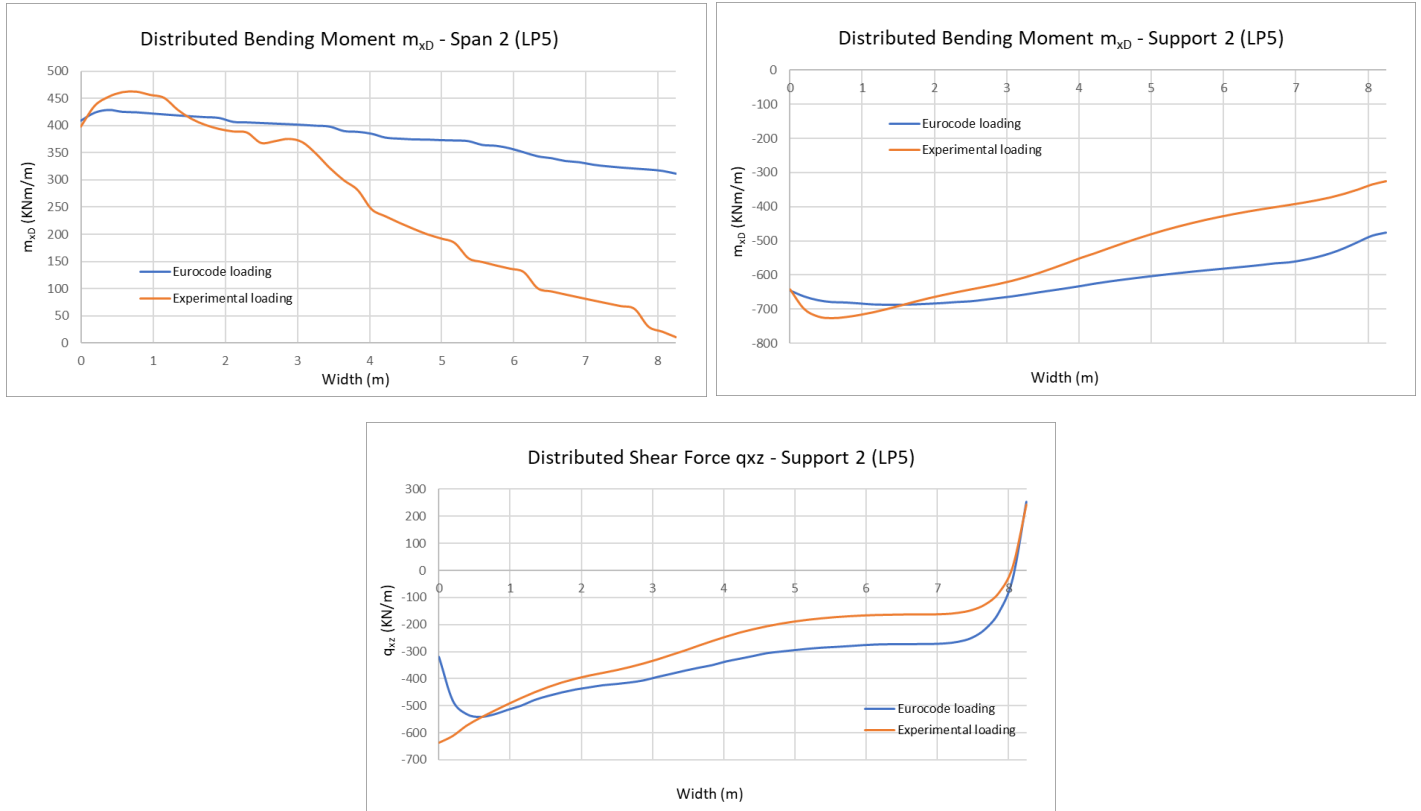


Figure 5.10: Distributed generalized design bending moment at Span 2 (top left) and Support 2 (top right), and generalized shear force at Support 2 (bottom) for Eurocode and experimental loading (LP5)

From these distributions of forces and moments, it can be seen that for the experimental loading more extreme values are obtained locally, especially regarding the distributed design bending moment at Span 2. In addition, the maximum moments are concentrated conspicuously in a small area along the width of the cross-section. Apropos the distributed shear force, it can be noticed that the maximum value for the experimental loading occurs at the edge of the cross-section, which is not the case for the Eurocode loading.

Furthermore, the vertical displacements of the plate model are depicted in Figure 5.11, in case of exerted loading according to LM1 and in case of field loading that causes the same design sagging bending moment for LP5.

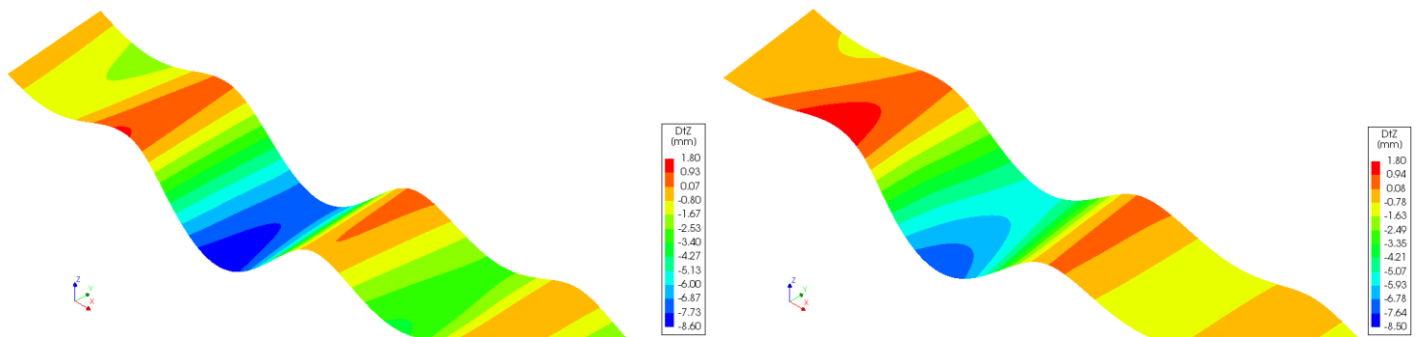


Figure 5.11: Vertical displacements for Eurocode (left) and experimental (right) loading (LP5)

Again, the more localized phenomena due to the experimental loading are evident. However, not significant differences are observed between the maximum values of the vertical displacement. The largest displacement downwards occurs for the Eurocode loading and the largest displacement upwards for the field loading.

Moreover, the comparison between the torsional moment generated for both loading types is of interest. The percentage of torsion that contributes to the design bending moment at the span, more specifically at the position where the loads are applied, and over the supports is displayed in *Table 5.6* for the design load combination and for all the examined loading scenarios.

LOADING POSITION		TORSION PERCENTAGE					
		1	2	3	4	5	6
		FLEXURE CRITICAL			SHEAR CRITICAL		
DESIGN							
Span	Eurocode loading (%)	6.3	4.5	8.3	9.7	8.1	7.7
	Experimental loading (%)	8.1	6.5	11.6	15.3	16.3	16.8
Support	Eurocode loading (%)	6.0	1.3	3.9	1.9	2.0	1.9
	Experimental loading (%)	11.8	7.8	9.8	9.1	8.2	8.1

*Table 5.6: Torsional moment ( $m_{xy}$ ) percentage of design bending moment ( $m_{xD}$ ) for Eurocode and experimental loading*

In the table above, the increased contribution of twisting moment for the experimental loading is obvious for all the examined cases. In specific, major raise can be noticed for the shear critical scenarios at the mid-span position, where also for the Eurocode loading the greatest participation of torsional moment is obtained.

#### 5.2.4. Failure field loading

Concerning the reasons explained in *Paragraph 4.2.3* for the analytical approach, the magnitude of the field loading that leads to shear and flexural failure of the bridge deck will be determined again according to the presented numerical approach.

The mean values of the concrete and the reinforcement parameters have been adopted and the field load that generates averaged design moment equal to the resistance of concrete before cracking ( $P_{Mcr}$ ), the resistance of the reinforcement before yielding ( $P_{My}$ ) and to the ultimate bending resistance ( $P_{Mu}$ ), have been specified. The field load that generates the same averaged shear forces as the shear capacity, calculated with both examined formulas ( $P_{V,EC}$ ,  $P_{V,prop}$ ) have been found as well.

For flexure critical positions, the proposed formula has not been applied, since there is no loading close to the supports. The resulted field load magnitudes are listed in *Table 5.7*.

FAILURE LOAD						
LOADING POSITION	1	2	3	4	5	6
	FLEXURE CRITICAL		SHEAR CRITICAL			
PREDICTED MAXIMUM FIELD LOAD: MEAN CAPACITY = SW + SD + FL						
$P_{Mcr,span}$ (kN)	560	540	780	1550	1585	1615
$P_{My,span}$ (kN)	1665	1670	2175	3480	3510	3475
$P_{Mu,span}$ (kN)	1950	1955	2545	3965	3965	3960
$P_{Mcr,sup}$ (kN)	560	530	1240	720	720	670
$P_{My,sup}$ (kN)	3790	2975	8000	4350	4130	4160
$P_{Mu,sup}$ (kN)	4515	3520	9570	5150	4895	4960
$P_{V,EC}$ (kN)	6655	4540	3870	2735	2720	2720
$P_{V,prop}$ (kN)	-		4845	3470	3475	3480

Table 5.7: Failure load - Numerical approach

It can be remarked that, evidently lower magnitudes are required for bending failure for LP1 and LP2 against the other loading scenarios. Regarding the shear failure loads, the smallest values are noticed for LP4, LP5 and LP6. The largest field load that is required is the one that leads to flexural failure over Support 2 for LP3.

Comparing the field load magnitudes for each loading scenario individually, considerably lower values are leading to flexural failure at the mid-span for LP1, LP2 and LP3, in contrast to the loads causing shear failure. On the contrary, for LP4, LP5 and LP6 the opposite results occur when the Eurocode formula for shear is applied. Nevertheless, if the proposed formula for loads close to supports is used, the values for shear failure and flexural failure due to yielding of the reinforcement at mid-span position become almost identical.

### 5.3. Discussion - Conclusions

In the previous paragraphs of this chapter, the Nieuwklap bridge was evaluated by using a numerical approach. For the purpose of this level of assessment a two-dimensional finite element model was constructed and a linear elastic analysis was performed.

According to the performed “Unity Checks” for the Eurocode loading, the Nieuwklap bridge has adequate shear capacity to withstand all the applied load combinations. However, it has been proven to have lacking bending moment capacity when the Tandem system of LM1 is exerted on the flexure critical positions. However, this result occurs only in case that the design load combination and the design material properties have been taken into account. For that reason, it cannot be directly entailed that the bridge is inadequate and has to be demolished, since it meets the criteria for usage and reconstruction.

Furthermore, by comparing the “Unity Checks” for each loading scenario, it can be initially assumed that, for concentrated loads applied on the flexure critical positions and on the shear critical position next to the end-support of the bridge flexural failure is the most possible failure mode. In case that the concentrated loads are applied on shear critical position next to a continuous support, an estimation for the failure mode is difficult to be made considering the “Unity Checks”, since different results are obtained based on the formula that has been used for the specification of the shear capacity.

A better estimation regarding the predicted failure mode can be made, by evaluating the resulted field load magnitudes that cause flexural and shear failure. An overview of these results is placed in *Table 5.8*, including the required loads for yielding of the reinforcement and for shear failure according to Eurocode shear provisions and to the proposed formula for slabs under concentrated loads close to supports.

FAILURE LOAD						
LOADING POSITION	1	2	3	4	5	6
	FLEXURE CRITICAL			SHEAR CRITICAL		
PREDICTED FAILURE MODE						
$P_{M_y,span}$ (kN)	1665	1670	2175	3480	3510	3475
$P_{V,EC}$ (kN)	6656	4540	3872	2735	2720	2720
<b>FAILURE MODE</b>	Bending	Bending	Bending	Shear	Shear	Shear
$P_{M_y,span}$ (kN)	1665	1670	2175	3480	3510	3475
$P_{V,prop}$ (kN)	-	-	4845	3470	3475	3480
<b>FAILURE MODE</b>	Bending	Bending	Bending	Shear/Bending	Shear/Bending	Shear/Bending

*Table 5.8: Predicted failure mode - Numerical approach*

Therefore, it can be surely stated that yielding of the reinforcement will lead to the bridge failure for the flexure critical loading positions and for the shear critical position located next to an end-support, since lower magnitudes of field load are required. Conversely, according to the Eurocode shear formula, smaller field load has to be exerted in order to cause shear failure for the shear critical positions located next to continuous supports. But in case that the additional bearing mechanisms of concrete slabs are taken into account, the field loads that lead to shear failure and yielding of the reinforcement have almost the same value, causing difficulties for the identification of the expected failure mode.

Finally, by carrying out a comparison between the Eurocode and the experimental loading, it can be concluded that higher local stresses are generated due to field loading and that the effects of torsional moment are highly considerable during the execution of the experiment.

## 5.4. Comparison with Analytical approach

After the completion of both the Analytical and the Numerical approach for the assessment of the reinforced concrete solid slab deck of the Nieuwklap bridge, the obtained results is of great importance to be compared in order to end up to some significant conclusions. The following tables include the results from a flexure critical scenario, a shear critical next to an end-support scenario and a shear critical next to a continuous support scenario.

At first, by the performed “Unity Checks” regarding the Eurocode loading (*Table 5.9*), it can be observed that lower values have been obtained for the analytical approach in comparison to the corresponding values for the numerical approach. However, this can be justified easily, by the fact that in the analytical model the shear forces and bending moments have been averaged along the whole width of the slab cross-section in contrast with the finite element model where a smaller width has been chosen for obtaining the average values for shear and bending moment. In addition, the influence of the twisting moment has been considered during the numerical approach, increasing considerably the results regarding the design bending moment.

UNITY CHECK COMPARISON						
LOADING POSITION	1		3		5	
	FLEXURE CRITICAL		SHEAR CRITICAL (END-SUPPORT)		SHEAR CRITICAL (MID-SUPPORT)	
DESIGN						
UNITY CHECK (LOAD/DESIGN CAPACITY)						
APPROACH	Analytical	Numerical	Analytical	Numerical	Analytical	Numerical
UC <sub>mxD,span</sub>	0.96	1.07	0.75	0.91	0.54	0.64
UC <sub>mxD,sup</sub>	0.79	0.81	0.69	0.70	0.76	0.81
UC <sub>vxz,EC</sub>	0.50	0.52	0.43	0.52	0.61	0.74
UC <sub>vxz,prop</sub>	0.48	0.50	0.41	0.50	0.58	0.71

Table 5.9: Unity Check comparison

Consequently, by comparing the equivalent proof load magnitudes (*Table 5.10*) acquired from both approaches, it can be noticed that for concentrated loads placed at the flexure critical positions the proof load values have been slightly overestimated by the analytical model. On the contrary, for concentrated loads applied at the shear critical positions, the analytical model seems to be somewhat conservative compared to the finite element model. A possible explanation regarding these differences, could be that, the effective width which has been considered for the analytical model is an approximation which justifies such an inconsistency of results. More specifically, for flexure critical positions the whole width of the slab has been regarded as effective for the analytical model which appears to be an overestimation according to the numerical model. In addition, the shear effective width for the shear critical cases seems to be larger than the one specified according to the French practice for the analytical model.

EQUIVALENT PROOF LOAD COMPARISON						
LOADING POSITION	1		3		5	
	FLEXURE CRITICAL		SHEAR CRITICAL (END-SUPPORT)		SHEAR CRITICAL (MID-SUPPORT)	
DESIGN						
EQUIVALENT PROOF LOAD = $0.25 \cdot SW + 0.25 \cdot SD + 1.50 \cdot (UDL + TS)$						
APPROACH	Analytical	Numerical	Analytical	Numerical	Analytical	Numerical
P <sub>M,span</sub> (kN)	1896	1552	1302	1632	1478	1936
P <sub>M,sup</sub> (kN)	3150	2272	4706	3712	2154	2512
P <sub>V</sub> (kN)	2798	2304	1278	1504	1430	1584

Table 5.10: Equivalent proof load comparison

Finally, regarding the prediction of the Nieuwklap bridge failure mode (*Table 5.11*), both approaches define that flexural failure due to yielding of the reinforcement will occur for experimental loading exerted at the flexure critical positions and the shear critical position next to the bridge end-support. Apropos the application of experimental loading at the shear critical positions next to continuous supports for both approaches, it is uncertain which failure mode will occur first, depending on the approximation that has been considered for the average shear capacity of the structure as has been already reported in *Paragraph 4.2.3* and in *Paragraph 5.2.4* for the analytical and the numerical approach respectively. It has to be remarked that for the calculation of the mean shear capacity the contribution of the longitudinal bent-up bars close to the supports has been omitted in both approaches.

FAILURE LOAD COMPARISON						
LOADING POSITION	1		3		5	
	FLEXURE CRITICAL		SHEAR CRITICAL (END-SUPPORT)		SHEAR CRITICAL (MID-SUPPORT)	
PREDICTED FAILURE MODE						
APPROACH	Analytical	Numerical	Analytical	Numerical	Analytical	Numerical
$P_{M_y, \text{span}}$ (kN)	2372	1665	2098	2175	3100	3510
$P_{V, EC}$ (kN)	8998	6656	3932	3872	3121	2720
<b>FAILURE MODE</b>	Bending	Bending	Bending	Bending	Shear/Bending	Shear
$P_{M_y, \text{span}}$ (kN)	2372	1665	2098	2175	3100	3510
$P_{V, \text{prop}}$ (kN)	-	-	4919	4845	3977	3475
<b>FAILURE MODE</b>	Bending	Bending	Bending	Bending	Bending	Shear/Bending

Table 5.11: Failure mode prediction comparison

# 6 Seismic design

In this chapter, the seismic evaluation of the Nieuwklap bridge will be presented.

Initially, the existing earthquake data in the Netherlands will be examined in order to estimate the occurrence probability of earthquakes with a specific magnitude and to define the suitable response spectra.

Then, a simplified linear static approach will take place and the resistance of the bridge deck and the bridge piers will be investigated under the seismic load combination.

Afterwards, a Modal response spectrum dynamic analysis will also be performed, by constructing two alternative models, obtaining all the important modes of the bridge contributing to its total structural response. Finally, the Nieuwklap bridge will be evaluated again under the combined action of the three components of the seismic excitation.

## 6.1. General

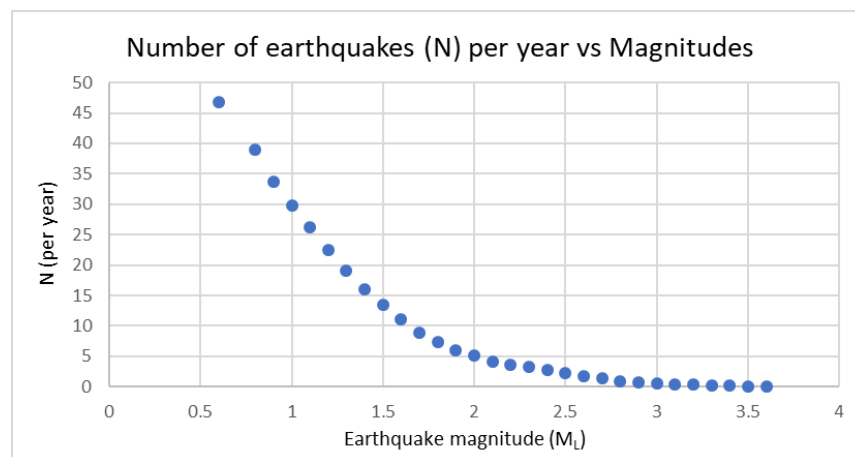
### 6.1.1. Earthquake data

In order to proceed with the seismic design of the Nieuwklap bridge, it has been considered essential to initially assess the existing data for seismic activity in the Netherlands, regarding the human-induced earthquakes. The Koninklijk Nederlands Meteorologisch Instituut (KNMI) [10], which is the official research institute in the Netherlands in the field of seismology, uses the Richter scale in order to measure the magnitude ( $M_i$ ) of the occurred earthquakes, which is also known as local magnitude and is a logarithmic scale, meaning that an increase of one magnitude unit corresponds to a ten times larger result. Also, when reference to earthquakes is made the return period ( $T_R$ ) is really important, which is defined as the mean time between earthquakes with a magnitude greater than  $M_L$  [76]. The occurrence of human-induced earthquakes regarding their magnitudes and their return period is of great significance to be estimated.

For the accomplishment of the above-mentioned purpose, the Earthquake catalog of the Netherlands, provided by KNMI [10] has been taken into account. All the human induced earthquakes with a larger magnitude than  $M_L=0.5$ , that have taken place in Groningen area the last 32 years, between 26-12-1986 and 22-08-2018, have been considered. By using these data, the total number of earthquakes per magnitude has been calculated for the examined period. Afterwards, the mean number of earthquakes per year has been found and finally for every magnitude  $M_L$ , the number of earthquakes ( $N$ ) with a greater or equal magnitude per year has been estimated (*Table 6.1*). Finally, a diagram is presented of the number of earthquakes  $N$  per year against earthquake magnitudes (*Figure 6.1*).

Human-Induced earthquakes data			
Magnitude ( $M_L$ )	Number of earthquakes in 32 years	Average number of earthquakes per year	N (per year)
0.6	249	7.78	46.81
0.8	168	5.25	39.03
0.9	129	4.03	33.78
1	113	3.53	29.75
1.1	117	3.66	26.22
1.2	112	3.50	22.56
1.3	96	3.00	19.06
1.4	84	2.63	16.06
1.5	76	2.38	13.44
1.6	70	2.19	11.06
1.7	50	1.56	8.88
1.8	44	1.38	7.31
1.9	27	0.84	5.94
2	29	0.91	5.09
2.1	16	0.50	4.19
2.2	15	0.47	3.69
2.3	17	0.53	3.22
2.4	14	0.44	2.69
2.5	15	0.47	2.25
2.6	14	0.44	1.78
2.7	13	0.41	1.34
2.8	8	0.25	0.94
2.9	2	0.06	0.69
3	6	0.19	0.63
3.1	2	0.06	0.44
3.2	6	0.19	0.38
3.3	1	0.03	0.19
3.4	2	0.06	0.16
3.5	2	0.06	0.09
3.6	1	0.03	0.03

Table 6.1: Human-induced earthquakes data

Figure 6.1: Number of earthquakes (N) vs magnitude ( $M_L$ )

The frequency of earthquake occurrence drops exponentially with the increasing earthquake magnitude and the following empirical formula can be formulated [76]:

$$\log_{10} N = a - \beta \cdot M_L \quad (6.1)$$

where,  $\alpha$  describes the total number of earthquakes in a region and  $\beta$  measures the relative number of large earthquakes compared to small ones and it takes typically values between 0.8 and 1.2.

In the following figure (*Figure 6.2*), a plot showing  $\log_{10}N$  as a function of magnitude  $M_L$  has been made and the data have been fitted with linear regression in order to estimate the constant coefficients  $\alpha$  and  $\beta$ .

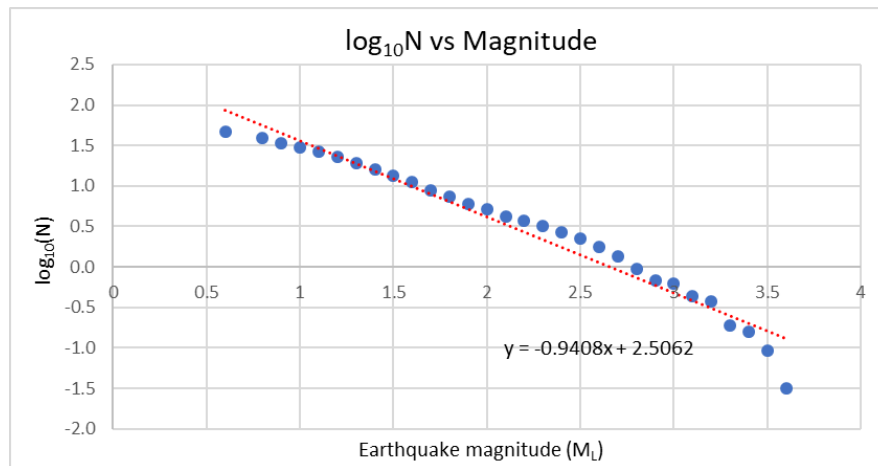


*Figure 6.2: Logarithm of the number of earthquakes (N) vs magnitude ( $M_L$ )*

From the presented diagram it can be deduced that:

$$a = 2.5062 \quad \& \quad \beta = 0.9408 \quad \rightarrow \quad \log_{10} N = 2.5062 - 0.9408 \cdot M_L \quad (6.2)$$

The deviations from the straight line, that can be observed in the previous diagram can be explained for the small and the high magnitudes. In the first case, the deviation is due to the fact that earthquakes with a magnitude smaller than the catalog completeness threshold were used, which is the minimum magnitude above which all earthquakes within a certain region are reliably recorded. In case of higher magnitudes, the change from power law to a faster decay is due to the fact that statistical data are very poor [77].

The magnitude of a human-induced earthquake in Groningen area, with a specific return period, can be estimated:

$$M_L = -\frac{\log_{10} N - 2.5062}{0.9408} \quad (6.3)$$

where,

$$N = \frac{1}{T_R} \quad (6.4)$$

Moreover, the probability that at least one earthquake with a magnitude greater than  $M_L$  will occur in a specified period  $t_r$ , also called the probability of exceedance, can be calculated for a specific return period [77]:

$$P = 1 - e^{-\frac{t_r}{T_R}} \quad (6.5)$$

For the purpose of the current project, and since the available data from KNMI correspond to specific return periods, it has been decided that earthquakes with return period of  $T_R=475$  years and  $T_R=2475$  years will be examined. The corresponding earthquake magnitudes and the probability of exceedance the next 50 years and 250 years for the two examined cases are listed in *Table 6.2*.

Earthquake occurrence			
Return period $T_R$ (years)	Magnitude $M_L$ (-)	Probability of exceedance in 50 years (%)	Probability of exceedance in 250 years (%)
475	5.5	10	40
2475	6.3	2	10

*Table 6.2: Earthquake occurrence*

### 6.1.2. Response spectra

The specification of the elastic horizontal and vertical response spectra of the area where the Nieuwklap bridge is located is an integral part of the seismic design and in order to be determined, specific characteristics such as the ground type of the area and the importance of the structure need to be identified. Moreover, the peak ground acceleration (PGA) is essential to be specified, due to the fact that the forces exerted on the structure are proportional to this value.

A representative horizontal elastic response spectrum can be established for the bridge location according to NPR 9998 Webtool [78] which gives a “Uniform Hazard Spectrum” at the surface level, which has been aligned with EN 1998-1:2004 [12]. On the other hand, due to the fact that there are no vertical accelerations provided by this Webtool, the procedure described in EN 1998-1:2004 [12] has to be followed, where two types of vertical response spectra are specified with regard to the magnitude of the earthquakes that contribute most to the seismic hazard. In order to decide which type of response spectrum is more suitable for our case, the horizontal response spectra according to these two types will be defined and will be compared with the given one from the NPR 9998 Webtool.

At first, the structure is considered to belong to importance class II, as recommended by EN 1998-2:2005 [13], so the importance factor is  $\gamma_I=1$ . The value of the PGA at surface level, including the

soil factor, has been defined according to the NPR 9998 Webtool [78] for both examined return periods mentioned in the previous paragraph. By obtaining the average shear wave velocity along a 30 m depth for the bridge location [14],  $v_{s,30} \approx 180 \text{ m/s}^2$ , the soil can be classified as Ground Type D. Moreover, the behaviour factor of the structure has been taken equal to  $q=1$ , since the bridge deck is not monolithically connected to the piers and the damping coefficient of the structure has been considered  $\xi=5\%$ , meaning that the damping correction factor is also equal to  $n=1$ . The obtained parameters according to the Eurocode and to the NPR 9998 for the horizontal response spectrum, for both return periods, are summarized in *Table 6.3*.

Horizontal elastic response spectra - $T_R = 475$ years				
Parameters		NPR 9998	EC8 - Type 1	EC8 - Type 2
PGA	$\alpha_g \cdot S$ (g)	0.066	0.066	0.066
Damping factor	$n$ (-)	1	1	1
Ratio	$p$ (-)	2.319	2.50	2.50
Characteristic Periods	$T_B$ (s)	0.198	0.20	0.10
	$T_C$ (s)	0.464	0.80	0.30
	$T_D$ (s)	0.849	2.00	1.20
Horizontal elastic response spectra - $T_R = 2475$ years				
Parameters		NPR 9998	EC8 - Type 1	EC8 - Type 2
PGA	$\alpha_g \cdot S$ (g)	0.114	0.114	0.114
Damping factor	$n$ (-)	1	1	1
Ratio	$p$ (-)	2.311	2.50	2.50
Characteristic Periods	$T_B$ (s)	0.226	0.20	0.10
	$T_C$ (s)	0.518	0.80	0.30
	$T_D$ (s)	1.005	2.00	1.20

*Table 6.3: Horizontal elastic response spectrum parameters*

For the horizontal components of the seismic action the elastic response spectrum is defined by the following expressions [14]:

$$0 \leq T \leq T_B : S_a(T) = a_g \cdot S \cdot \left[ 1 + \frac{T}{T_B} \cdot (n \cdot p - 1) \right] \quad (6.6)$$

$$T_B \leq T \leq T_C : S_a(T) = a_g \cdot S \cdot n \cdot p \quad (6.7)$$

$$T_C \leq T \leq T_D : S_a(T) = a_g \cdot S \cdot n \cdot p \cdot \left[ \frac{T_C}{T} \right] \quad (6.8)$$

$$T_D \leq T \leq 4s : S_a(T) = a_g \cdot S \cdot n \cdot p \cdot \left[ \frac{T_C \cdot T_D}{T} \right] \quad (6.9)$$

The obtained horizontal response spectra for both examined return periods according to NPR 9998 and to Type 1 and Type 2 of the Eurocode 8 are illustrated in *Figure 6.3*.

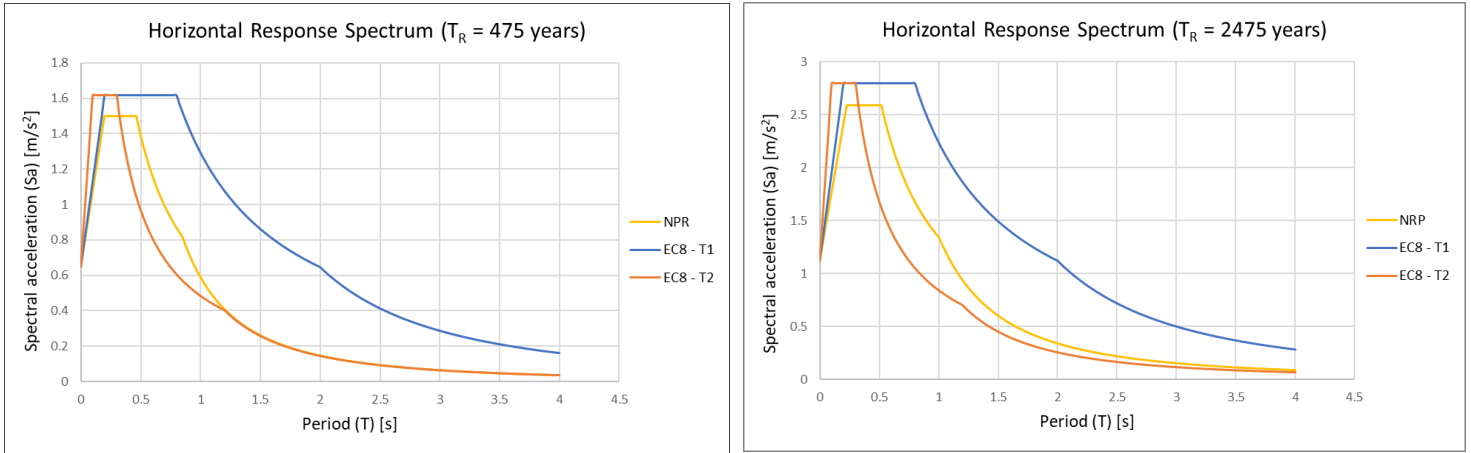


*Figure 6.3: Horizontal elastic response spectra for an earthquake with return period  $T_R=475$  years (left) and  $T_R=2475$  years (right)*

It can be observed that the shape of the response spectrum defined by NPR 9998 Webtool corresponds better with the response spectrum Type 2 of the Eurocode. For that reason, it is decided to define the vertical elastic response spectrum of the structure according to the Type 2 response spectrum of the Eurocode 8, for which the vertical PGA is defined as  $\alpha_{vg}/\alpha_g=0.45$  and the soil parameter  $S=1$ . The parameters for the vertical response spectrum are summarized in *Table 6.4*.

Vertical elastic response spectra - EC8 - Type 2			
Parameters		TR = 475 years	TR = 2475 years
PGA	$\alpha_{vg}$ (g)	0.030	0.051
Damping factor	n (-)	1	1
Ratio	p (-)	3	3
Characteristic Periods	$T_B$ (s)	0.05	0.05
	$T_C$ (s)	0.15	0.15
	$T_D$ (s)	1.00	1.00

*Table 6.4: Vertical elastic response spectrum parameters*

For the vertical components of the seismic action the elastic response spectrum is defined by the following expressions [12]:

$$0 \leq T \leq T_B : S_{av}(T) = a_{vg} \cdot \left[ 1 + \frac{T}{T_B} \cdot (n \cdot p - 1) \right] \tag{6.10}$$

$$T_B \leq T \leq T_C : S_{av}(T) = a_{vg} \cdot n \cdot p \tag{6.11}$$

$$T_C \leq T \leq T_D : S_{av}(T) = a_{vg} \cdot n \cdot p \cdot \left[ \frac{T_C}{T} \right] \quad (6.12)$$

$$T_D \leq T \leq 4s : S_{av}(T) = a_{vg} \cdot n \cdot p \cdot \left[ \frac{T_C \cdot T_D}{T} \right] \quad (6.13)$$

The obtained vertical response spectra for both examined return periods according to Type 2 of the Eurocode 8 are illustrated in *Figure 6.4*.

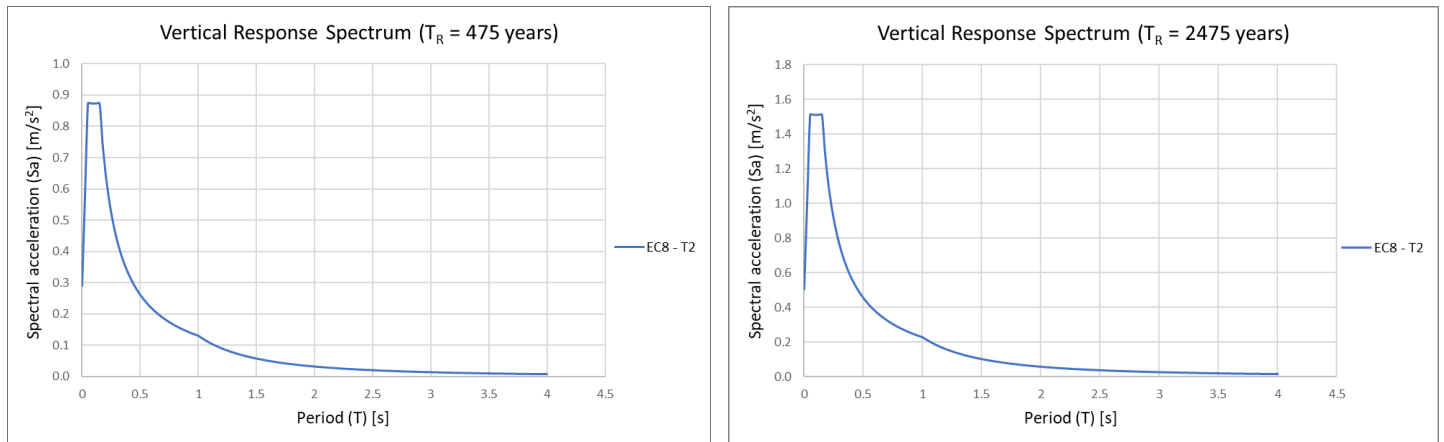


*Figure 6.4: Vertical elastic response spectra for an earthquake with return period  $T_R=475$  years (left) and  $T_R=2475$  years (right)*

## 6.2. Fundamental mode method

Initially, for the determination of the seismic resistance of the Nieuwklap bridge a simplified approach has been used, the fundamental mode method. According to this method, equivalent static forces are derived from the inertia forces corresponding to the fundamental mode and natural period of the structure in every direction which is examined, by using the site-dependent response spectrum. Simplifications regarding the shape of the first mode and the estimation of the fundamental period have been considered.

### 6.2.1. Vertical component

In order to apply this method for the vertical component of the seismic excitation on the bridge deck some simplifications have been taken into account. First, the deck of the Nieuwklap bridge has been considered as a continuous beam exactly as the model presented in *Paragraph 4.1.1* and with the same supporting conditions. The mass is assumed to be concentrated in the middle of each span, which is a conservative estimation, in particular for the bending moments, due to the fact that the equivalent vertical static forces will be applied on these flexure critical positions.

Concerning the stiffness derivation, vertical unit forces have been applied in the middle position of every span, at the point of the mass concentration, and the obtained vertical displacements  $u_{z(F_z=1)}$  have been found.

$$K_{z,i} = \frac{F_z(=1)}{u_{z,i}} \quad (6.14)$$

Afterwards, the fundamental natural period of each span has been calculated by using its mass:

$$T_{z,i} = 2\pi \cdot \sqrt{\frac{m_i}{K_{z,i}}} \quad (6.15)$$

Then, by obtaining the corresponding value from the vertical elastic response spectrum (*Figure 6.4*), the equivalent vertical static forces have been found, for both examined return periods:

$$F_{z,i} = m_i \cdot S_{av}(T_{z,i}) \quad (6.16)$$

The obtained data are summarized in *Table 6.5* for both cases:

Equivalent vertical static forces					
Position		Span 1 & Span 7	Span 2 & Span 6	Span 3 & Span 5	Span 4
Stiffness	K (kN/m)	357515	251423	247967	247740
Mass	m (ton)	153.06	193.24	193.24	193.24
Fundamental period	T (s)	0.130	0.174	0.175	0.175
T <sub>R</sub> = 475 years					
Spectral acceleration	S <sub>av</sub> (m/s <sup>2</sup> )	0.873	0.752	0.748	0.748
Vertical static force	F <sub>v</sub> (kN)	133.58	145.38	144.55	144.55
T <sub>R</sub> = 2475 years					
Spectral acceleration	S <sub>av</sub> (m/s <sup>2</sup> )	1.511	1.303	1.295	1.295
Vertical static force	F <sub>v</sub> (kN)	231.28	251.72	250.28	250.28

*Table 6.5: Equivalent vertical static forces*

The equivalent vertical forces have been applied on the bridge deck with three alternative ways, estimating the fundamental mode shapes, which are illustrated in *Figure 6.5*.

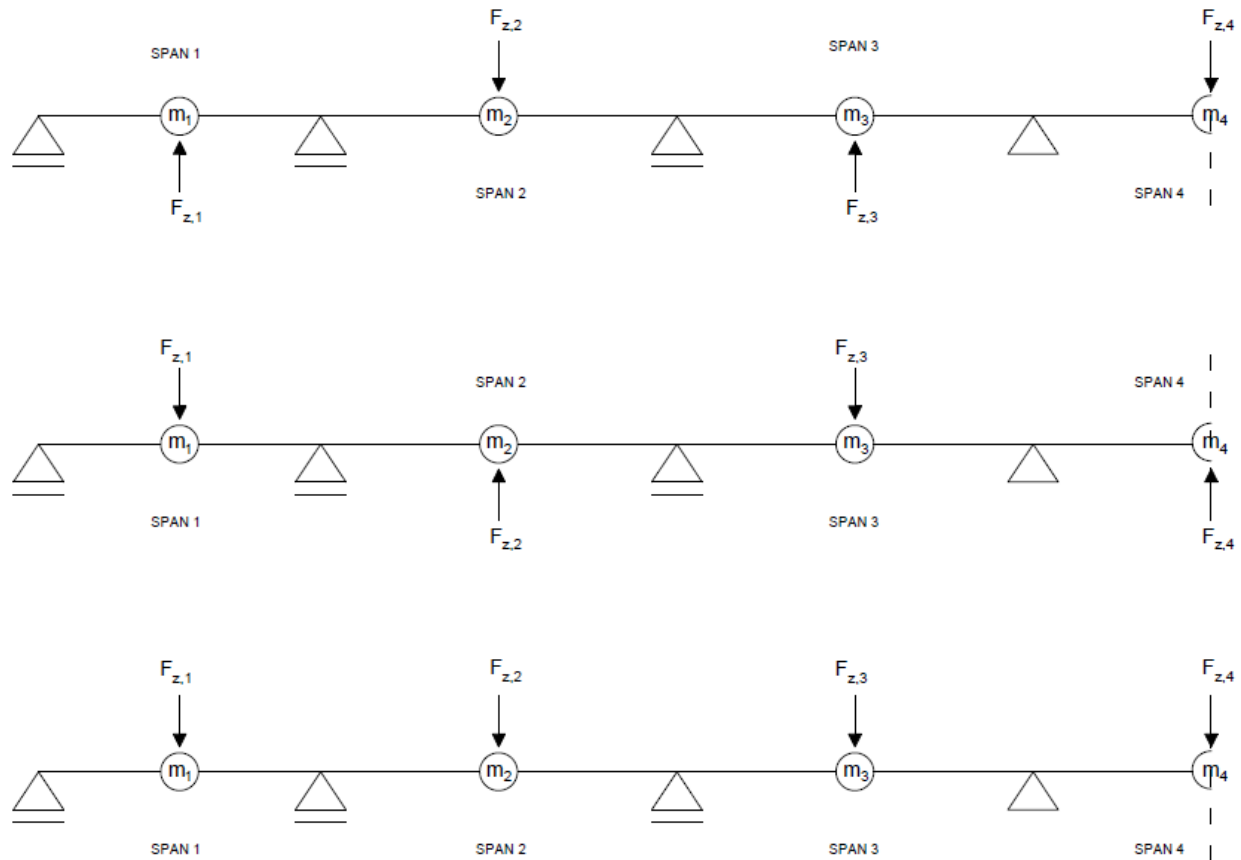


Figure 6.5: Equivalent vertical static forces alternative applications

The effect of the vertical seismic action  $E_z$  has to be evaluated by taking into account the presence of all the other loads that are exerted on the structure and have been described in *Paragraph 4.1.2*, by the following load combination [14]:

$$U = SW + SD + \psi_{E,LL} \cdot LL + E_z \quad (6.17)$$

The combination coefficient  $\psi_{E,LL}$  takes into account the likelihood of the traffic loading not being present over the entire bridge deck during the earthquake and according to EN 1998-2:2005 [13] it is for the LM1 on road bridges equal to:  $\psi_{E,LL} = 0.2$

From the three alternative ways of application of the vertical seismic excitation (*Figure 6.5*), the maximum resulted cross-section forces, for the presented load combination, are summarized in *Table 6.6*. The examined positions are the same as depicted in *Figure 4.3*.

Then, a “Unity Check” has been performed, corresponding to the capacity calculated in *Paragraph 4.1.3*, in order to evaluate the Nieuwklap bridge deck with regards to its earthquake resistance (*Table 6.7*).

VERTICAL SEISMIC LOADING						
LOADING POSITION	1	2	3	4	5	6
	FLEXURE CRITICAL		SHEAR CRITICAL			
$T_R = 475$ years						
LOAD = SW + SD + 0.2*(UDL + TS) + Ez						
$M_{Ed,span}$ (kNm/m)	273.61	281.85	254.04	248.24	251.78	250.67
$M_{Ed,sup}$ (kNm/m)	-366.09	-386.15	-363.99	-369.82	-372.09	-382.64
$V_{Ed}$ (kN/m)	160.59	-158.71	-109.89	170.61	-169.86	170.19
$T_R = 2475$ years						
LOAD = SW + SD + 0.2*(UDL + TS) + Ez						
$M_{Ed,span}$ (kNm/m)	311.11	324.16	291.55	285.74	294.09	292.99
$M_{Ed,sup}$ (kNm/m)	-389.88	-409.95	-387.79	-393.62	-395.89	-405.09
$V_{Ed}$ (kN/m)	168.64	-165.25	-116.59	178.65	-177.07	176.54

Table 6.6: Vertical seismic loading - Fundamental mode method

UNITY CHECKS						
LOADING POSITION	1	2	3	4	5	6
	FLEXURE CRITICAL		SHEAR CRITICAL			
$T_R = 475$ years						
UNITY CHECK (LOAD/DESIGN CAPACITY)						
$UC_{M,span}$	0.41	0.43	0.38	0.37	0.39	0.39
$UC_{M,sup}$	0.44	0.46	0.43	0.44	0.44	0.46
$UC_{V,EC}$	0.24	0.24	0.16	0.25	0.25	0.25
$T_R = 2475$ years						
UNITY CHECK (LOAD/DESIGN CAPACITY)						
$UC_{M,span}$	0.47	0.50	0.44	0.43	0.45	0.45
$UC_{M,sup}$	0.47	0.49	0.46	0.47	0.47	0.48
$UC_{V,EC}$	0.25	0.25	0.17	0.26	0.26	0.26

Table 6.7: Unity Check - Vertical seismic loading - Fundamental mode method

From the “Unity Check”, it can be observed that the Nieuwklap bridge has sufficient shear and bending moment capacity to withstand the vertical seismic excitation, for both examined return periods. In specific the “Unity Check” for bending moment never exceeds the 0.50 value, even for the flexure critical positions, and the “Unity Check” for shear force is smaller than 0.26 for all the examined loading scenarios.

### 6.2.2. Horizontal components

The fundamental mode method for the horizontal components of the seismic excitation has been applied by using the rigid deck model approach, according to EN 1998-2:2005 [13]. This approach is considered suitable for the longitudinal direction of straight bridges with continuous deck, and for the transverse direction of symmetric rigid decks, where small movements of the pier tops can be observed. Therefore, because these requirements are fulfilled by the Nieuwklap bridge, the above-mentioned approach has been selected.

At first, in order to derive the equivalent horizontal forces acting on the structure in the longitudinal and in the transverse direction, the stiffnesses of the resisting members have to be calculated. Regarding the longitudinal direction, it can be stated that, the total effect of the seismic excitation

is carried from the two middle piers, where the connection between them and the deck does not allow translation in any horizontal direction. However, in the transverse direction, except from the middle piers, the seven pendulums located over each pier, contribute significantly to the seismic resistance of the bridge. In order to calculate the stiffness of the pier and the pendulum, it has been assumed that they are clamped on the ground and the below-piers respectively. The side and the front view of a middle-pier and a pendulum are illustrated in *Figure 6.6*.

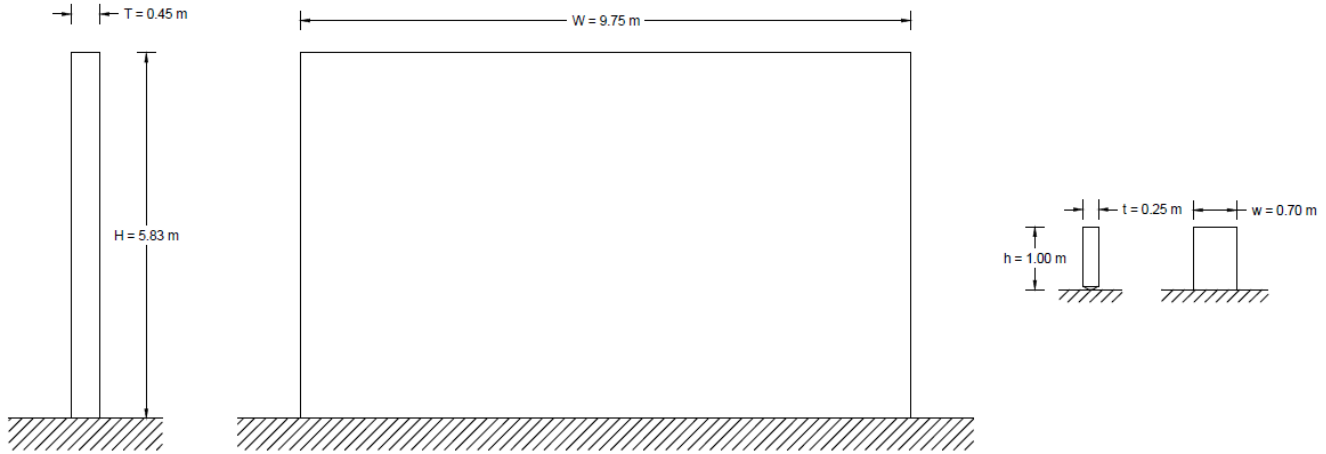


Figure 6.6: Side and front-view of a middle-pier (left) and a pendulum (right) with dimensions (m)

The bending stiffness of the pier in the longitudinal direction can be obtained:

$$K_{x,pier} = \frac{3 \cdot E_c \cdot I_y}{H^3} \quad (6.18)$$

The stiffnesses of the pier and of a single pendulum, due to the contribution of bending and shear can be calculated:

$$K_{y,pier} = \frac{E_c \cdot T}{4 \cdot \left(\frac{H}{W}\right)^3 + 1.2 \cdot \left[2 \cdot (1 + \nu) \cdot \left(\frac{H}{W}\right)\right]} \quad (6.19)$$

$$K_{y,pendulum} = \frac{E_c \cdot t}{4 \cdot \left(\frac{h}{w}\right)^3 + 1.2 \cdot \left[2 \cdot (1 + \nu) \cdot \left(\frac{h}{w}\right)\right]} \quad (6.20)$$

Finally, the total stiffnesses of the Nieuwklap bridge in the longitudinal direction and in the transverse direction are:

$$K_{x,total} = 2 \cdot K_{x,pier} \quad (6.21)$$

$$K_{y,total} = 2 \cdot K_{y,pier} + 6 \cdot (7 \cdot K_{y,pendulum}) \quad (6.22)$$

Then, the fundamental periods in both directions can be obtained by using the total effective mass of the structure, equal to the mass of the deck plus the mass of the upper half of the piers.

$$T_x = 2\pi \cdot \sqrt{\frac{M}{K_{x,total}}} \quad \& \quad T_y = 2\pi \cdot \sqrt{\frac{M}{K_{y,total}}} \quad (6.23)$$

Finally, the applying equivalent horizontal static forces can be found by obtaining the corresponding values from the horizontal elastic response spectrum (*Figure 6.3*).

$$F_x = M \cdot S_a(T_x) \quad \& \quad F_y = M \cdot S_a(T_y) \quad (6.24)$$

The obtained data are summarized in *Table 6.8* for both return periods.

Equivalent horizontal static forces			
Direction		Longitudinal	Transverse
Stiffness pier	K (kN/m)	35389	5670263
Stiffness pendulum	K (kN/m)	-	505792
Total stiffness	K (kN/m)	70777	32583785
Mass	M (ton)	1337.48	1337.48
Fundamental period	T (s)	0.864	0.040
$T_R = 475$ years			
Spectral acceleration	$S_a$ (m/s <sup>2</sup> )	0.791	0.819
Horizontal static force	$F_h$ (kN)	1058.14	1095.05
$T_R = 2475$ years			
Spectral acceleration	$S_a$ (m/s <sup>2</sup> )	1.551	1.379
Horizontal static force	$F_h$ (kN)	2074.24	1844.45

*Table 6.8: Equivalent horizontal static forces*

Due to the fact that, the equivalent static force in the longitudinal direction is carried by the two middle piers, the cross-section shear force and the bending moment at the bottom of the pier can be easily obtained:

$$V_{Ed,x,pier} = \frac{F_x}{2} [kN] \quad \& \quad M_{Ed,y,pier} = \frac{F_x}{2} \cdot H [kNm] \quad (6.25)$$

The horizontal breaking and acceleration forces due to traffic loading [3], acting in the longitudinal direction, have not been considered, since their contribution found to be insignificant comparing with the corresponding seismic excitation.

In the transverse direction the equivalent horizontal static force can be distributed along the bridge deck, proportionally to the distribution of the mass. Since the mass of the deck is evenly distributed along the length  $L$  of the bridge, the equivalent distributed lateral force is:

$$q_y = \frac{F_y}{L} \text{ [kN/m]} \tag{6.26}$$

By applying this distributed force, the reaction forces in the transverse direction can be found by using the structural software SAP2000. The top view of the static scheme of the distributed lateral load application is illustrated in *Figure 6.7*.

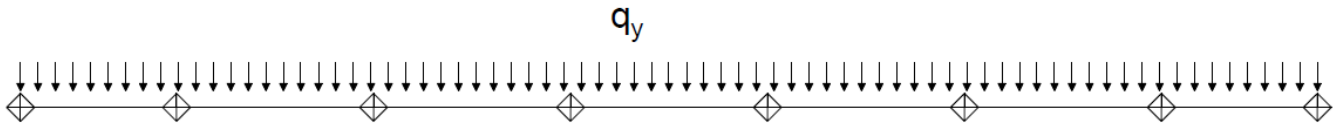


*Figure 6.7: Lateral load application static scheme - Top view*

The maximum cross-section forces can be obtained for the middle-pier and the pendulums respectively, assuming that this force is evenly distributed among the 7 pendulums of each pier:

$$V_{Ed,y, pier} = R_{y,i} \text{ [kN]} \quad \& \quad M_{Ed,x, pier} = R_{y,i} \cdot H \text{ [kNm]} \tag{6.27}$$

$$V_{Ed,y, pendulum} = \frac{R_{y,i}}{7} \text{ [kN]} \quad \& \quad M_{Ed,x, pendulum} = \frac{R_{y,i}}{7} \cdot h \text{ [kNm]} \tag{6.28}$$

The resulted cross-section forces, due to the horizontal seismic excitation in both directions and for both examined return periods are listed in *Table 6.6*.

HORIZONTAL SEISMIC LOADING				
DIRECTION	LONGITUDINAL (Ex)		TRANSVERSE (Ey)	
	PIER	PENDULUM	PIER	PENDULUM
<b>T<sub>R</sub> = 475 years</b>				
M <sub>Ed</sub> (kNm)	3084.48	-	968.71	23.84
V <sub>Ed</sub> (kN)	529.07	-	166.16	23.84
<b>T<sub>R</sub> = 2475 years</b>				
M <sub>Ed</sub> (kNm)	6046.41	-	1631.88	40.16
V <sub>Ed</sub> (kN)	1037.12	-	279.91	40.16

*Table 6.9: Horizontal seismic loading - Fundamental mode method*

In the longitudinal direction the static equivalent forces are acting out-of-plane on the piers and they are much higher than in the longitudinal direction. Concerning this fact, in order to identify if the structure is able to withstand the horizontal seismic loading the shear and the bending moment capacity of the pier only in the longitudinal direction will be calculated. Regarding the transverse direction of the seismic excitation, since the bridge is supported by shear walls, which are earthquake resistant elements it has been assumed that their capacity is sufficient against the exerted static equivalent in-plane forces and the derivation of their resistance by using a strut-and-tie model is considered out of the scope of the current project. For that reason, only the resistance of the pendulums will be calculated in the transverse direction.

The formulas presented in *Paragraph 4.1.3* have been used, for the ultimate bending moment capacity and the shear capacity estimation, without taking into account the vertical axial forces, which are contributing positively to the shear resistance. The characteristic material properties (*Table 3.2, Table 3.3*) have been considered and the reinforcement layout has been obtained from the given structural plans (*Appendix A*). The bending moment and the shear capacity of a middle-pier out-of-plane and of a single pendulum are listed in *Table 6.10*.

Then, a “Unity Check” has been performed, in order to evaluate the supports of Nieuwklap bridge regarding their earthquake resistance.

Capacity			
Parameters		Pier (Longitudinal)	Pendulum (Transverse)
Reinforcement area	$A_s$ (mm <sup>2</sup> /m)	20944	9852
Reinforcement ratio	$\rho_l$ (%)	4.65	1.41
Shear capacity			
Design shear stress capacity	$V_{Rd,c}$ (MPa)	1.339	0.816
Minimum shear stress capacity	$V_{min}$ (MPa)	1.258	1.089
Design shear capacity	$V_{Rd,c}$ (kN)	5222.03	179.67
Bending moment capacity			
Ultimate moment capacity	$M_{ud}$ (kNm)	7122.47	151.57

*Table 6.10: Shear and bending moment capacity of middle-pier out-of-plane and pendulum*

UNITY CHECKS		
DIRECTION	LONGITUDINAL (Ex)	TRANSVERSE (Ey)
	PIER	PENDULUM
$T_R = 475$ years		
UC <sub>M</sub>	0.43	0.16
UC <sub>V</sub>	0.10	0.13
$T_R = 2475$ years		
UC <sub>M</sub>	0.85	0.26
UC <sub>V</sub>	0.20	0.22

*Table 6.11: Unity Check - Horizontal seismic loading - Fundamental mode method*

It can be observed that the supports of the Nieuwklap bridge have sufficient shear and bending moment capacity to withstand the horizontal seismic excitation, for both examined return periods.

### 6.3. Modal response spectrum analysis

In order to describe more accurately the seismic behaviour of the Nieuwklap Bridge, a linear dynamic analysis has been applied, which is called response spectrum analysis. By using this method, the peak dynamic responses of all significant modes of the structure can be calculated. The overall response of the structure is obtained by statistical combination of the maximum modal contributions [13].

For the evaluation of the Nieuwklap bridge two different models have been constructed by using the structural software SAP2000. In both idealizations the slab part of the bridge has been considered as a continuous beam as *Paragraph 4.1.1*. The substantial difference with the previous constructed models is the replication of the supporting conditions, due to the fact that, by applying rigid supports the global seismic response of the bridge cannot be described realistically. For that reason, two alternatives were adopted; in the first one, the supports have been represented as springs with translation stiffness in both horizontal directions, equal to the one calculated in the previous paragraph (*Table 6.8*), and in the second one a 3D model of the bridge, by modelling also the piers of the structure, has been constructed. The model with the spring supports is depicted in *Figure 6.8* and the model, in which the piers have been modelled in *Figure 6.9*.

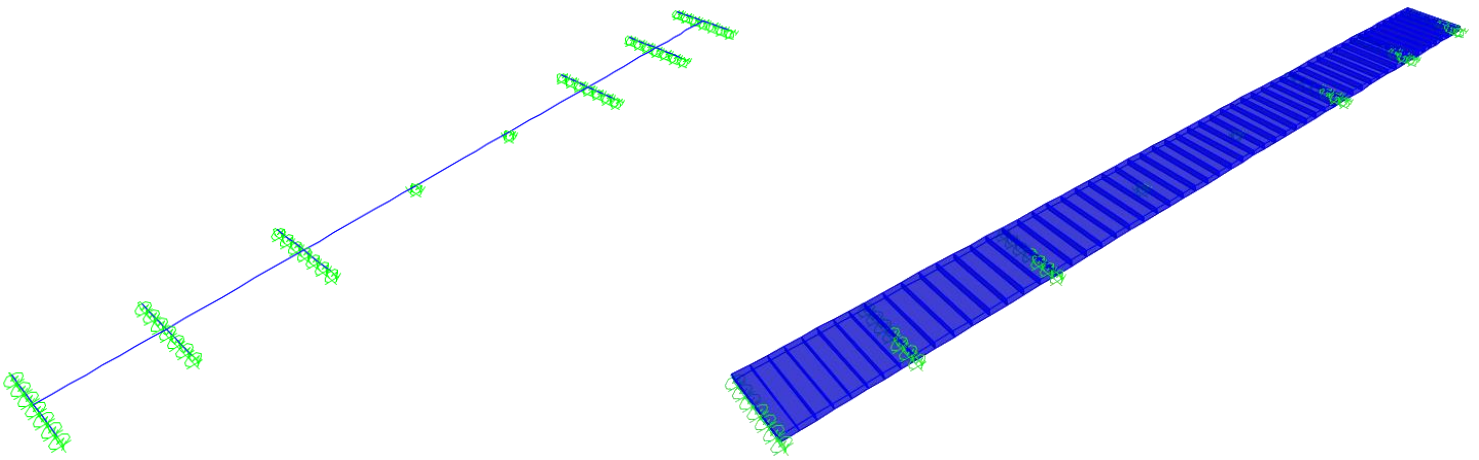


Figure 6.8: Model with spring supports - Standard view (left) and Extrude view (right)

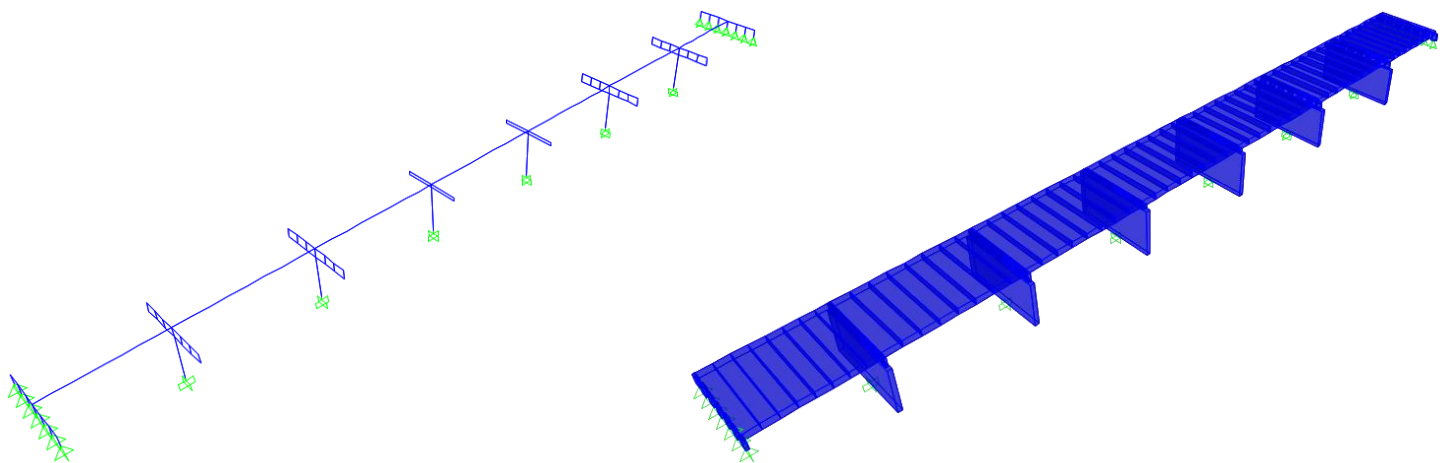


Figure 6.9: Model with piers - Standard view (left) and Extrude view (right)

### 6.3.1. Modal analysis

Initially, all the modes with significant contribution to the total structural response have to be taken into account, which means that all the modes with a mass participation over 5% of the total mass of the structure have to be considered. The sum of these effective modal masses ( $m_i$ ) has to be at least 90% of the total mass ( $M$ ) in all the relevant, for the model, directions. So, the condition is:

$$\sum_{i=1}^N m_i \geq 0.9 \cdot M \quad (6.29)$$

For the combination of the modal responses the method of the Complete Quadratic Combination (CQC) has been considered, which is a more accurate procedure for the prediction of the probable maximum value  $E$  of a seismic action effect, estimating the likelihood of the peak response and not the peak response itself. It is expressed as:

$$E = \sqrt{\sum_i \sum_j E_i \cdot r_{ij} \cdot E_j} \quad (6.30)$$

In addition, due to the simultaneous occurrence of all the directional components of the seismic action, the probable maximum action effect can be estimated by applying the SRSS (Square Root of the Sum of Squares) rule to the maximum action effects  $E_x$ ,  $E_y$  and  $E_z$ :

$$E = \sqrt{E_x^2 + E_y^2 + E_z^2} \quad (6.31)$$

The response spectra for the vertical and the horizontal direction, have been already defined for both examined return periods in *Paragraph 6.1.2*

The modal participating mass ratios of the significant modes for both constructed models, regarding all degrees of freedom (translations and rotations), are presented in the following tables (*Table 6.12*, *Table 6.13*). The corresponding modal shapes are included in *Appendix E*.

MODAL PARTICIPATING MASS RATIOS - SPRING SUPPORTS							
Mode	T (s)	$u_x$	$u_y$	$u_z$	$r_x$	$r_y$	$r_z$
1	0.843	1	0	0	0	0	0
2	0.183	0	0	0.051	0	0	0
3	0.097	0	0	0.037	0	0	0
4	0.086	0	0	0	0	0.773	0
5	0.083	0	0	0.763	0	0	0
6	0.047	0	0	0	0	0.046	0
7	0.046	0	0	0	0	0	0.715
8	0.045	0	0.864	0	0	0	0
9	0.035	0	0	0	0	0	0.192
10	0.030	0	0.093	0	0	0	0
11	0.025	0	0	0	0	0	0.082
12	0.018	0	0	0	0	0.043	0
13	0.017	0	0	0.095	0	0	0
14	0.013	0	0	0	0	0.046	0
SUM (%)		100	96	95	0	91	99

Table 6.12: Modal participation mass ratios - Model with spring supports

MODAL PARTICIPATING MASS RATIOS - PIERS							
Mode	T (s)	$u_x$	$u_y$	$u_z$	$r_x$	$r_y$	$r_z$
1	0.867	0.921	0	0	0	0	0
2	0.183	0	0	0.053	0	0	0
3	0.135	0.051	0	0	0	0	0
4	0.088	0	0	0	0	0.638	0
5	0.086	0	0	0.617	0	0	0
6	0.048	0	0	0	0	0	0.695
7	0.047	0	0.862	0	0.666	0	0
8	0.044	0	0	0	0	0.037	0
9	0.041	0	0.022	0	0.020	0	0
10	0.035	0	0	0	0	0	0.182
11	0.029	0	0.077	0	0.068	0	0
12	0.022	0	0	0	0	0	0.080
13	0.021	0	0	0	0	0.056	0
14	0.021	0	0	0.076	0	0	0
15	0.019	0	0	0	0	0.049	0
16	0.018	0	0	0.097	0	0	0
17	0.015	0	0	0	0	0.080	0
18	0.010	0	0	0.061	0	0	0
19	0.009	0	0.019	0	0.040	0	0
20	0.007	0	0	0	0	0.026	0
21	0.005	0	0	0	0.035	0	0
22	0.005	0	0	0	0.018	0	0
23	0.005	0	0	0	0.035	0	0
24	0.005	0	0	0	0	0.033	0
25	0.005	0	0	0	0.014	0	0
SUM (%)		97	98	90	90	92	96

Table 6.13: Modal participation mass ratios - Model with piers

It can be seen that, less modes are necessary in order to describe the behaviour of the simplified model with the spring supports, since the condition for the mass participation is met earlier. In addition, the rotation around the longitudinal axis of the bridge cannot be described, if the piers have not been modelled.

### 6.3.2. Seismic action

For the seismic evaluation of the Nieuwklap bridge, the vertical and horizontal components of the occurring earthquake have to be combined. Therefore, for the computation of the action effects the following combinations of seismic components can be defined, one for each direction:

$$\begin{aligned}
 E_{z,comb} &= E_z \quad + \quad 0.3 \cdot E_x \quad + \quad 0.3 \cdot E_y \\
 E_{x,comb} &= 0.3 \cdot E_z \quad + \quad E_x \quad + \quad 0.3 \cdot E_y \\
 E_{y,comb} &= 0.3 \cdot E_z \quad + \quad 0.3 \cdot E_x \quad + \quad E_y
 \end{aligned}
 \tag{6.32}$$

Finally, in order to combine the seismic action with the other exerted loads, as described in *Paragraph 6.2.1* for the vertical component, three combinations have been taken into account, by using the elastic response spectra defined in *Paragraph 6.1.2*:

$$\begin{aligned}
 U_z &= SW + SD + 0.2 \cdot LL + E_{z,comb} \\
 U_x &= SW + SD + 0.2 \cdot LL + E_{x,comb} \\
 U_y &= SW + SD + 0.2 \cdot LL + E_{y,comb}
 \end{aligned}
 \tag{6.33}$$

The maximum generated cross-section forces of the bridge deck from the vertical seismic excitation ( $U_z$ ) for the presented load combination, are listed in Table 6.14. The examined cases, regarding the position where the concentrated Tandem system loading is applied, are the same as depicted in *Figure 4.3*.

VERTICAL SEISMIC LOADING						
LOADING POSITION	1	2	3	4	5	6
	FLEXURE CRITICAL			SHEAR CRITICAL		
$T_R = 475$ years						
$U_z = SW + SD + 0.2 \cdot (UDL + TS) + E_{z,comb}$						
$M_{Ed,span}$ (kNm/m)	239.83	236.68	220.26	214.45	206.61	205.50
$M_{Ed,sup}$ (kNm/m)	-356.21	-376.27	-354.11	-359.94	-362.21	-371.25
$V_{Ed}$ (kN/m)	158.34	-156.56	-106.67	168.35	-166.70	168.30
$T_R = 2475$ years						
$U_z = SW + SD + 0.2 \cdot (UDL + TS) + E_{z,comb}$						
$M_{Ed,span}$ (kNm/m)	252.62	246.03	233.06	227.25	215.96	214.86
$M_{Ed,sup}$ (kNm/m)	372.77	392.84	370.68	376.50	378.78	385.37
$V_{Ed}$ (kN/m)	164.73	161.52	111.01	174.75	171.60	173.26

Table 6.14: Vertical seismic loading - Response spectrum analysis

Afterwards, the results of the “Unity Check” are presented (Table 6.15), where the earthquake resistance of the bridge deck is verified.

UNITY CHECKS						
LOADING POSITION	1	2	3	4	5	6
	FLEXURE CRITICAL			SHEAR CRITICAL		
$T_R = 475$ years						
UNITY CHECK (LOAD/DESIGN CAPACITY)						
$UC_{M,span}$	0.36	0.36	0.33	0.32	0.32	0.32
$UC_{M,sup}$	0.43	0.45	0.42	0.43	0.43	0.44
$UC_{V,EC}$	0.23	0.23	0.16	0.25	0.25	0.25
$T_R = 2475$ years						
UNITY CHECK (LOAD/DESIGN CAPACITY)						
$UC_{M,span}$	0.38	0.38	0.35	0.34	0.33	0.33
$UC_{M,sup}$	0.45	0.47	0.44	0.45	0.45	0.46
$UC_{V,EC}$	0.24	0.24	0.16	0.26	0.25	0.26

Table 6.15: Unity Check - Vertical seismic loading - Response spectrum analysis

Moreover, the generated forces and bending moments, on the middle piers and the pendulums supporting the deck of the Nieuwklap bridge, due to the horizontal seismic combinations and for

both return periods, can also be found for the two constructed models. In regards with the model in which the spring supports have been applied, the procedure in order to find the cross-section forces through the reaction forces is similar to the one described in *Paragraph 6.2.2* for the simplified approach. For the model, in which the piers have been modelled, the results are obtained directly from the software. In the following tables the resulting shear forces and bending moments are presented for the longitudinal (*Table 6.16*) and the transverse (*Table 6.18*) seismic load combination. Additionally, the corresponding “Unity Check” is depicted for both cases. More specifically, the “Unity Check” has been performed, regarding the bending moment and shear capacity of the middle-piers out of their plane ( $M_{Ed,y}$ ,  $V_{Ed,x}$ ) and the capacity of a single pendulum in the transverse direction ( $M_{Ed,x}$ ,  $V_{Ed,y}$ ), for both horizontal seismic combinations (*Table 6.17*, *Table 6.19*).

LONGITUDINAL SEISMIC LOADING				
MODEL	SPRING SUPPORTS		PIERS	
	PIER	PENDULUM	PIER	PENDULUM
$U_x = SW + SD + 0.2*(UDL + TS) + Ex,comb$				
$T_R = 475$ years				
$M_{Ed,y}$ (kNm)	3060.40	-	3083.02	-
$M_{Ed,x}$ (kNm)	229.63	7.25	286.46	19.24
$V_{Ed,x}$ (kN)	524.94	-	530.38	-
$V_{Ed,y}$ (kN)	39.39	7.25	49.25	9.08
$T_R = 2475$ years				
$M_{Ed,y}$ (kNm)	5895.24	-	6061.56	-
$M_{Ed,x}$ (kNm)	386.02	12.13	480.69	22.10
$V_{Ed,x}$ (kN)	1011.19	-	1042.78	-
$V_{Ed,y}$ (kN)	66.21	12.13	82.64	15.18

Table 6.16: Longitudinal seismic loading - Response spectrum analysis

UNITY CHECKS				
MODEL	SPRING SUPPORTS		PIERS	
	PIER (Longitudinal)	PENDULUM (Transverse)	PIER (Longitudinal)	PENDULUM (Transverse)
$T_R = 475$ years				
$UC_M$	0.43	0.05	0.43	0.13
$UC_V$	0.10	0.05	0.10	0.05
$T_R = 2475$ years				
$UC_M$	0.83	0.08	0.85	0.15
$UC_V$	0.19	0.07	0.20	0.08

Table 6.17: Unity Check - Longitudinal seismic loading - Response spectrum analysis

TRANSVERSE SEISMIC LOADING				
MODEL	SPRING SUPPORTS		PIERS	
	PIER	PENDULUM	PIER	PENDULUM
$U_y = SW + SD + 0.2*(UDL + TS) + E_{y,comb}$				
$T_R = 475$ years				
$M_{Ed,y}$ (kNm)	918.12	-	924.91	-
$M_{Ed,x}$ (kNm)	765.43	24.16	954.87	28.55
$V_{Ed,x}$ (kN)	157.48	-	159.11	-
$V_{Ed,y}$ (kN)	131.29	24.16	164.15	30.19
$T_R = 2475$ years				
$M_{Ed,y}$ (kNm)	1768.57	-	1818.47	-
$M_{Ed,x}$ (kNm)	1286.74	40.44	1602.29	37.71
$V_{Ed,x}$ (kN)	303.36	-	312.83	-
$V_{Ed,y}$ (kN)	220.71	40.44	275.45	50.63

Table 6.18: Transverse seismic loading - Response spectrum analysis

UNITY CHECKS				
MODEL	SPRING SUPPORTS		PIERS	
	PIER (Longitudinal)	PENDULUM (Transverse)	PIER (Longitudinal)	PENDULUM (Transverse)
$T_R = 475$ years				
$UC_M$	0.13	0.16	0.13	0.19
$UC_V$	0.03	0.13	0.03	0.17
$T_R = 2475$ years				
$UC_M$	0.25	0.27	0.26	0.25
$UC_V$	0.06	0.23	0.06	0.28

Table 6.19: Unity Check - Transverse seismic loading - Response spectrum analysis

It can be clearly observed that the Nieuwklap bridge has sufficient resistance against both horizontal seismic combinations. The highest value of the “Unity Check” is observed for the out of plane bending of the middle pier under longitudinal seismic excitation, which was expected, due to the fact that this earthquake component is carried exclusively by this vertical structural element. Furthermore, it is worth to be mentioned that there are no significant deviations between the values obtained from both models.

## 6.4. Discussion - Conclusions

In this chapter, the Nieuwklap bridge was evaluated regarding its earthquake resistance by using the fundamental mode method and a modal response spectrum analysis.

Initially, for the specification of the vertical elastic response spectrum it can be identified that for the location of the bridge the horizontal response spectrum Type 2 according to Eurocode 8 corresponds better to the uniform hazard spectrum of the area and for that reason this type has to be selected for the vertical seismic excitation.

Furthermore, by performing “Unity Checks” for the vertical seismic load combination, with both methods and for both examined return periods, it can be concluded that the bridge deck can

withstand easily the acting seismic forces, which cannot be considered as a critical load combination (*Table 6.20*).

UNITY CHECK COMPARISON - VERTICAL SEISMIC LOADING						
LOADING POSITION	1		3		5	
	FLEXURE CRITICAL		SHEAR CRITICAL (END-SUPPORT)		SHEAR CRITICAL (MID-SUPPORT)	
APPROACH	Fundamental mode method	Response spectrum analysis	Fundamental mode method	Response spectrum analysis	Fundamental mode method	Response spectrum analysis
<b><math>T_R = 475</math> years</b>						
<b>UNITY CHECK (LOAD/DESIGN CAPACITY)</b>						
$UC_{M,span}$	0.41	0.36	0.38	0.33	0.39	0.32
$UC_{M,sup}$	0.44	0.43	0.43	0.42	0.44	0.43
$UC_{V,EC}$	0.24	0.23	0.16	0.16	0.25	0.25
<b><math>T_R = 2475</math> years</b>						
<b>UNITY CHECK (LOAD/DESIGN CAPACITY)</b>						
$UC_{M,span}$	0.47	0.38	0.44	0.35	0.45	0.33
$UC_{M,sup}$	0.47	0.45	0.46	0.44	0.47	0.45
$UC_{V,EC}$	0.25	0.24	0.17	0.16	0.26	0.25

*Table 6.20: Unity Check comparison - Vertical seismic loading*

Likewise, regarding the horizontal seismic excitation, the evaluation of the bridge middle-piers and pendulum supports with both the fundamental mode method and the response spectrum analysis, proves that this type of structures are able to withstand earthquake loading acting in both horizontal directions (*Table 6.21*).

UNITY CHECK COMPARISON - HORIZONTAL SEISMIC LOADING						
DIRECTION	LONGITUDINAL (Ex)			TRANSVERSE (Ey)		
	PIER			PENDULUM		
APPROACH	Fundamental mode method	Response spectrum analysis (Spring supports)	Response spectrum analysis (Piers)	Fundamental mode method	Response spectrum analysis (Spring supports)	Response spectrum analysis (Piers)
<b><math>T_R = 475</math> years</b>						
<b>UNITY CHECK (LOAD/DESIGN CAPACITY)</b>						
$UC_M$	0.43	0.43	0.43	0.16	0.16	0.19
$UC_V$	0.10	0.10	0.10	0.13	0.13	0.17
<b><math>T_R = 2475</math> years</b>						
<b>UNITY CHECK (LOAD/DESIGN CAPACITY)</b>						
$UC_M$	0.85	0.83	0.85	0.26	0.27	0.25
$UC_V$	0.20	0.19	0.20	0.22	0.23	0.28

*Table 6.21: Unity Check comparison - Horizontal seismic loading*

Comparing the results from the fundamental mode method and the two models that were used for the modal response spectrum analysis important information can be obtained. At first, it can be observed that the resulting generated forces and bending moments have similar values, with the simplified approach to be slightly conservative, as expected, particularly regarding the sagging bending moments.

Moreover, in *Table 6.22* the acquired fundamental periods for each direction of the seismic excitation, for all the constructed models, have been summarized and it is evident that there are not significant differences between the resulting values. Therefore, it can be concluded that the

fundamental mode method is a quite accurate estimation of the seismic behaviour of the Nieuwklap bridge.

FUNDAMENTAL PERIODS (s)			
MODEL	Longitudinal	Transverse	Vertical
Simplified approach	0.864	0.040	0.130 - 0.175
Springs supports	0.843	0.045	0.183
Piers	0.867	0.048	0.183

*Table 6.22: Fundamental period for each direction of seismic excitation*

Finally, comparing the two models constructed for the modal analysis, it can be deduced that both of them are describing accurately the real problem. By modelling the piers, a better sense of the bridge seismic behaviour and its modal shapes can be gained, but on the other hand, by using suitable spring supports, significant computational time can be saved.

# 7 Conclusions and Recommendations

In this chapter, the conclusions derived from the presented research are listed down, with regards to the problem definition and the project objectives that have been introduced in the first chapter, followed by recommendations for further studies.

In the course of this research, two main objectives have been formulated. At first, an accurate prediction of the dominant failure mode of the Nieuwklap bridge under collapse testing has been considered of great importance, in order to achieve also a better estimation of the more possible failure mode of other existing reinforced concrete solid slab bridges in the Netherlands with similar characteristics. Then, because of the increased seismic activity in the Groningen area, the earthquake-resistance evaluation of the Nieuwklap bridge has been regarded essential in order to assess bridges that have been constructed without taking the earthquake factor into account and are located in seismic active zones.

## 7.1. Conclusions

The following conclusions can be derived from the performed static analysis of the Nieuwklap bridge, by using the first two Levels of Assessment.

- The Nieuwklap bridge has sufficient shear capacity against all the load combinations, defined by RBK, and the traffic loading (LM1), defined by Eurocode 2, for all the examined shear- and flexure-critical loading scenarios. However, it is proven to have borderline insufficient bending moment capacity when the concentrated loads are applied on the flexure-critical positions and the design load combination is used. Therefore, since it meets the requirements for usage and reconstruction limit states, it can be stated that the Nieuwklap bridge is able to withstand the loads specified according to the current standards, fulfilling the code requirements.
- Considering only the plate part of the deck of the Nieuwklap bridge, it can be deduced that under a collapse loading test, flexural failure, due to yielding of the reinforcement, will occur first for experimental loading applied on the flexure-critical positions and on the shear-critical position, which is located next to the end-supports of the bridge. Regarding the shear-critical loading scenarios next to a continuous support, the dominant failure mode under collapse testing is unclear. Concerning these observations, it can be concluded that, if the whole geometry of the deck is taken into account, including the edge beams and the bent-up bars located at the shear critical areas, shear failure is not likely possible to occur before yielding of the longitudinal reinforcement, even for loading applied

at the shear-critical positions. The most likely possible scenario is that shear cracks will make their appearance in the concrete and then the occurring shear stresses will be transferred to the existing bent-up bars of the reinforcement, preventing a brittle shear failure.

- Comparing the loading type that will be applied during the field experiment with the Eurocode loading, it can be deduced that more intense localized phenomena are caused by the experimental loading, since higher stresses are generated in the areas where the tandem loads are applied. In addition, the increase of the torsional moment contribution is found to be around 6%, when the field loading is exerted on the structure compared to the loading type that the Eurocode defines.
- The use of an analytical approach for the evaluation of the Nieuwklap bridge can be useful in case of limited computational time, underestimating the generated stresses by approximately 10%, but not affecting the final result. On the other hand, the specification of equivalent magnitudes for proof loading and failure loading is more complicated, using estimations for the determination of the effective shear width. However, with both approaches the same failure mode has been predicted under collapse testing of the Nieuwklap bridge for the different loading scenarios.

From the seismic evaluation of the Nieuwklap bridge, by using linear-static and a linear-dynamic (modal) analysis, the following conclusions can be derived.

- The Nieuwklap bridge has adequate earthquake resistance against vertical and horizontal seismic excitation, even for earthquakes with a return period of 2475 years. In specific, the vertical seismic load combination, defined by Eurocode 8, is found to be not critical regarding the shear and bending moment capacity of the bridge deck, generating almost half the stresses compared with the traffic loading (LM1) defined by Eurocode 2. In addition, the piers and the pendulums, supporting the bridge, are able to withstand the horizontal seismic excitation in both the longitudinal and the transverse direction for both examined earthquake return periods.
- For the specification of the vertical elastic response spectrum, the response spectrum Type 2 according to Eurocode 8, is suitable for bridges located in the same area as the Nieuwklap bridge, since it corresponds better to the provided horizontal uniform hazard spectrum.
- The fundamental modes and modal shapes of the Nieuwklap bridge can be estimated rather accurately by using the fundamental mode method. However, the complete seismic behaviour of the structure and the influence of all the significant modes contributing to the total response can be examined only by performing a modal analysis. Both models, that were constructed for the application of the modal response spectrum analysis, achieve a quite precise description of the bridge seismic behaviour.

## 7.2. Recommendations

Recommendations for future work that can be made, regarding the static analysis and the prediction of the failure mode of reinforced concrete solid slab bridges, are listed below.

- In order to determine the probability of a certain failure mode under collapse testing, reliability methods of assessment are beneficial to be implemented in this kind of

structures, when the dominant failure mode cannot be identified accurately through the lower levels of assessment.

- Aiming at a closer description of the behaviour of the Nieuwklap bridge or of other similar structures, the construction of a non-linear finite element model is recommended. By performing a non-linear analysis, a load-displacement diagram and a possible crack pattern of the structure can also be obtained, providing a deeper insight of the actual capacity of the structure.
- Regarding the analytical approach that has been applied in this project, it can be stated that, the assumptions that have been considered for the shear effective width in order to calculate the equivalent proof loads and the failure loads may need refinement, leading to more accurate results closer to the ones obtained through the numerical approach.
- In order to succeed a more complete comparison between the experimental loading and the Eurocode loading, and to describe better the bridge behaviour under field loading, the transverse bending moment ( $m_{yy}$ ) and the transverse shear force ( $q_{yz}$ ) are suggested to be evaluated by performing a finite element analysis.

Furthermore, suggestions for future studies regarding the seismic evaluation of concrete bridges are also listed.

- Aiming in a better understanding of the effects of the seismic excitation on concrete bridges, the execution of non-linear static pushover analysis is considered significant. By representing the earthquake components with monotonically increasing loads and taking into account also the second-order-effects, a force-displacement curve (“capacity curve”) of the structure could be obtained and the formation of plastic hinges could be estimated.
- Non-linear dynamic time-history analysis could be also an option for the verification of the earthquake resistance of the bridge in combination with the performed in this research response spectrum analysis. In case of available ground motion time-histories acquired from the bridge location, or from the Groningen area generally, this analysis can be performed in order to identify the actual pattern of hinge formation and to determine the strength requirements for the prevention of non-ductile failure modes.



# References

- [1] Rijkswaterstaat, "Inventarisatie kunstwerken," p. 31, 2007.
- [2] E. Lantsoght, C. van der Veen and A. de Boer, "Recommendations for the shear assessment of reinforced concrete slab bridges from experiments," *Structural Engineering International*, pp. 23:418-426, 2013.
- [3] CEN, "Eurocode 1: Actions on structures - Part 2: Traffic loads on bridges, NEN-EN 1991-2:2003," Brussels: Comité Européen de Normalisation (p. 168), 2003.
- [4] CEN, "Eurocode 2: Design of concrete structures - Part 1-1: General rules and rules for buildings, NEN-EN 1992-1-1:2005," Brussels: Comité Européen de Normalisation (p.229), 2005.
- [5] Stichting Commissie Voorschriften Beton, "Provisions concrete VB 1977 - Part E: Reinforced concrete, additional provisions (NEN 3865) (in Dutch)," Delft: Nederlands Normalisatie Instituut, 1977.
- [6] J. C. Walraven, "Residual shear bearing capacity of existing bridges," in *fib Bulletin 57, Shear and punching shear in RC and FRC elements, Proceedings of a workshop*, Salò, Lake Garda, Italy, (p.129-138), 2010.
- [7] E. Lantsoght, "Shear in reinforced concrete slabs under concentrated loads close to supports (Ph.D. Thesis)," Delft University of Technology, Delft, 2013.
- [8] E. Lantsoght, "Overview of existing information of proof load tests executed by Delft University of Technology," Delft University of Technology, Delft, 2016.
- [9] Wikipedia, "Nieuwklap," 2014. [Online]. Available: <https://nl.wikipedia.org/wiki/Nieuwklap>. [Accessed 5 July 2018].
- [10] Koninklijk Nederlands Meteorologisch Instituut , "KNMI," 2018. [Online]. Available: <https://www.knmi.nl/kennis-en-datacentrum/uitleg/aardbevingen-door-gaswinning>. [Accessed 15 August 2018].
- [11] Wikipedia, "Groningen gas field," [Online]. Available: [https://en.wikipedia.org/wiki/Groningen\\_gas\\_field](https://en.wikipedia.org/wiki/Groningen_gas_field). [Accessed 3 September 2018].
- [12] CEN, "Eurocode 8: Design of structures for earthquake resistance - Part 1: General rules, seismic actions and rules for buildings, EN 1998-1:2004," Brussels: Comité Européen de Normalisation (p. 168), 2004.
- [13] CEN, "Eurocode 8: Design of structures for earthquake resistance - Part 2: Bridges, EN 1998-2:2005," Brussels: Comité Européen de Normalisation (p. 168), 2005.

- [14] NEN, “Nederlandse Praktijkrichtlijn 9998: Assessment of structural safety of buildings in case of erection, reconstruction and disapproval - Basic rules for seismic actions: induced earthquakes, NPR 9998:2017,” 2017.
- [15] Fib. , “Model Code 2010: final draft,” Lausanne: International Federation for Structural Concrete, 2012.
- [16] Rijkswaterstaat, “Guidelines Assessment Bridges - assessment of structural safety of an existing bridge at reconstruction, usage and disapproval (in Dutch),” Delft, 2013.
- [17] E. Lantsoght, C. van der Veen, A. de Boer and J. Walraven, “Proposal for the extension of the Eurocode shear formula for one-way slabs under concentrated loads,” *Engineering Structures*, vol. 95, pp. 16-24, 2015.
- [18] AASHTO, “Manual for Bridge Evaluation,” American Association of State Highway and Transportation Officials, Washington D.C., 2011.
- [19] D. Veneziano, D. Galeota and M. Giammatteo, “Analysis of bridge proof-load data I: Model and statistical procedures,” *Structural Safety*, pp. 91-104, 1984.
- [20] E. Brühwiler, T. Vogel, T. Lang and P. Luechinger, “Swiss standards for existing structures,” *Structural Engineering International*, pp. 275-280, 2012.
- [21] D. Cochet, P. Corfdir, G. Delfosse, Y. Jaffre, T. Kretz, G. Lacoste, D. Lefaucheur, V. Khac and M. Prat, “Load tests on highway bridges and pedestrian bridges (in French),” Bagneux-Cedex: Service d’Etudes techniques des routes et autoroutes, 2004.
- [22] E. Lantsoght, C. van der Veen, A. de Boer and D. Hordijk, “Proof load testing of reinforced concrete slab bridges in the Netherlands,” in *9th Annual Meeting of the Transportation Research Board*, Washington D.C., 2017.
- [23] Institution of Civil Engineers National Steering Committee for the Load Testing of Bridges, “Guidelines for the supplementary load testing of bridges,” *Thomas Telford Publications*, p. 73, 1998.
- [24] NRA, “Load testing for bridge assessment,” National Roads Authority, Dublin, 2014.
- [25] Deutscher Ausschuss für Stahlbeton, “DAfStb-Richtlinie: Belastungsversuche an Betonbauwerken,” in *Deutscher Ausschuss für Stahlbeton*, Berlin, (p.7), 2000.
- [26] ACI Committee 437, “Code requirements for load testing of existing concrete structures (ACI 437.2 M-13) and commentary,” American Concrete Institute, Farmington Hills, MA, 2013.
- [27] V. Werner, “Stop criteria for proof loading,” Delft University of Technology, Delft, 2016.
- [28] E. Lantsoght, Y. Yang, C. van der Veen and A. de Boer, “Development of Stop Criteria for Proof Loading,” *Life-Cycle of Engineering Systems*, pp. 1064-1071, 2017.

- [29] E. Lantsoght, Y. Yang, C. van der Veen and A. Bosman, "Analysis of beam experiments for stop criteria," Delft University of Technology, Delft, 2016.
- [30] E. Lantsoght, Y. Yang, C. van der Veen, A. de Boer and D. A. Hordijk, "Ruytenschildt Bridge: Field and laboratory testing," *Engineering Structures*, 2016.
- [31] N. Bagge, "Failure tests on concrete bridges: Have we learnt the lessons?," *Structure and Infrastructure Engineering*, vol. 14, no. 3, pp. 292-319, 2018.
- [32] G. Dieteren and J. Uijl, "Evaluation Proof load Heidijk (in Dutch)," TNO/Delft University of Technology, Delft, 2009.
- [33] G. Kappahn, "Experimental determination of the safety of the superstructure of bridge Nr. 12 (14H04) in road N240 at Medemblik (in German)," Markkleeberg, Germany, (p.70), 2009.
- [34] R. Koekkoek, Y. Yang, S. Fennis and D. Hordijk, "Assessment of Viaduct Vlijmen Oost by Proof Loading," Delft University of Technology, Delft, 2015.
- [35] S. Fennis and D. Hordijk, "Proof loading Halvemaans Bridge Alkmaar (in Dutch)," Delft University of Technology, Delft, 2014.
- [36] R. Koekkoek, E. Lantsoght and D. Hordijk, "Proof loading of the ASR affected viaduct Zijlweg over highway A59," Delft University of Technology, Delft, 2015.
- [37] E. Lantsoght, R. Koekkoek, Y. Yang, C. van der Veen, A. de Boer and D. Hordijk, "Proof load testing of the viaduct De Beek," in *39th IABSE Symposium*, Vancouver, 2017.
- [38] E. Lantsoght, C. van der Veen and A. de Boer, "Shear and Moment Capacity of the Ruytenschildt Bridge," *IABMAS 2016*, p. 8, 2016.
- [39] R. Cope, "Flexural shear failure of reinforced concrete slab bridges," in *Proceedings of the Institution of Civil Engineers Part 2 - Research and Theory*, (p.559-583), 1985.
- [40] E. Lantsoght, C. van der Veen, A. de Boer and D. Hordijk, "Collapse test and moment capacity of the Ruytenschildt reinforced concrete slab bridge," *Structure and Infrastructure Engineering*, 2016.
- [41] P. Regan, "Shear resistance of members without shear reinforcement," Polytechnic of Central London, London, UK, 1987.
- [42] E. Lantsoght, C. van der Veen and J. C. Walraven, "Shear in one-way slabs under a concentrated load close to the support," *ACI Struct J*, pp. 110:275-284, 2013.
- [43] E. Lantsoght, C. van der Veen, A. de Boer and J. C. Walraven, "Influence of width on shear capacity of reinforced concrete members," *ACI Struct J*, pp. 111:1441-1450, 2014.
- [44] E. Lantsoght, C. van der Veen, J. C. Walraven and A. de Boer, "Experimental investigation on shear capacity of reinforced concrete slabs with plain bars and slabs on elastomeric bearings," *Eng Struct*, pp. 103:1-14, 2015.

- [45] R. J. Cope and P. V. Rao, "Moment redistribution in skewed slab bridges," (p. 419-451), 1983.
- [46] Rijkswaterstaat, "Assumptions QS slabs 2012 – Skew factors 2012 (in Dutch)," Utrecht, 2013a.
- [47] E. Lantsoght, C. van der Veen, A. de Boer and J. C. Walraven, "Transverse load redistribution and effective shear width in reinforced concrete slabs," *Heron*, p. 29, 2016.
- [48] Y. Yang, J. den Uijl and J. C. Walraven, "The critical shear displacement theory: on the way to extending the scope of shear design and assessment for members without shear reinforcement," *Struct Conc*, p. 25, 2016.
- [49] E. Lantsoght, C. van der Veen and A. de Boer, "Modified bond model for shear in slabs under concentrated loads," in *FIB symposium*, Copenhagen: Concrete Innovation and Design, 2015.
- [50] J. Vecchio and P. Collins, "The Modified Compression-Field Theory for Reinforced Concrete Elements Subjected to Shear," *ACI Journal*, vol. 83, no. 22, pp. 219-231, 1986.
- [51] B. Belletti, C. Damoni, MAN Hendriks and A. de Boer, "Analytical and numerical evaluation of the design shear resistance of reinforced concrete slabs," *Struct Conc*, pp. 15:317-330, 2014.
- [52] A. Muttoni and M. Fernández Ruiz, "Shear strength in one- and two-way slabs according to the critical shear crack theory," in *International FIB symposium*, Amsterdam: Fédération Internationale du Béton, 2008.
- [53] Z. Procházková, E. Lantsoght and C. van der Veen, "FEM analyses: Shear tests of Reinforced Concrete Slabs," Delft University of Technology, Delft, 2012.
- [54] E. Lantsoght, A. de Boer, C. van der Veen and J. Walraven, "Effective shear width of concrete slab bridges," *Proc Inst Civil Eng – Bridge Eng*, pp. 168:287-298, 2015.
- [55] R. Vergoossen, M. Naaktgeboren, M. Hart, A. de Boer and E. van Vugt, "Quick scan on shear in existing slab type viaducts," in *International IABSE conference on assessment, upgrading and refurbishment of infrastructures*, Rotterdam (p.8), 2013.
- [56] E. Lantsoght, A. de Boer and C. van der Veen, "Determination of distribution width for shear stresses at support in reinforced concrete slab bridges," St. Anton am Arlberg (Austria), (p.9), 2014.
- [57] Rijkswaterstaat, "Guidelines for nonlinear finite element analysis of concrete structures," (p.65), 2012.
- [58] E. Lantsoght, "Probabilistic approach to determine the increased shear capacity in reinforced concrete slabs under a concentrated load," Delft University of Technology, Delft, 2012.

- [59] R. Koekkoek, E. Lantsoght, Y. Yang, A. de Boer and D. Hordijk, "Defining loading criteria for proof loading of existing reinforced concrete bridges," in *Performance-based approaches for concrete structures*, Cape Town, (p.10).
- [60] N. Wang, B. Ellingwood and A. Zureick, "Bridge rating using system reliability assessment, Part II: improvement to bridge rating practices," *J Bridge Eng*, pp. 16:863-871, 2011.
- [61] JCSS, JCSS probabilistic model code - Part 3: resistance models, 2001.
- [62] CEN, "Eurocode - Basis of structural design, NEN-EN 1990:2002," Brussels: Comité Européen de Normalisation (p. 103), 2002.
- [63] Code Committee 351001, "Assessment of structural safety of an existing structure at repair or unfit for use - Basic Requirements, NEN 8700:2011 (in Dutch)," Delft: Civil center for the execution of research and standard, Dutch Normalisation Institute, 2011.
- [64] M. Pimentel, E. Brühwiler and D. Rosowsky, "Safety examination of existing concrete structures using the global resistance safety factor concept," *Eng Struct*, p. 70:130-143, 2014.
- [65] C. Higgins, T. Daniels, D. Rosowsky, T. Miller and S. Yim, "Assessment and risk ranking of conventionally reinforced concrete bridges for shear," *Transport Res Rec: Des Struct*, pp. 110-117, 2005.
- [66] T. Braml, A. Taffe, S. Feistkorn and O. Wurzer, "Assessment of existing structures using probabilistic analysis methods in combination with nondestructive testing methods," *Struct Eng Int*, p. 23:376-385, 2013.
- [67] A. Nowak, A. Yamani and S. Tabsh, "Probabilistic models for resistance of concrete bridge girders," *Struct J*, p. 91, 1994.
- [68] Steenbergen RDJM, Vrouwenvelder ACWM, "Safety philosophy for existing structures and partial factors for traffic loads on bridges," *Heron*, pp. 55:123-140, 2010.
- [69] E. Lantsoght, C. van der Veen, A. de Boer and D. Hordijk, "Probabilistic prediction of the failure mode of the Ruytenschildt Bridge," *Engineering Structures*, pp. 127:549-558, 2016.
- [70] S. B. Keivani, "Seismic Evaluation of Existing Reinforced Concrete Bridges in Ottawa Region," Ottawa University, Ottawa, Ontario, 2003.
- [71] C. Choo, I. Harik and P. Yuan, "Detailed seismic evaluation of bridges along I-24 in Western Kentucky," Kentucky Transportation Center, Lexington, Kentucky, 2006.
- [72] M. Vinay Kumar and C. Shivananad, "Seismic Performance Evaluation of Existing Bridge," *International Journal of Science, Engineering and Technology Research (IJSETR)*, vol. 5, no. 5, pp. 1596-1602, 2016.
- [73] E. Lantsoght, "Bezwijktest Nieuwklapbrug: voorbereidingsrapport," Delft University of Technology, Delft, 2018.

- [74] CEN, "Eurocode 2: Design of concrete structures - Part 2: Concrete bridges - Design and detailing rules, EN 1992-2:2005," Brussels: Comité Européen de Normalisation (p.229), 2005.
- [75] DIANA FEA, "DIANA User's manual," [Online]. Available: <https://dianafea.com/manuals/d101/Diana.html>.
- [76] P. Shearer, Introduction to Seismology, Cambridge: Cambridge University Press, 2009.
- [77] A. Tsouvalas and P. Ditmar, *Lecture Notes: Structural Reponse to Earthquakes (CIE5260)*, Delft: TU Delft, 2017.
- [78] NEN, "Webtool NPR 9998," NEN, [Online]. Available: <http://seismischekrachten.nen.nl/webtool.php>.

# List of Figures

Figure 1.1: Building year of concrete viaducts and bridges in the Netherlands [1] .....	1
Figure 1.2: View of the Nieuwklap Bridge [9] .....	2
Figure 1.3: Location of the Groningen gas field [11] .....	3
Figure 1.4: Annual number of earthquakes in the Groningen gas field with a magnitude ( $M_L$ ) higher than 1.5 [10].....	3
Figure 2.1: Truncation of probability density function of resistance after proof load test [22] .....	10
Figure 2.2: Determination of the effective width according to Dutch practice (left) and to French practice (right) [47].....	13
Figure 2.3: Principle of Levels of Approximation according to Fib Model Code [15].....	14
Figure 2.4: Schematization of different methods of structural analysis .....	16
Figure 3.1: Location of the Nieuwklap bridge .....	17
Figure 3.2: Bridge construction location .....	18
Figure 3.3: South view of the Nieuwklap Bridge .....	18
Figure 3.4: New bridge under construction.....	19
Figure 3.5: Sideview of the Nieuwklap bridge with dimensions (m) .....	19
Figure 3.6: Overview of the Nieuwklap bridge with dimensions (m).....	19
Figure 3.7: Cross-section of the Nieuwklap bridge close to supports with dimensions (m) .....	20
Figure 3.8: Cross-section of the bridge with the position of the saw cut .....	22
Figure 4.1: Simplified mechanical scheme of the Nieuwklap bridge .....	26
Figure 4.2: Load Model 1 for normal traffic loading [3].....	27
Figure 4.3: Loading positions of the concentrated loads.....	29
Figure 4.4: Different approaches for the determination and values of the effective width for skewed slabs .....	30
Figure 4.5: Effective width of the Tandem system of LM1 .....	30
Figure 4.6: Superposition of shear stress due to a concentrated load over the effective width with the distributed load over the full slab width .....	31
Figure 4.7: Thorenfeldt's stress-strain parabola .....	32
Figure 4.8: Simplified concrete stress block .....	33
Figure 4.9: Moment-curvature ( $M-\kappa$ ) diagrams for characteristic and mean material properties.....	34
Figure 4.10: Stresses generated by EC loading (left) and proof loading (right).....	38
Figure 5.1: Global view of the Finite element model with the supports .....	44
Figure 5.2: Mesh discretization - Top view detail.....	44

Figure 5.3: Characteristic plate bending element (left) and Q12PL element (right) [75].....	45
Figure 5.4: Shear critical layout of the Tandem system (LP3) .....	47
Figure 5.5: FEM plan view with notional lanes and wheel prints (LP4) .....	47
Figure 5.6: FEM global view with applied loads according to Eurocode 2 (LP4) .....	47
Figure 5.7: Distributed bending moment for Span 1 with ( $m_{xD}$ ) and without ( $m_{xx}$ ) torsion inclusion (LP1).....	48
Figure 5.8: Generalized shear forces (top) and bending moments (bottom) (LP6) .....	49
Figure 5.9: Averaged shear forces (left) and averaged design bending moments (right) (LP6) .	49
Figure 5.10: Distributed generalized design bending moment at Span 2 (top left) and Support 2 (top right), and generalized shear force at Support 2 (bottom) for Eurocode and experimental loading (LP5) .....	53
Figure 5.11: Vertical displacements for Eurocode (left) and experimental (right) loading (LP5) .	53
Figure 6.1: Number of earthquakes (N) vs magnitude ( $M_L$ ) .....	60
Figure 6.2: Logarithm of the number of earthquakes (N) vs magnitude ( $M_L$ ).....	61
Figure 6.3: Horizontal elastic response spectra for an earthquake with return period $T_R=475$ years (left) and $T_R=2475$ years (right).....	64
Figure 6.4: Vertical elastic response spectra for an earthquake with return period $T_R=475$ years (left) and $T_R=2475$ years (right).....	65
Figure 6.5: Equivalent vertical static forces alternative applications .....	67
Figure 6.6: Side and front-view of a middle-pier (left) and a pendulum (right) with dimensions (m) .....	69
Figure 6.7: Lateral load application static scheme - Top view.....	71
Figure 6.8: Model with spring supports - Standard view (left) and Extrude view (right) .....	73
Figure 6.9: Model with piers - Standard view (left) and Extrude view (right) .....	73

# List of Tables

Table 3.1: Longitudinal reinforcement layout for Span 1, Span 2 and over the Supports.....	20
Table 3.2: Material properties of concrete .....	21
Table 3.3: Material properties of reinforcement steel.....	22
Table 4.1: Acting loads on beam model .....	27
Table 4.2: Bending moment capacity .....	33
Table 4.3: Shear capacity .....	35
Table 4.4: Sectional forces and moments - Eurocode loading - Analytical approach.....	36
Table 4.5: Unity Check - Eurocode loading - Analytical approach .....	37
Table 4.6: Equivalent proof load - Analytical approach.....	39
Table 4.7: Failure load - Analytical approach .....	40
Table 4.8: Predicted failure mode - Analytical approach.....	42
Table 5.1: Finite element type characteristics .....	45
Table 5.2: Acting loads FEM .....	46
Table 5.3: Averaged forces and moments - Eurocode loading - Numerical approach .....	50
Table 5.4: Unity Check - Eurocode loading - Numerical approach .....	51
Table 5.5: Equivalent proof load - Numerical approach .....	52
Table 5.6: Torsional moment ( $m_{xy}$ ) percentage of design bending moment ( $m_{xD}$ ) for Eurocode and experimental loading.....	54
Table 5.7: Failure load - Numerical approach.....	55
Table 5.8: Predicted failure mode - Numerical approach.....	56
Table 5.9: Unity Check comparison.....	57
Table 5.10: Equivalent proof load comparison .....	57
Table 5.11: Failure mode prediction comparison.....	58
Table 6.1: Human-induced earthquakes data.....	60
Table 6.2: Earthquake occurrence .....	62
Table 6.3: Horizontal elastic response spectrum parameters .....	63
Table 6.4: Vertical elastic response spectrum parameters .....	64
Table 6.5: Equivalent vertical static forces .....	66
Table 6.6: Vertical seismic loading - Fundamental mode method.....	68
Table 6.7: Unity Check - Vertical seismic loading - Fundamental mode method.....	68
Table 6.8: Equivalent horizontal static forces .....	70

---

Table 6.9: Horizontal seismic loading - Fundamental mode method.....	71
Table 6.10: Shear and bending moment capacity of middle-pier out-of-plane and pendulum....	72
Table 6.11: Unity Check - Horizontal seismic loading - Fundamental mode method .....	72
Table 6.12: Modal participation mass ratios - Model with spring supports .....	74
Table 6.13: Modal participation mass ratios - Model with piers.....	75
Table 6.14: Vertical seismic loading - Response spectrum analysis.....	76
Table 6.15: Unity Check - Vertical seismic loading - Response spectrum analysis.....	76
Table 6.16: Longitudinal seismic loading - Response spectrum analysis.....	77
Table 6.17: Unity Check - Longitudinal seismic loading - Response spectrum analysis .....	77
Table 6.18: Transverse seismic loading - Response spectrum analysis.....	78
Table 6.19: Unity Check - Transverse seismic loading - Response spectrum analysis.....	78
Table 6.20: Unity Check comparison - Vertical seismic loading.....	79
Table 6.21: Unity Check comparison - Horizontal seismic loading .....	79
Table 6.22: Fundamental period for each direction of seismic excitation .....	80

# APPENDICES



# Appendix A

## Structural plans

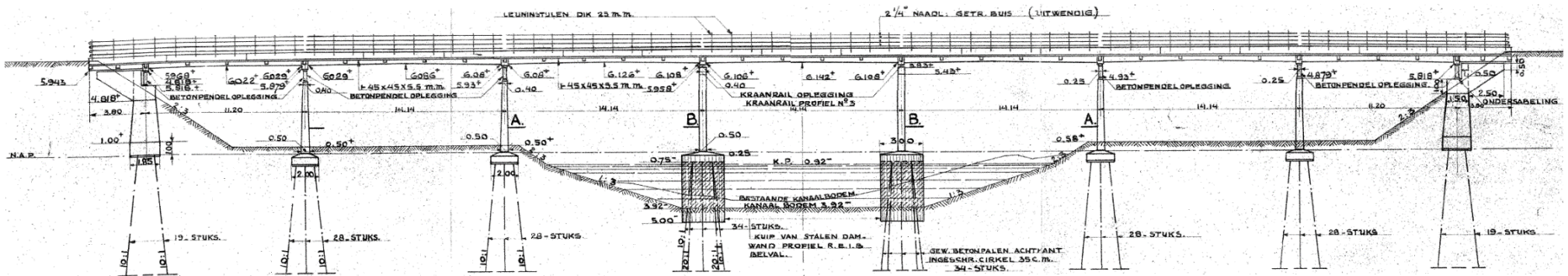


Figure A.1: Bridge side-view with dimensions [m]

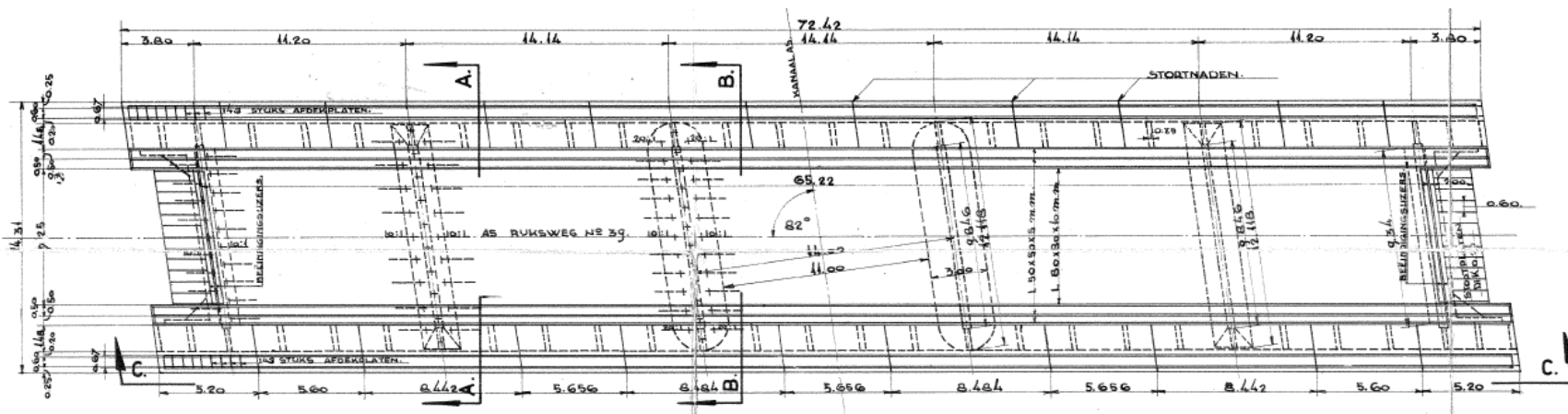


Figure A.2: Bridge top view (5-span version) with dimensions [m]

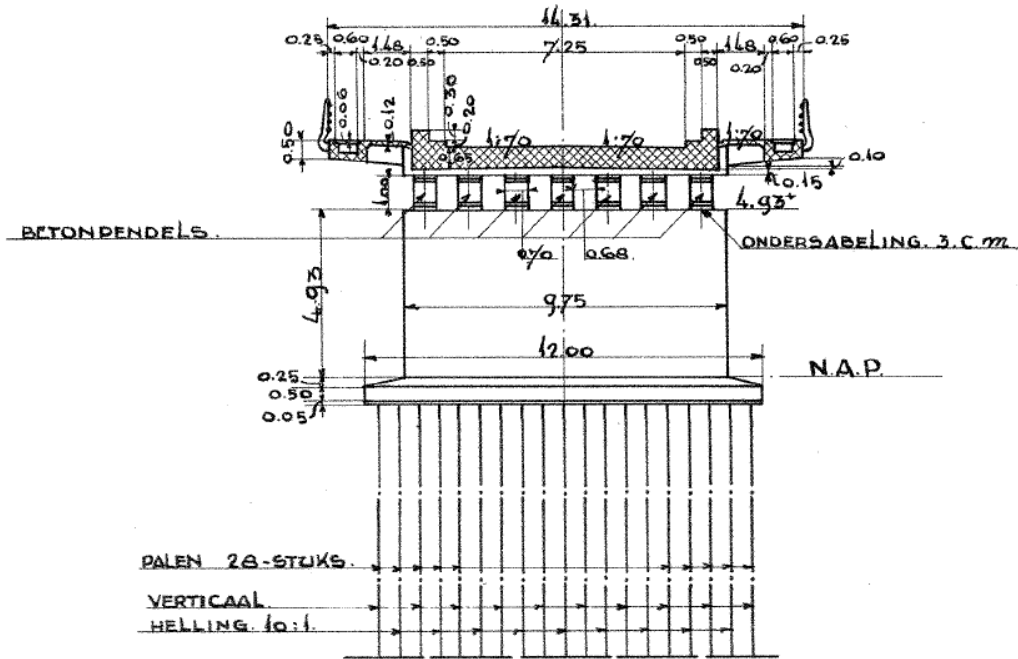


Figure A.4: Cross-section A-A with dimensions [m]

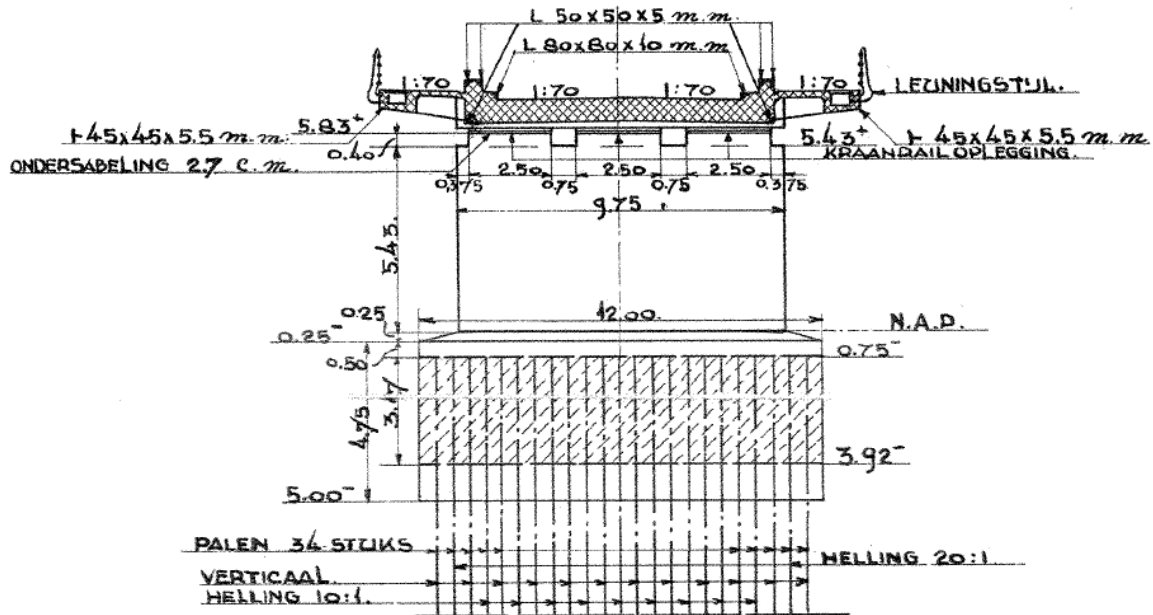


Figure A.3: Cross-section B-B with dimensions [m]

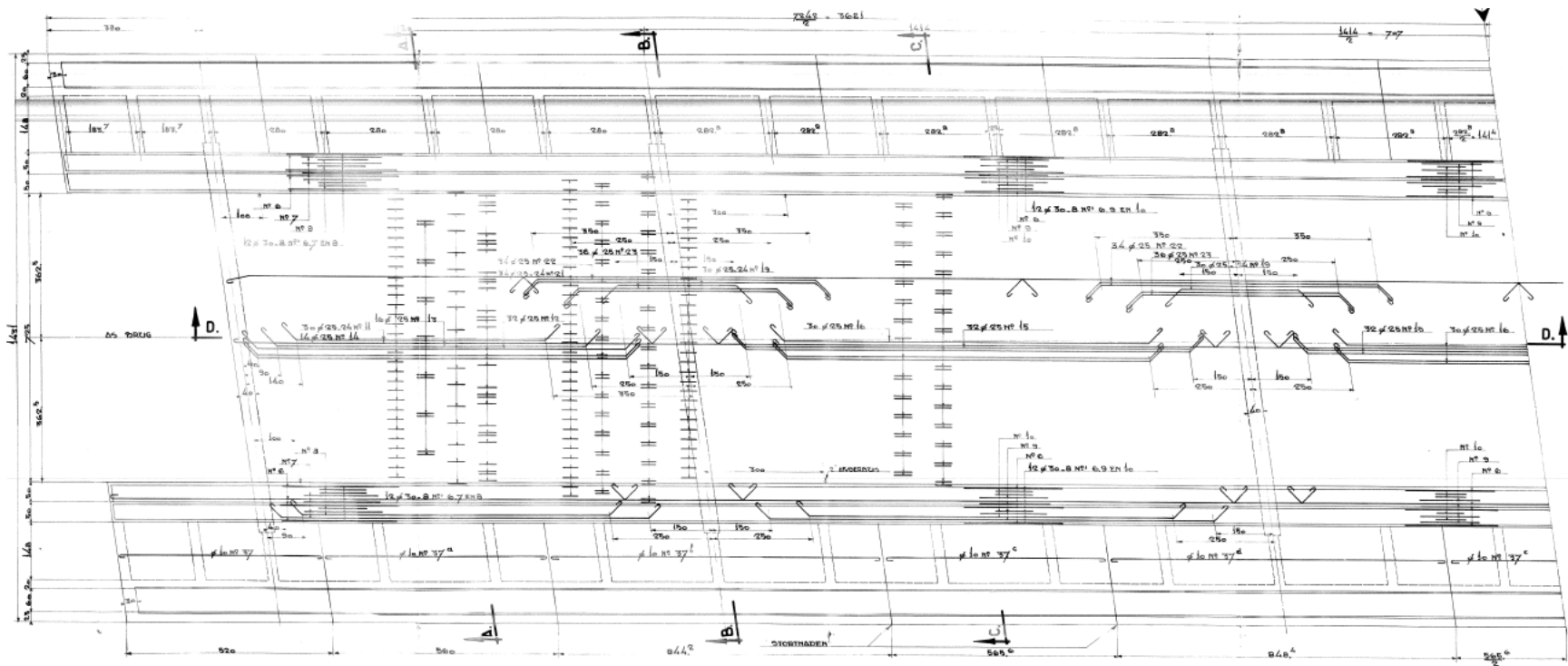


Figure A.5: Longitudinal reinforcement layout with dimensions [cm]

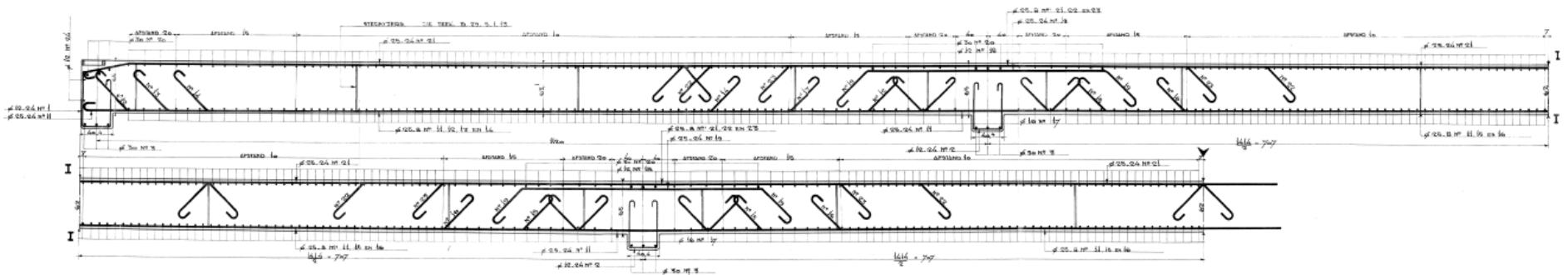


Figure A.6: Reinforcement cross-section D-D with dimensions [cm]

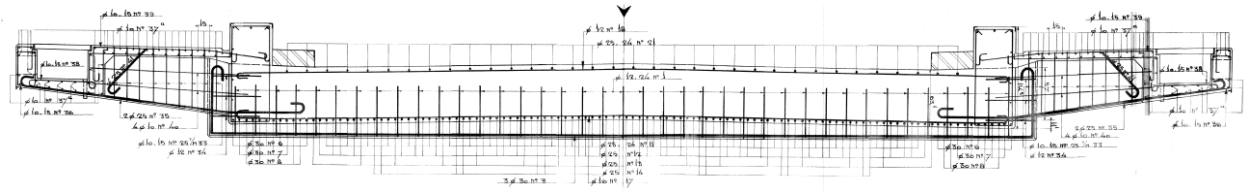


Figure A.7: Reinforcement cross-section A-A with dimensions [cm]

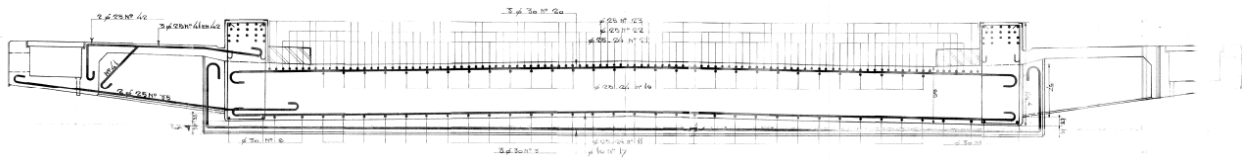


Figure A.8: Reinforcement cross-section B-B with dimensions [cm]

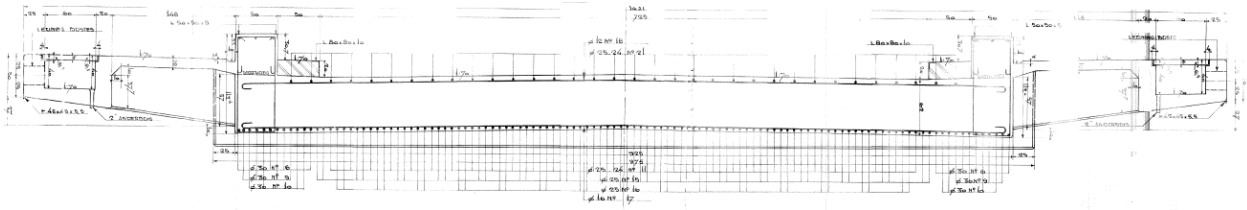


Figure A.9: Reinforcement cross-section C-C with dimensions [cm]

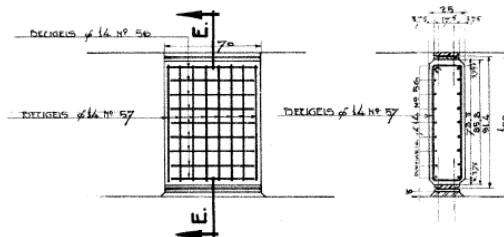


Figure A.10: Concrete pendulum reinforcement layout

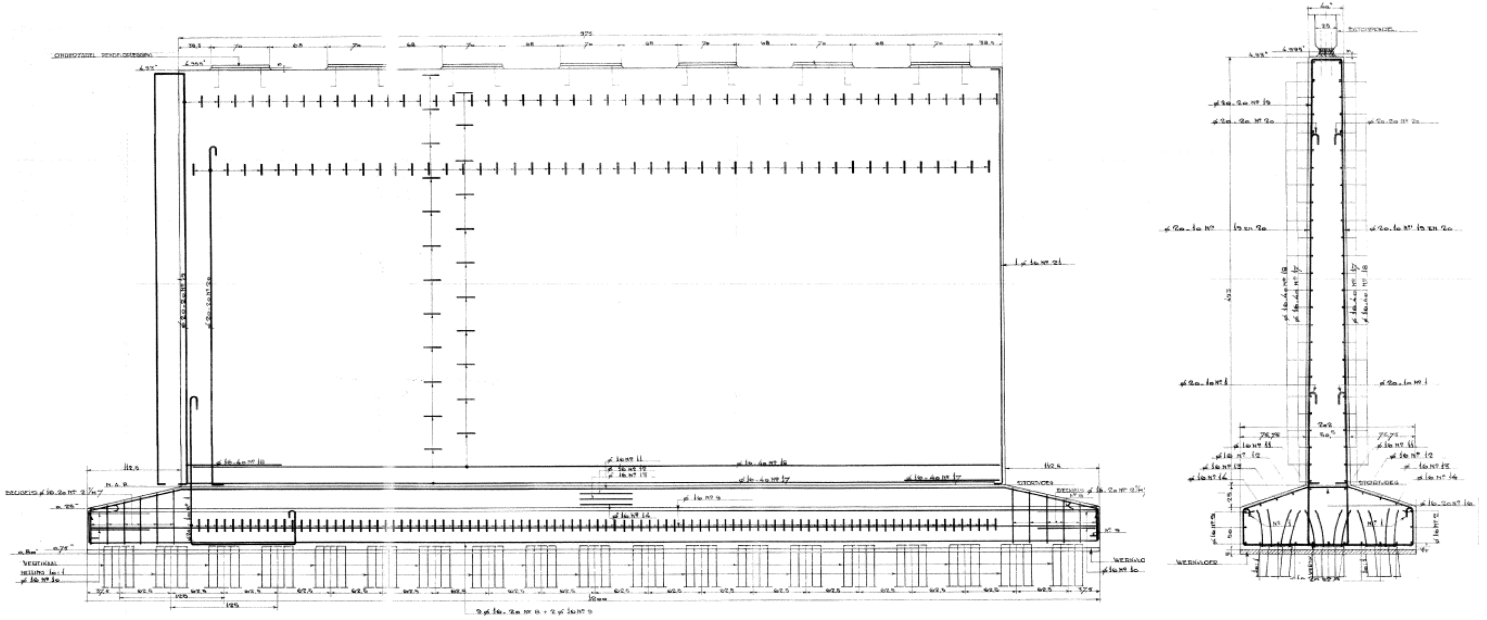


Figure A.12: Pier with pendulum reinforcement layout

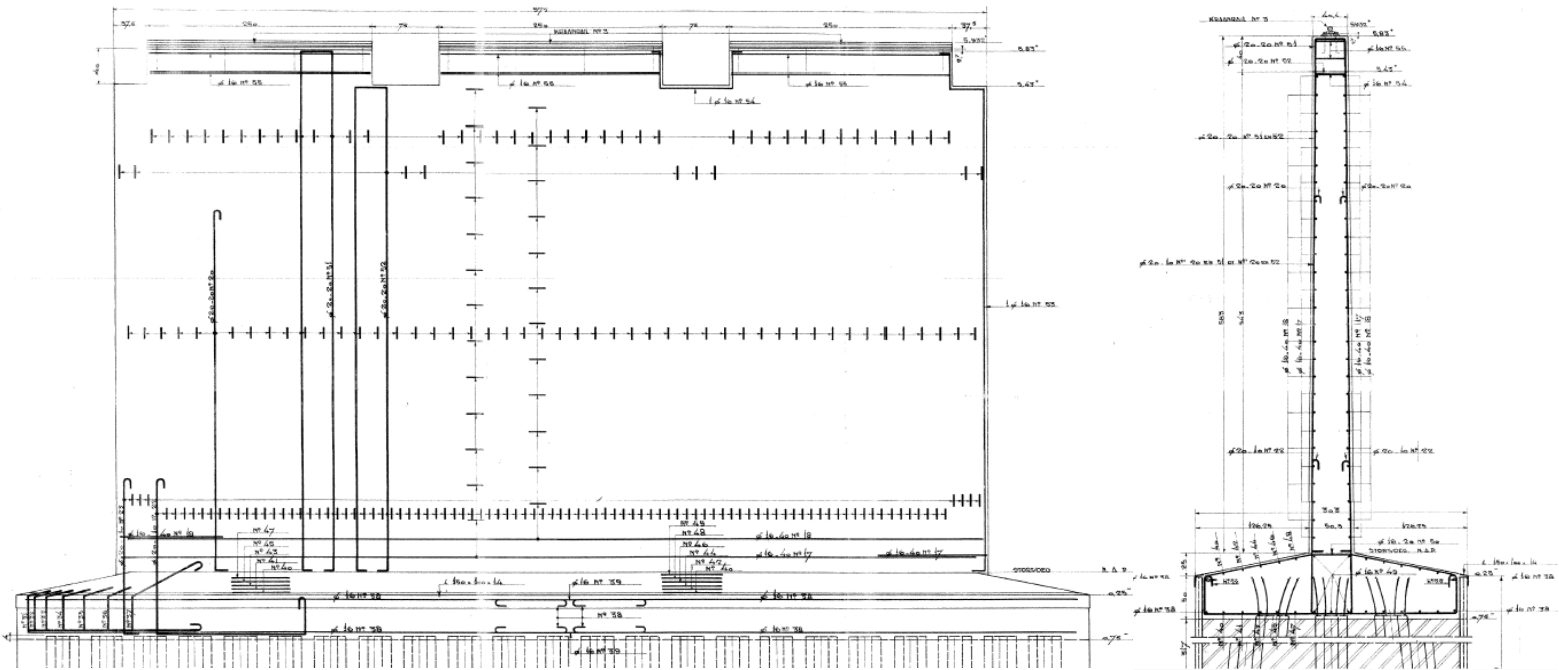


Figure A.11: Middle-pier reinforcement layout



# Appendix B

## Analytical Calculations

### 1. Bending Moment Capacity - SPAN 1

#### 1.1. Input - Parameters

The input that was used for the calculation of the bending moment capacity of Span 1 is summarized in the following table:

Input - Parameters		
Concrete initial Young's Modulus	$E_{c,0}$ (MPa)	22000
Steel Young's Modulus	$E_s$ (MPa)	200000
Mean compressive strength	$f_{cm}$ (MPa)	70
Design compressive strength	$f_{cd}$ (MPa)	33.33
Mean yielding strength	$f_{ym}$ (MPa)	242
Design yielding strength	$f_{yd}$ (MPa)	191
Slab width	$b$ (mm)	8250
Slab height	$h$ (mm)	631
Cover	$c$ (mm)	45
Reinforcement diameter	$\emptyset$ (mm)	25
Bottom longitudinal reinforcement area	$A_{s,bot}$ (mm <sup>2</sup> )	6136
Top longitudinal reinforcement area	$A_{s,top}$ (mm <sup>2</sup> )	2045

Table B.1: Input - Parameters for bending moment capacity calculation

Concrete Young's modulus:

$$E_c = E_{c,0} \cdot \left(\frac{f_{cd}}{10}\right)^{0.3} = 31570 \text{ MPa}$$

Effective depth to the longitudinal reinforcement:

$$d_l = h - c = 586 \text{ mm}$$

## 1.2. Cracking moment capacity

Depth of compression zone at onset of cracking:

$$c_{cr} = \frac{b \cdot \frac{h^2}{2} + \left(\frac{E_s}{E_c} - 1\right) \cdot A_{s,bot} \cdot d_l + \left(\frac{E_s}{E_c} - 1\right) \cdot A_{s,top} \cdot d_l \cdot \left(c - \frac{\emptyset}{2}\right)}{b \cdot h + \left(\frac{E_s}{E_c} - 1\right) \cdot A_{s,bot} + \left(\frac{E_s}{E_c} - 1\right) \cdot A_{s,top}} = 316.65 \text{ mm}$$

Moment of inertia of the gross (uncracked) section:

$$I_{gross} = b \cdot \frac{c_{cr}^3}{3} + b \cdot \frac{(h - c_{cr})^3}{3} + \left(\frac{E_s}{E_c} - 1\right) \cdot A_{s,bot} \cdot (d_l - c_{cr})^2 + \left(\frac{E_s}{E_c} - 1\right) \cdot A_{s,top} \cdot \left(c_{cr} - c - \frac{\emptyset}{2}\right)^2 = 1.76 \cdot 10^{11} \text{ mm}^4$$

### Design Properties

Design rupture strength of concrete:

$$f_{rd} = \frac{7.5}{12} \cdot \sqrt{f_{cd}} = 3.608 \text{ MPa}$$

Design cracking moment capacity:

$$M_{crd} = f_{rd} \cdot \frac{I_{gross}}{(h - c_{cr}) \cdot b} = 244.67 \text{ kNm/m}$$

And the corresponding curvature is:

$$\kappa_{crd} = \frac{\varepsilon_{crd}}{h - c_{cr}} = \frac{f_{rd}/E_c}{h - c_{cr}} = 3.64 \cdot 10^{-7} \text{ 1/mm}$$

### Mean Properties

Mean rupture strength of concrete:

$$f_{rm} = \frac{7.5}{12} \cdot \sqrt{f_{cm}} = 5.229 \text{ MPa}$$

Mean cracking moment capacity:

$$M_{crm} = f_{rm} \cdot \frac{I_{gross}}{(h - c_{cr}) \cdot b} = 354.56 \text{ kNm/m}$$

And the corresponding curvature is:

$$\kappa_{crm} = \frac{\varepsilon_{crm}}{h - c_{cr}} = \frac{f_{rm}/E_c}{h - c_{cr}} = 5.27 \cdot 10^{-7} \text{ 1/mm}$$

### 1.3. Yielding moment capacity

The moment capacity at yielding, is based on the stress-strain diagram for concrete as specified by Thorenfeldt's parabola.

#### Design Properties

Steel strain at yielding:

$$\varepsilon_{sy} = \frac{f_{yd}}{E_s} = 0.010$$

The value of concrete strain is changed until:

$$\varepsilon_c = \varepsilon_{sy} \cdot \frac{c_y}{d_l - c_y}$$

And is found:

$$\varepsilon_c = 0.00058$$

The formulas for the calculations of the parameters defined by Thorenfeldt are:

$$n_{th} = 0.8 + \frac{f_{cd}}{17} = 2.76$$

$$\varepsilon_0 = \frac{f_{cd}}{E_c} \cdot \left( \frac{n_{th}}{n_{th} - 1} \right) = 0.0017$$

$$\beta_1 = \frac{\ln[1 + (\varepsilon_c/\varepsilon_0)^2]}{\varepsilon_c/\varepsilon_0} = 0.33$$

$$k_2 = 1 - 2 \cdot \frac{\varepsilon_c/\varepsilon_0 - \arctan(\varepsilon_c/\varepsilon_0)}{(\varepsilon_c/\varepsilon_0)^2 \cdot \beta_1} = 0.34$$

Thus, the concrete stress according to Thorenfeldt's parabola is:

$$f_{c,th} = \frac{0.9 \cdot f_{cd} \cdot n_{th} \cdot \varepsilon_c / \varepsilon_0}{n_{th} - 1 + (\varepsilon_c / \varepsilon_0)^{n_{th}}} = 16.03 \text{ MPa}$$

Depth of compression zone at yielding of the reinforcement:

$$c_y = \frac{A_{s,bot} \cdot f_{yd}}{\beta_1 \cdot f_{c,th}} = 220.93 \text{ mm}$$

Design yielding moment capacity:

$$M_{yd} = \beta_1 \cdot f_{c,th} \cdot c_y \cdot (d_l - k_2 \cdot c_y) = 599.39 \text{ kNm/m}$$

And the corresponding curvature:

$$\kappa_{yd} = \frac{\varepsilon_{sy}}{d_l - c_y} = 2.33 \cdot 10^{-6} \text{ 1/mm}$$

### Mean Properties

Steel strain at yielding:

$$\varepsilon_{sy} = \frac{f_{ym}}{E_s} = 0.012$$

The value of concrete strain is changed until:

$$\varepsilon_c = \varepsilon_{sy} \cdot \frac{c_y}{d_l - c_y}$$

And is found:

$$\varepsilon_c = 0.00080$$

The formulas for the calculations of the parameters defined by Thorenfeldt are:

$$n_{th} = 0.8 + \frac{f_{cm}}{17} = 4.92$$

$$\varepsilon_0 = \frac{f_{cm}}{E_c} \cdot \left( \frac{n_{th}}{n_{th} - 1} \right) = 0.0028$$

$$\beta_1 = \frac{\ln[1 + (\varepsilon_c/\varepsilon_0)^2]}{\varepsilon_c/\varepsilon_0} = 0.28$$

$$k_2 = 1 - 2 \cdot \frac{\varepsilon_c/\varepsilon_0 - \arctan(\varepsilon_c/\varepsilon_0)}{(\varepsilon_c/\varepsilon_0)^2 \cdot \beta_1} = 0.34$$

Thus, the concrete stress according to Thorenfeldt's parabola is:

$$f_{c,th} = \frac{0.9 \cdot f_{cm} \cdot n_{th} \cdot \varepsilon_c/\varepsilon_0}{n_{th} - 1 + (\varepsilon_c/\varepsilon_0)^{n_{th}}} = 22.85 \text{ MPa}$$

Depth of compression zone at yielding of the reinforcement:

$$c_y = \frac{A_{s,bot} \cdot f_{ym}}{\beta_1 \cdot f_{c,th}} = 234.07 \text{ mm}$$

Mean yielding moment capacity:

$$M_{ym} = \beta_1 \cdot f_{c,th} \cdot c_y \cdot (d_l - k_2 \cdot c_y) = 752.42 \text{ kNm/m}$$

And the corresponding curvature:

$$\kappa_{ym} = \frac{\varepsilon_{sy}}{d_l - c_y} = 3.05 \cdot 10^{-6} \text{ 1/mm}$$

## 1.4. Ultimate bending moment capacity

The ultimate bending moment is calculated based on a rectangular stress block diagram.

### Design Properties

Depth of compression zone at the ultimate bending moment:

$$c_{ult} = \frac{A_{s,bot} \cdot f_{yd}}{0.85 \cdot \beta_{ult} \cdot f_{cd}} = 51.03 \text{ mm}$$

where,

$$\beta_{ult} = 0.85 - 0.05 \cdot \frac{f_{cd} - 28}{7} = 0.81$$

Design ultimate bending moment capacity:

$$M_{ud} = 0.85 \cdot f_{cd} \cdot \beta_{ult} \cdot c_{ult} \cdot \left( d_l - \frac{\beta_{ult} \cdot c_{ult}}{2} \right) = 663.55 \text{ kNm/m}$$

The corresponding curvature is calculated also:

$$\kappa_{ult,d} = \frac{\varepsilon_{cu}}{c_{ult}} = 5.88 \cdot 10^{-5} \text{ 1/mm}$$

where,

$$\varepsilon_{cu} = 0.003$$

### Mean Properties

Depth of compression zone at the ultimate bending moment:

$$c_{ult} = \frac{A_{s,bot} \cdot f_{ym}}{0.85 \cdot \beta_{ult} \cdot f_{cm}} = 38.39 \text{ mm}$$

where,

$$\beta_{ult} = 0.85 - 0.05 \cdot \frac{f_{cm} - 28}{7} = 0.65$$

Mean ultimate bending moment capacity:

$$M_{um} = 0.85 \cdot f_{cm} \cdot \beta_{ult} \cdot c_{ult} \cdot \left( d_l - \frac{\beta_{ult} \cdot c_{ult}}{2} \right) = 851.62 \text{ kNm/m}$$

The corresponding curvature is calculated also:

$$\kappa_{ult,m} = \frac{\varepsilon_{cu}}{c_{ult}} = 7.81 \cdot 10^{-5} \text{ 1/mm}$$

where,

$$\varepsilon_{cu} = 0.003$$

## 2. Shear capacity

### 2.1. Input - Parameters

The input that was used for the calculation of the shear capacity is summarized in the following table:

Input - Parameters		
Mean compressive strength	$f_{cm}$ (MPa)	70
Characteristic compressive strength	$f_{ck}$ (MPa)	50
Mean yielding strength	$f_{ym}$ (MPa)	242
Characteristic yielding strength	$f_{yk}$ (MPa)	220
Slab width	$b$ (mm)	8250
Effective depth	$d_l$ (mm)	605
Reinforcement ratio	$\rho_l$ (%)	1.47
Design calibration factor	$C_{Rd,c}$ (-)	0.12
Average calibration factor	$C_{Rm,c}$ (-)	0.15
Supported length	$l_{sup}$ (mm)	4900

Table B.2: Input - Parameters for shear capacity calculation

$$k = 1 + \sqrt{d_l/200} = 1.575$$

### 2.2. Eurocode formula

The shear capacity of the slab is calculated according to EC2 for members without shear reinforcement not subjected to axial forces:

$$V_{R,c} = C_{R,c} \cdot k \cdot (100 \cdot \rho_l \cdot f_c)^{1/3} \cdot d_l \geq v_{min} \cdot d_l [kN/m]$$

#### Design Properties

The design shear stress capacity:

$$v_{Rd,c} = C_{Rd,c} \cdot k \cdot (100 \cdot \rho_l \cdot f_{ck})^{1/3} = 0.793 \text{ MPa}$$

The lower bound of the shear capacity:

$$v_{min} = 1.08 \cdot k^2 \cdot \left(\frac{f_{ck}}{f_{yk}}\right)^{1/2} = 1.018 \text{ MPa}$$

So, the design capacity is:

$$V_{Rd,c} = 615.68 \text{ kN/m}$$

### Mean Properties

The mean shear stress capacity:

$$v_{Rm,c} = C_{Rm,c} \cdot k \cdot (100 \cdot \rho_l \cdot f_{cm})^{1/3} = 1.109 \text{ MPa}$$

The lower bound of the shear capacity:

$$v_{min} = 1.08 \cdot k^{\frac{3}{2}} \cdot \left( \frac{f_{cm}}{f_{ym}} \right)^{1/2} = 1.148 \text{ MPa}$$

So, the mean capacity is:

$$V_{Rm,c} = 694.58 \text{ kN/m}$$

### 2.3. Proposed formula for concrete slabs

The shear capacity of the slab is calculated according to a proposed formula for concrete slabs under concentrated loads close to supports:

$$V_{R,c,prop} = C_{R,c} \cdot k \cdot (100 \cdot \rho_l \cdot f_c)^{\frac{1}{3}} \cdot \left( 1.9 - \frac{f_c}{225} \right) \cdot 0.5 \cdot \left( \frac{l_{sup}}{b} + 1 \right) \cdot d_l \geq v_{min} \cdot d_l \text{ [kN/m]}$$

### Design Properties

The design shear stress capacity:

$$v_{Rd,c,prop} = C_{Rd,c} \cdot k \cdot (100 \cdot \rho_l \cdot f_{ck})^{\frac{1}{3}} \cdot \left( 1.9 - \frac{f_{ck}}{225} \right) \cdot 0.5 \cdot \left( \frac{l_{sup}}{b} + 1 \right) = 1.060 \text{ MPa}$$

The lower bound of the shear capacity:

$$v_{min} = 1.08 \cdot k^{\frac{3}{2}} \cdot \left( \frac{f_{ck}}{f_{yk}} \right)^{1/2} = 1.018 \text{ MPa}$$

So, the design capacity is:

$$V_{Rd,c} = 641.38 \text{ kN/m}$$

## Mean Properties

The mean shear stress capacity:

$$v_{Rm,c,prop} = C_{Rm,c} \cdot k \cdot (100 \cdot \rho_l \cdot f_{cm})^{\frac{1}{3}} \cdot \left(1.9 - \frac{f_{cm}}{225}\right) \cdot 0.5 \cdot \left(\frac{l_{sup}}{b} + 1\right) = 1.404 \text{ MPa}$$

The lower bound of the shear capacity:

$$v_{min} = 1.08 \cdot k^{\frac{3}{2}} \cdot \left(\frac{f_{cm}}{f_{ym}}\right)^{1/2} = 1.148 \text{ MPa}$$

So, the mean capacity is:

$$V_{Rm,c} = 849.37 \text{ kN/m}$$

## 3. Analytical approach - LP4

### 3.1. Eurocode loading - Evaluation

The design loads acting on the Nieuwklap bridge according to NEN-EN 1991-2:2003 [3] are the following:

- LL: traffic loading as described by Load Model 1, consisting of two partial systems, the double-axle concentrated loads, which are called tandem system (TS), and the uniformly distributed loads (UDL) on each notional lane and the remaining area
- SW: dead load, due to the self-weight of the bridge
- SD: asphalt loading

The loading is applied by representing the loads that are acting on the deck surface as distributed loads and the tandem system of LM1 is represented as point loads. The acting loads on the beam model according to the standards are calculated:

$$SW = b \cdot h_{slab} \cdot \gamma_c = 8.25 \cdot 0.65 \cdot 25 = 134 \text{ kN/m}$$

$$SD = w_{slab} \cdot t_{asph} \cdot \gamma_{asph} = 7.25 \cdot 0.12 \cdot 23 = 20 \text{ kN/m}$$

$$UDL = w_1 \cdot q_1 + w_2 \cdot q_2 + w_r \cdot q_r = 3 \cdot 9 + 3 \cdot 2.5 + 1.25 \cdot 2.5 = 37.625 \text{ kN/m}$$

$$TS = 2 \cdot (Q_1 + Q_2) = 2 \cdot (300 + 200) = 2 \cdot 500 \text{ kN}$$

These load cases have been combined according to the load combinations defined by RBK [16], for this example only the design load combination will be displayed:

$$\text{Design: } U = 1.25 \cdot SW + 1.25 \cdot SD + 1.50 \cdot LL$$

In order to facilitate the calculations of the sectional forces and moments for the continuous beam model the structural software SAP2000 was used and the results for the LP4 scenario are illustrated in the following figures.

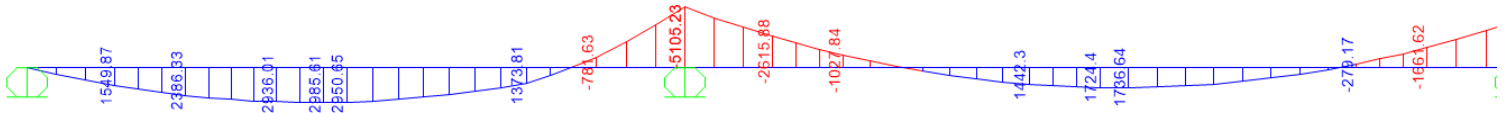


Figure B.1: Bending moment (kNm)

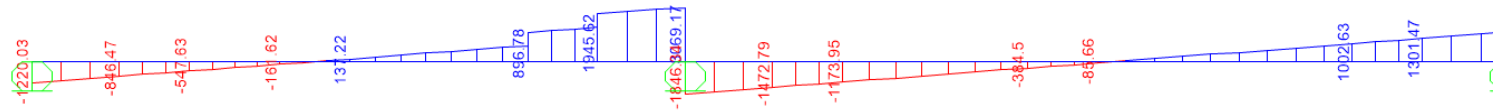


Figure B.2: Shear force (kN)

The resulted sectional forces and moments, from Eurocode loading application have been averaged along the whole width of the concrete slab, even for the Tandem system, considering that the whole bridge deck is effective under this type of loading, since the tandems have been placed next to each other.

$$M_{Ed,span} = \frac{2985.61}{b} = \frac{2985.61}{8.25} = 361.89 \text{ kNm/m}$$

$$M_{Ed,sup} = -\frac{5105.23}{b} = -\frac{5105.23}{8.25} = -619.71 \text{ kNm/m}$$

$$V_{Ed} = \frac{3069.17}{b} = \frac{3069.17}{8.25} = 372.14 \text{ kN/m}$$

Then, a “Unity Check” is performed, which is a ratio of the stresses caused by the applied loads to the corresponding capacity of the structure.

$$UC_{M,span} = \frac{M_{Ed,span}}{M_{ud,span1}} = \frac{361.89}{663.55} = 0.55$$

$$UC_{M,sup} = \frac{M_{Ed,sup}}{M_{ud,sup}} = \frac{619.71}{837.22} = 0.74$$

$$UC_{V,EC} = \frac{V_{Ed}}{V_{Rd,c}} = \frac{372.14}{615.68} = 0.60$$

$$UC_{V,prop} = \frac{V_{Ed}}{V_{Rd,c,prop}} = \frac{372.14}{641.38} = 0.58$$

### 3.2. Equivalent proof load

The effective width of the equivalent proof load tandems, which generate the same stresses as the Eurocode loading, is considered with a horizontal load spreading under a 45° angle from the far side of the concentrated experimental loads, taking into account the skew angle of the concrete deck. The effective width is assumed to be the same for both axes.

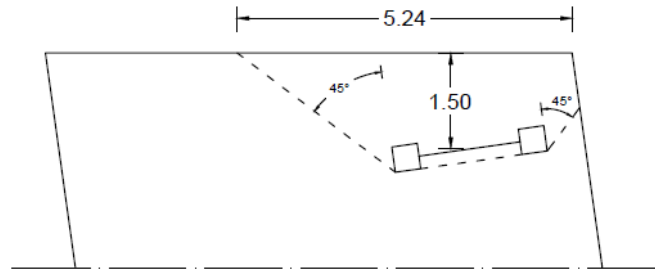


Figure B.3: Calculation of effective width (m)

In order to determine the shear force that has to be generated from the proof loading for the beam model, an equivalency has been assumed between the shear stresses due to Eurocode loading and field loading. For the LP4 loading scenario and the design load combination the calculation procedure for the equivalent shear force is described below.

$$\tau_{comb,EC} = \tau_{comb,PL} \rightarrow \gamma_G \cdot (\tau_{SW} + \tau_{SD}) + \gamma_Q \cdot \tau_{LL} = \tau_{SW} + \tau_{SD} + \tau_{PL}$$

$$\rightarrow \tau_{PL} = (\gamma_G - 1) \cdot (\tau_{SW} + \tau_{SD}) + \gamma_Q \cdot \tau_{LL}$$

$$\rightarrow V_{PL} = [(\gamma_G - 1) \cdot (V_{SW} + V_{SD}) + \gamma_Q \cdot V_{LL}] \cdot \frac{b_{skew}}{b}$$

$$\rightarrow V_{PL} = [(1.25 - 1) \cdot 1085.83 + 1.50 \cdot (265.13 + 876.78)] \cdot \frac{5.24}{8.25} = 1260.35 \text{ kN}$$

Using the structural software SAP2000 and by trial-and-error it is obtained that the required total proof load that generates the same shear stresses as the Eurocode loading is:

$$P_V = 2 \cdot 719 = 1438 \text{ kN}$$

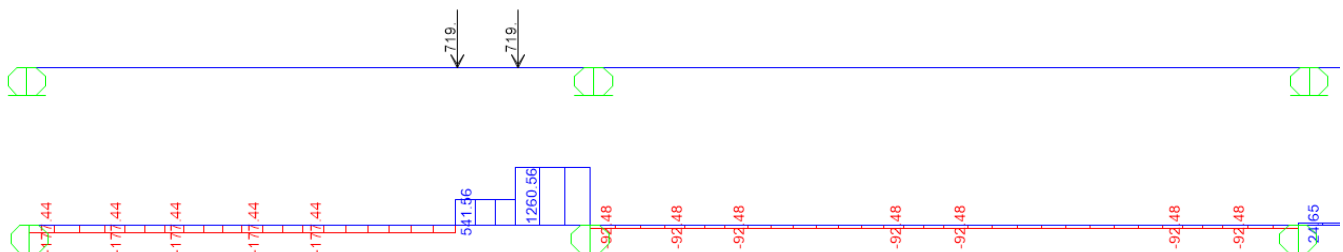


Figure B.4: Calculation of the equivalent proof load (kN)

### 3.3.Failure load

For the determination of the effective shear width of the failure loading, all the three approaches for skewed slabs have been considered. The effective width is assumed to be the same for both axles.

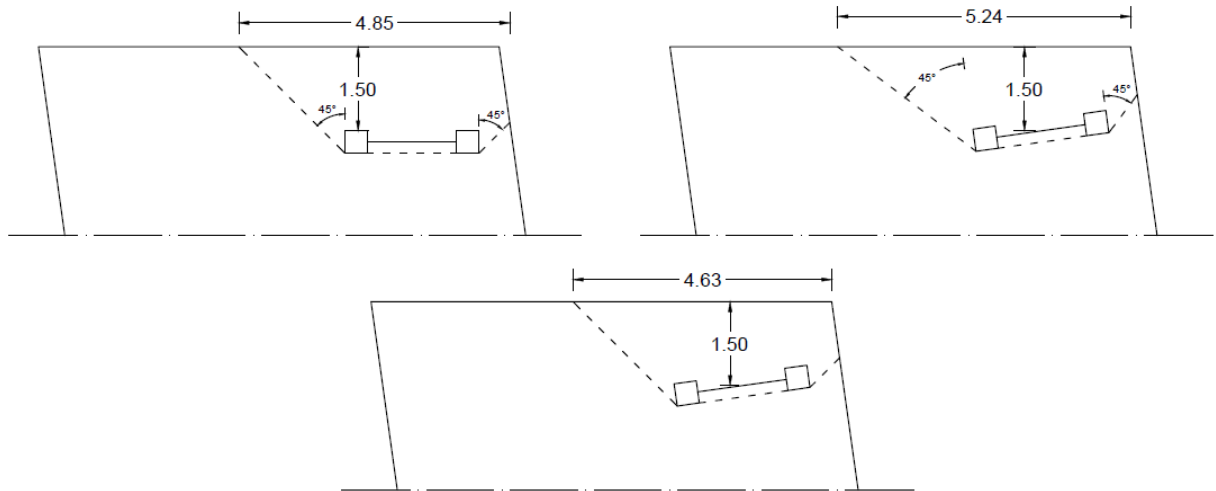


Figure B.5: Calculation of effective width (m)

The shear force that has to be caused from the failure loading in order to reach the ultimate shear resistance for the mean material properties can be determined as:

$$\tau_{Rm} = \tau_{comb,FL} \rightarrow \tau_{Rm} = \tau_{SW} + \tau_{SD} + \tau_{FL}$$

$$\rightarrow V_{FL} = [\tau_{Rm} \cdot b - (V_{SW} + V_{SD})] \cdot \frac{b_{eff}}{b}$$

For shear capacity estimation according to Eurocode and for  $b_{str}$ :

$$V_{FL} = [694.58 \cdot 8.25 - 1085.83] \cdot \frac{4.85}{8.25} = 2730.38 \text{ kN}$$

For shear capacity estimation according to Eurocode and for  $b_{skew}$ :

$$V_{FL} = [694.58 \cdot 8.25 - 1085.83] \cdot \frac{5.24}{8.25} = 2949.93 \text{ kN}$$

For shear capacity estimation according to Eurocode and for  $b_{para}$ :

$$V_{FL} = [694.58 \cdot 8.25 - 1085.83] \cdot \frac{4.63}{8.25} = 2606.52 \text{ kN}$$

With the same procedure as the equivalent proof loads using SAP2000, the required failure load is found:

$$P_{V,EC,str} = 2 \cdot 1557 = 3114 \text{ kN}$$

$$P_{V,EC,skew} = 2 \cdot 1683 = 3366 \text{ kN}$$

$$P_{V,EC,para} = 2 \cdot 1486 = 2972 \text{ kN}$$

And the mean value can be defined:

$$P_{V,EC,mean} = 3151 \text{ kN}$$

For shear capacity estimation according to the proposed formula and for  $b_{str}$  :

$$V_{FL} = [849.37 \cdot 8.25 - 1085.83] \cdot \frac{4.85}{8.25} = 3481.11 \text{ kN}$$

For shear capacity estimation according to the proposed formula and for  $b_{skew}$  :

$$V_{FL} = [849.37 \cdot 8.25 - 1085.83] \cdot \frac{5.24}{8.25} = 3761.03 \text{ kN}$$

For shear capacity estimation according to the proposed formula and for  $b_{para}$  :

$$V_{FL} = [849.37 \cdot 8.25 - 1085.83] \cdot \frac{4.63}{8.25} = 3323.20 \text{ kN}$$

With the same procedure as the equivalent proof loads using SAP2000, the required failure load is found:

$$P_{V,prop,str} = 2 \cdot 1984 = 3968 \text{ kN}$$

$$P_{V,prop,skew} = 2 \cdot 2145 = 4290 \text{ kN}$$

$$P_{V,prop,para} = 2 \cdot 1893 = 3786 \text{ kN}$$

And the mean value can be defined:

$$P_{V,prop,mean} = 4015 \text{ kN}$$



# Appendix C

## Finite Element Model

### The \*.dat file of the Model

```
: Diana Datafile written by Diana 10.1
'UNITS'
FORCE KN
'DIRECTIONS'
  1 1.000000000E+00 0.000000000E+00 0.000000000E+00
  2 0.000000000E+00 1.000000000E+00 0.000000000E+00
  3 0.000000000E+00 0.000000000E+00 1.000000000E+00
'MODEL'
DIMENS "3D"
GRAVDI 3
GRAVAC -9.810000000E+00
'COORDINATES'
  1 2.314680000E+01 7.450000000E+00 -1.224646799E-17
  2 2.314680000E+01 7.050000000E+00 -1.224646799E-17
  3 2.274680000E+01 7.050000000E+00 1.224646799E-17
  4 2.274680000E+01 7.450000000E+00 1.224646799E-17
  5 2.314680000E+01 5.450000000E+00 -1.224646799E-17
  6 2.314680000E+01 5.050000000E+00 -1.224646799E-17
  7 2.274680000E+01 5.050000000E+00 1.224646799E-17
  8 2.274680000E+01 5.450000000E+00 1.224646799E-17
  9 2.194680000E+01 7.450000000E+00 -1.224646799E-17
 10 2.194680000E+01 7.050000000E+00 -1.224646799E-17
 11 2.154680000E+01 7.050000000E+00 1.224646799E-17
 12 2.154680000E+01 7.450000000E+00 1.224646799E-17
 13 2.194680000E+01 5.450000000E+00 -1.224646799E-17
 14 2.194680000E+01 5.050000000E+00 -1.224646799E-17
 15 2.154680000E+01 5.050000000E+00 1.224646799E-17
 16 2.154680000E+01 5.450000000E+00 1.224646799E-17
 17 2.198050000E+01 4.450000000E+00 -1.224646799E-17
 18 2.198050000E+01 4.050000000E+00 -1.224646799E-17
 19 2.158050000E+01 4.050000000E+00 1.224646799E-17
 20 2.158050000E+01 4.450000000E+00 1.224646799E-17
.....
20083 8.585315151E+01 3.333333333E-01 3.228348784E-17
20084 8.565315151E+01 3.333333333E-01 3.3281991569E-17
20085 8.545315151E+01 3.333333333E-01 3.4280495299E-17
20086 8.525315151E+01 3.333333333E-01 3.5278999029E-17
20087 8.505315151E+01 3.333333333E-01 3.6277502758E-17
20088 8.485315151E+01 3.333333333E-01 3.7276006488E-17
20089 8.465315151E+01 3.333333333E-01 3.8274510217E-17
20090 8.445315151E+01 3.333333333E-01 3.9273013947E-17
20091 8.425315151E+01 3.333333333E-01 4.0271517677E-17
20092 8.405315151E+01 3.333333333E-01 4.1270021406E-17
20093 8.385315151E+01 3.333333333E-01 4.2268525136E-17
20094 8.365315151E+01 3.333333333E-01 4.3267028866E-17
20095 8.345315151E+01 3.333333333E-01 4.4265532595E-17
20096 8.325315151E+01 3.333333333E-01 4.5264036325E-17
20097 8.305315151E+01 3.333333333E-01 4.6262540054E-17
20098 8.285315151E+01 3.333333333E-01 4.7261043784E-17
20099 8.265315151E+01 3.333333333E-01 4.8259547514E-17
20100 8.245315151E+01 3.333333333E-01 4.9258051243E-17
20101 8.225315151E+01 3.333333333E-01 5.0256554973E-17
20102 8.205315151E+01 3.333333333E-01 5.1255058703E-17
```

'MATERI'  
 1 NAME "Concrete"  
 MCNAME CONCR  
 MATMDL LEI  
 POISON 2.0000000000E-01  
 YOUNG 3.1570900000E+07  
 ASPECT  
 'GEOMET'  
 1 NAME "Deck"  
 GCNAME SHEET  
 GEOMDL PLATE  
 KFAC 1.5000000000E+00  
 XAXIS 1.0000000000E+00 0.0000000000E+00 0.0000000000E+00  
 THICK 6.5000000000E-01

'ELEMENTS'  
 SET "Deck"  
 CONNECT  
 1 Q12PL 4 84 3169 81  
 2 Q12PL 81 3169 82 1  
 3 Q12PL 84 3 83 3169  
 4 Q12PL 3169 83 2 82  
 5 Q12PL 8 88 3170 85  
 6 Q12PL 85 3170 86 5  
 7 Q12PL 88 7 87 3170  
 8 Q12PL 3170 87 6 86  
 9 Q12PL 12 92 3171 89  
 10 Q12PL 89 3171 90 9  
 11 Q12PL 92 11 91 3171  
 12 Q12PL 3171 91 10 90  
 13 Q12PL 16 96 3172 93  
 14 Q12PL 93 3172 94 13  
 15 Q12PL 96 15 95 3172  
 16 Q12PL 3172 95 14 94  
 17 Q12PL 20 100 3173 97  
 18 Q12PL 97 3173 98 17  
 19 Q12PL 100 19 99 3173  
 20 Q12PL 3173 99 18 98

.....  
 19587 Q12PL 20083 1917 1916 20084  
 19588 Q12PL 20084 1916 1915 20085  
 19589 Q12PL 20085 1915 1914 20086  
 19590 Q12PL 20086 1914 1913 20087  
 19591 Q12PL 20087 1913 1912 20088  
 19592 Q12PL 20088 1912 1911 20089  
 19593 Q12PL 20089 1911 1910 20090  
 19594 Q12PL 20090 1910 1909 20091  
 19595 Q12PL 20091 1909 1908 20092  
 19596 Q12PL 20092 1908 1907 20093  
 19597 Q12PL 20093 1907 1906 20094  
 19598 Q12PL 20094 1906 1905 20095  
 19599 Q12PL 20095 1905 1904 20096  
 19600 Q12PL 20096 1904 1903 20097  
 19601 Q12PL 20097 1903 1902 20098  
 19602 Q12PL 20098 1902 1901 20099  
 19603 Q12PL 20099 1901 1900 20100  
 19604 Q12PL 20100 1900 1899 20101  
 19605 Q12PL 20101 1899 1898 20102  
 19606 Q12PL 20102 1898 64 1954

MATERIAL 1  
 GEOMETRY 1  
 'LOADS'  
 CASE 1  
 NAME "Selfweight"  
 ELEMEN

/ 33-872 / FACE  
FORCE -2.7600000000E+00  
DIRECT 3  
/ 33-872 / FACE  
FORCE -1.6250000000E+01  
DIRECT 3  
/ 873-1712 /  
FACE  
FORCE -2.7600000000E+00  
DIRECT 3  
/ 873-1712 /  
FACE  
FORCE -1.6250000000E+01  
DIRECT 3  
/ 1713-2757 /  
FACE  
FORCE -2.7600000000E+00  
DIRECT 3  
/ 1713-2757 /  
FACE  
FORCE -1.6250000000E+01  
DIRECT 3  
/ 2758-3802 /  
FACE  
FORCE -2.7600000000E+00  
DIRECT 3  
/ 2758-3802 /  
FACE  
FORCE -1.6250000000E+01  
DIRECT 3  
/ 3803-4867 /  
FACE  
FORCE -2.7600000000E+00  
DIRECT 3  
/ 3803-4867 /  
FACE  
FORCE -1.6250000000E+01  
DIRECT 3  
/ 4868-5932 /  
FACE  
FORCE -2.7600000000E+00  
DIRECT 3  
/ 4868-5932 /  
FACE  
FORCE -1.6250000000E+01  
DIRECT 3  
/ 5933-6997 /  
FACE  
FORCE -2.7600000000E+00  
DIRECT 3  
/ 5933-6997 /  
FACE  
FORCE -1.6250000000E+01  
DIRECT 3  
/ 6998-8062 /  
FACE  
FORCE -2.7600000000E+00  
DIRECT 3  
/ 6998-8062 /  
FACE  
FORCE -1.6250000000E+01  
DIRECT 3  
/ 8063-9127 /  
FACE  
FORCE -2.7600000000E+00

DIRECT 3  
/ 8063-9127 /  
FACE  
FORCE -1.6250000000E+01  
DIRECT 3  
/ 9128-10192 /  
FACE  
FORCE -2.7600000000E+00  
DIRECT 3  
/ 9128-10192 /  
FACE  
FORCE -1.6250000000E+01  
DIRECT 3  
/ 10193-11257 /  
FACE  
FORCE -2.7600000000E+00  
DIRECT 3  
/ 10193-11257 /  
FACE  
FORCE -1.6250000000E+01  
DIRECT 3  
/ 11258-12322 /  
FACE  
FORCE -2.7600000000E+00  
DIRECT 3  
/ 11258-12322 /  
FACE  
FORCE -1.6250000000E+01  
DIRECT 3  
/ 12323-13162 /  
FACE  
FORCE -2.7600000000E+00  
DIRECT 3  
/ 12323-13162 /  
FACE  
FORCE -1.6250000000E+01  
DIRECT 3  
/ 13163-14002 /  
FACE  
FORCE -2.7600000000E+00  
DIRECT 3  
/ 13163-14002 /  
FACE  
FORCE -1.6250000000E+01  
DIRECT 3  
/ 14003-14215 /  
FACE  
FORCE -1.6250000000E+01  
DIRECT 3  
/ 14216-14428 /  
FACE  
FORCE -1.6250000000E+01  
DIRECT 3  
/ 14429-14641 /  
FACE  
FORCE -1.6250000000E+01  
DIRECT 3  
/ 14642-14854 /  
FACE  
FORCE -1.6250000000E+01  
DIRECT 3  
/ 14855-15067 /  
FACE  
FORCE -1.6250000000E+01  
DIRECT 3

/ 15068-15235 /  
FACE  
FORCE -1.6250000000E+01  
DIRECT 3  
/ 15236-15403 /  
FACE  
FORCE -1.6250000000E+01  
DIRECT 3  
/ 15404-15829 /  
FACE  
FORCE -2.7600000000E+00  
DIRECT 3  
/ 15404-15829 /  
FACE  
FORCE -1.6250000000E+01  
DIRECT 3  
/ 15830-16255 /  
FACE  
FORCE -2.7600000000E+00  
DIRECT 3  
/ 15830-16255 /  
FACE  
FORCE -1.6250000000E+01  
DIRECT 3  
/ 16256-16681 /  
FACE  
FORCE -2.7600000000E+00  
DIRECT 3  
/ 16256-16681 /  
FACE  
FORCE -1.6250000000E+01  
DIRECT 3  
/ 16682-17107 /  
FACE  
FORCE -2.7600000000E+00  
DIRECT 3  
/ 16682-17107 /  
FACE  
FORCE -1.6250000000E+01  
DIRECT 3  
/ 17108-17533 /  
FACE  
FORCE -2.7600000000E+00  
DIRECT 3  
/ 17108-17533 /  
FACE  
FORCE -1.6250000000E+01  
DIRECT 3  
/ 17534-17869 /  
FACE  
FORCE -2.7600000000E+00  
DIRECT 3  
/ 17534-17869 /  
FACE  
FORCE -1.6250000000E+01  
DIRECT 3  
/ 17870-18205 /  
FACE  
FORCE -2.7600000000E+00  
DIRECT 3  
/ 17870-18205 /  
FACE  
FORCE -1.6250000000E+01  
DIRECT 3  
/ 18206-18418 /

FACE  
FORCE -1.6250000000E+01  
DIRECT 3  
/ 18419-18631 /  
FACE  
FORCE -1.6250000000E+01  
DIRECT 3  
/ 18632-18844 /  
FACE  
FORCE -1.6250000000E+01  
DIRECT 3  
/ 18845-19057 /  
FACE  
FORCE -1.6250000000E+01  
DIRECT 3  
/ 19058-19270 /  
FACE  
FORCE -1.6250000000E+01  
DIRECT 3  
/ 19271-19438 /  
FACE  
FORCE -1.6250000000E+01  
DIRECT 3  
/ 19439-19606 /  
FACE  
FORCE -1.6250000000E+01  
DIRECT 3  
CASE 2  
NAME UDL  
ELEMEN  
/ 33-872 / FACE  
FORCE -9.0000000000E+00  
DIRECT 3  
/ 873-1712 /  
FACE  
FORCE -2.5000000000E+00  
DIRECT 3  
/ 1713-2757 /  
FACE  
FORCE -9.0000000000E+00  
DIRECT 3  
/ 2758-3802 /  
FACE  
FORCE -2.5000000000E+00  
DIRECT 3  
/ 3803-4867 /  
FACE  
FORCE -9.0000000000E+00  
DIRECT 3  
/ 4868-5932 /  
FACE  
FORCE -2.5000000000E+00  
DIRECT 3  
/ 5933-6997 /  
FACE  
FORCE -9.0000000000E+00  
DIRECT 3  
/ 6998-8062 /  
FACE  
FORCE -2.5000000000E+00  
DIRECT 3  
/ 8063-9127 /  
FACE  
FORCE -9.0000000000E+00  
DIRECT 3

/ 9128-10192 /  
FACE  
FORCE -2.5000000000E+00  
DIRECT 3  
/ 10193-11257 /  
FACE  
FORCE -9.0000000000E+00  
DIRECT 3  
/ 11258-12322 /  
FACE  
FORCE -2.5000000000E+00  
DIRECT 3  
/ 12323-13162 /  
FACE  
FORCE -9.0000000000E+00  
DIRECT 3  
/ 13163-14002 /  
FACE  
FORCE -2.5000000000E+00  
DIRECT 3  
/ 15404-15829 /  
FACE  
FORCE -2.5000000000E+00  
DIRECT 3  
/ 15830-16255 /  
FACE  
FORCE -2.5000000000E+00  
DIRECT 3  
/ 16256-16681 /  
FACE  
FORCE -2.5000000000E+00  
DIRECT 3  
/ 16682-17107 /  
FACE  
FORCE -2.5000000000E+00  
DIRECT 3  
/ 17108-17533 /  
FACE  
FORCE -2.5000000000E+00  
DIRECT 3  
/ 17534-17869 /  
FACE  
FORCE -2.5000000000E+00  
DIRECT 3  
/ 17870-18205 /  
FACE  
FORCE -2.5000000000E+00  
DIRECT 3  
CASE 3  
NAME TS  
ELEMEN  
/ 1-4 / FACE  
FORCE -9.3750000000E+02  
DIRECT 3  
/ 5-8 / FACE  
FORCE -9.3750000000E+02  
DIRECT 3  
/ 9-12 / FACE  
FORCE -9.3750000000E+02  
DIRECT 3  
/ 13-16 / FACE  
FORCE -9.3750000000E+02  
DIRECT 3  
/ 17-20 / FACE  
FORCE -6.2500000000E+02

```

DIRECT 3
/ 21-24 / FACE
FORCE -6.2500000000E+02
DIRECT 3
/ 25-28 / FACE
FORCE -6.2500000000E+02
DIRECT 3
/ 29-32 / FACE
FORCE -6.2500000000E+02
DIRECT 3
COMBIN
1 1 1.0000000000E+00
2 2 1.0000000000E+00
3 3 1.0000000000E+00
4 1 1.2500000000E+00 2 1.5000000000E+00 3 1.5000000000E+00
5 1 1.1500000000E+00 2 1.3000000000E+00 3 1.3000000000E+00
6 1 1.1500000000E+00 2 1.2500000000E+00 3 1.2500000000E+00
7 1 1.1000000000E+00 2 1.2500000000E+00 3 1.2500000000E+00
'SUPPOR'
NAME "Supports"
/ 65-70 77 80 / TR 2
/ 33-80 1953-2211 2672-2708 / TR 3
/ 39-42 50 51 58 59 67 68 73 74 2027-2100 / TR 1
'END'

```

## The \*.dcf file of the analysis for output at the integration points

```

*LINSTA LABEL="Structural linear static"
SOLVE PARDIS
BEGIN OUTPUT
TEXT "Output linear static analysis"
BINARY
SELECT LOADS ALL /
STRESS TOTAL DISMOM LOCAL INTPNT
STRESS TOTAL DISFOR LOCAL INTPNT
END OUTPUT
*END

```

# Appendix D

## Response spectra



### Responspectrum data gedownload van de Webtool NPR 9998

Datum van download: 2018-06-08 15:13

Dataset: 2017-06-22\_GMMv4\_Surf

Herhalingsjijd [jaar]: 475

Richting: Horizontaal

#### Locatie

RD (x, y) [m]: 229646, 585766

GPS (lat, lng) [°]: 53.253237, 6.505635

#### Ontw. NPR 9998:2017 parameters

a\_g S [g] 0,0659

p [-] 2,319

T\_B [s] 0,198

T\_C [s] 0,464

T\_D [s] 0,849

#### UHS-data

T [s]	S_a [g]
-------	---------

0,01	0,0659
------	--------

0,025	0,0652
-------	--------

0,05	0,0749
------	--------

0,075	0,0918
-------	--------

0,1	0,1085
-----	--------

0,125	0,1222
-------	--------

0,15	0,1352
------	--------

0,175	0,1438
-------	--------

0,2	0,1497
-----	--------

0,25	0,1499
------	--------

0,3	0,1576
-----	--------

0,4	0,1531
-----	--------

0,5	0,1344
-----	--------

0,6	0,1162
-----	--------

0,7	0,1042
-----	--------

0,85	0,0827
------	--------

1	0,0587
---	--------

1,5	0,0322
-----	--------

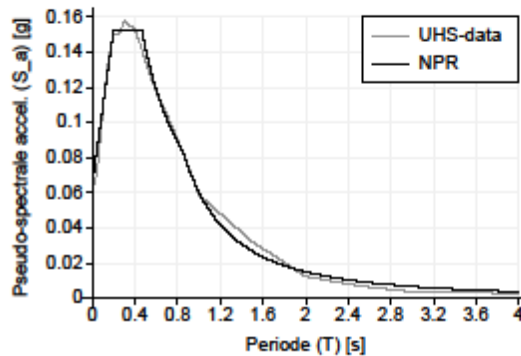
2	0,0124
---	--------

2,5	0,007
-----	-------

3	0,0037
---	--------

4	0,0028
---	--------

5	0,0027
---	--------



Horizontal response spectrum for 475 years return period

## Responspectrum data gedownload van de Webtool NPR 9998

Datum van download: 2018-06-08 16:47

Dataset: 2017-06-22\_GMMv4\_Surf

Herhalingstijd [jaar]: 2475

Richting: Horizontaal

### Locatie

RD (x, y) [m]: 229646, 585766

GPS (lat, lng) [°]: 53.253237, 6.505635

### Ontw. NPR 9998:2017 parameters

a\_g S [g] 0,1141

p [-] 2,311

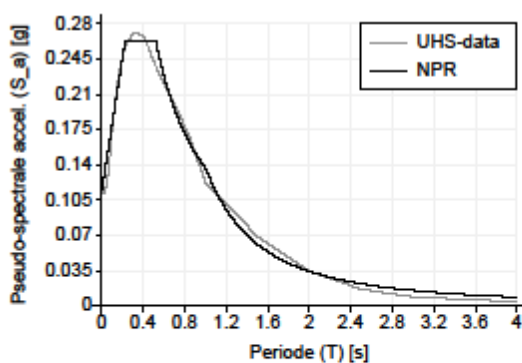
T\_B [s] 0,226

T\_C [s] 0,518

T\_D [s] 1,005

### UHS-data

T [s]	S_a [g]
0,01	0,1141
0,025	0,1116
0,05	0,1219
0,075	0,1432
0,1	0,1737
0,125	0,1973
0,15	0,2192
0,175	0,2349
0,2	0,2463
0,25	0,2618
0,3	0,2706
0,4	0,269
0,5	0,2426
0,6	0,2196
0,7	0,201
0,85	0,166
1	0,1225
1,5	0,0688
2	0,0344
2,5	0,0165
3	0,0087
4	0,0041
5	0,0032

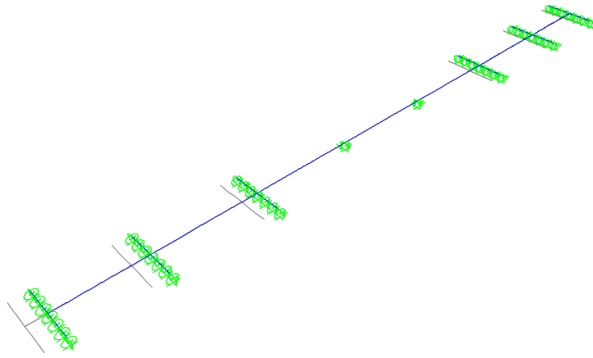


Horizontal response spectrum for 2475 years return period

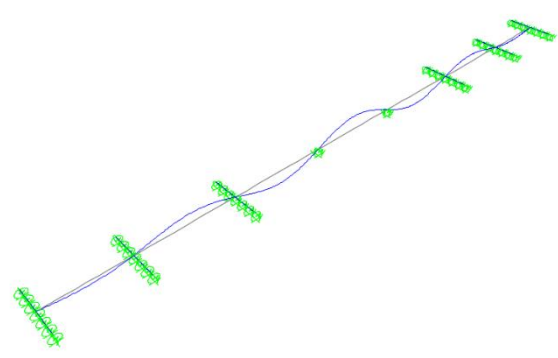
# Appendix E

## Modal shapes

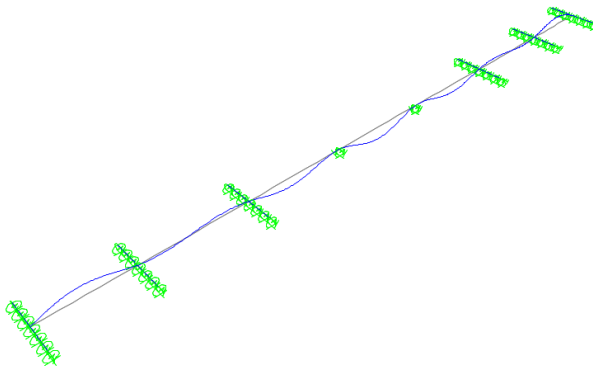
Model with spring supports



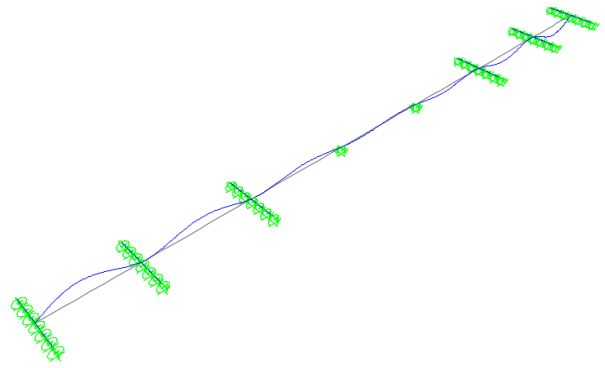
Mode 1



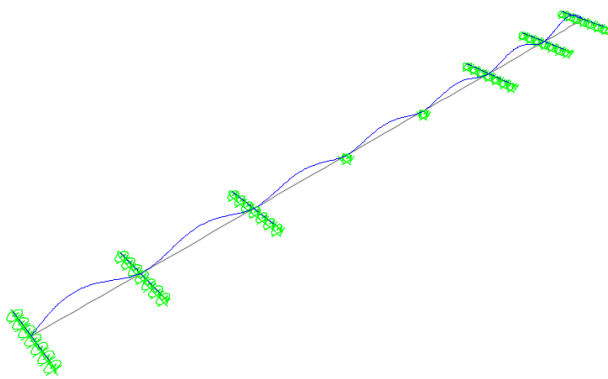
Mode 2



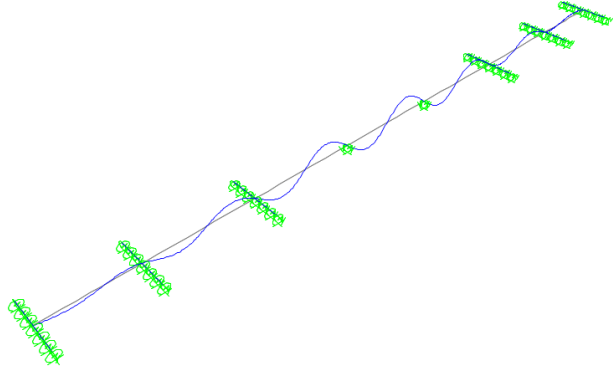
Mode 3



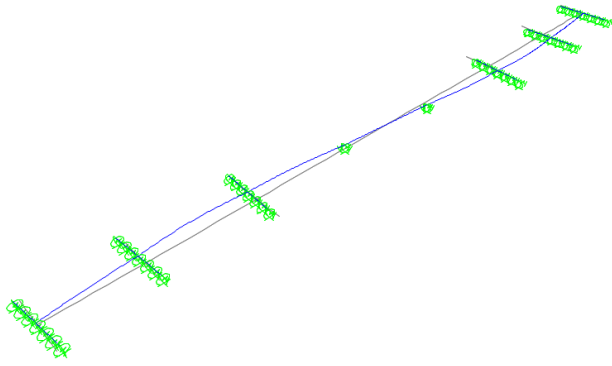
Mode 4



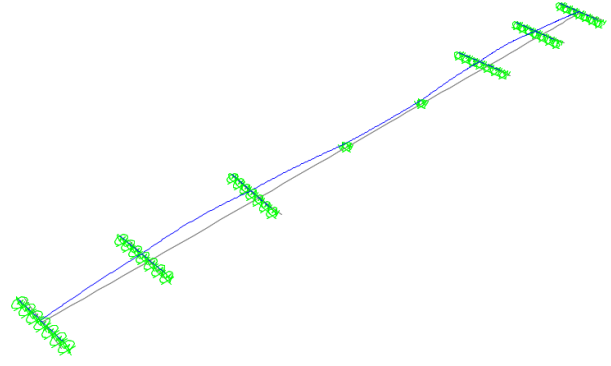
Mode 5



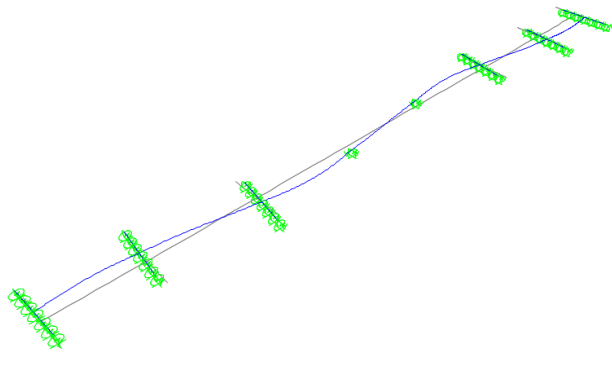
Mode 6



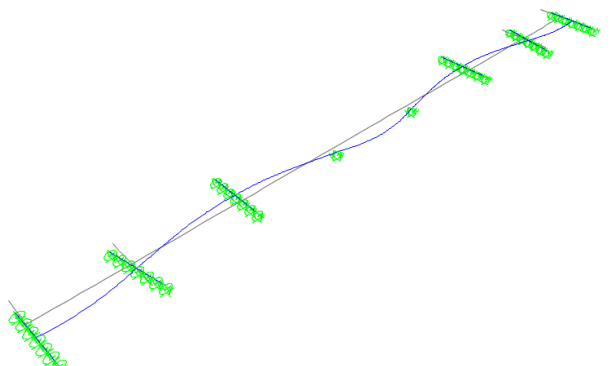
Mode 7



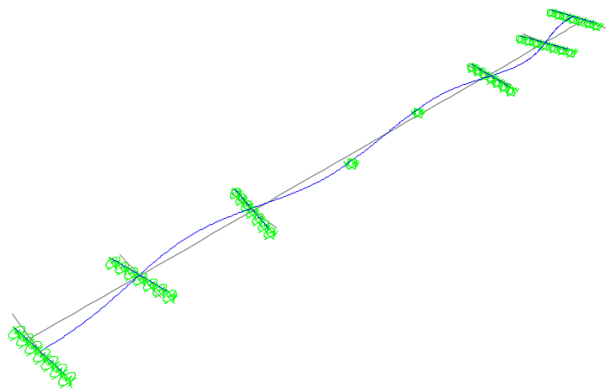
Mode 8



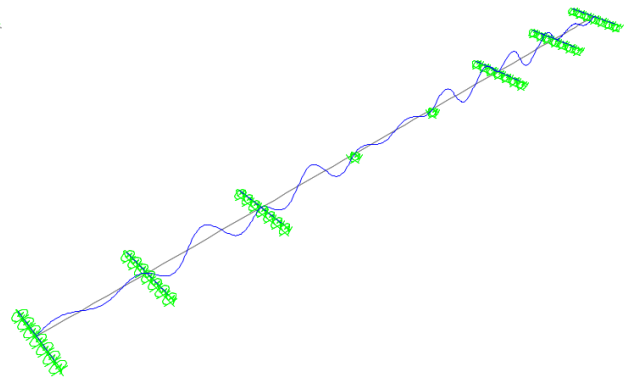
Mode 9



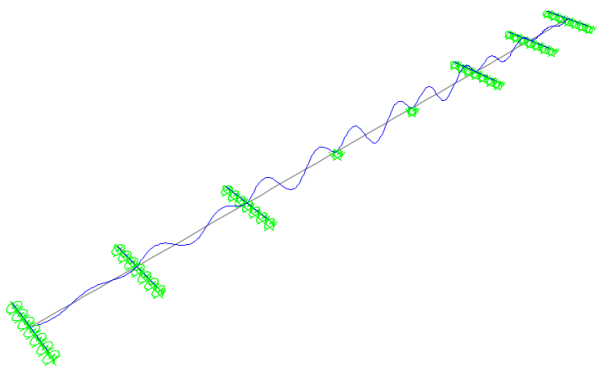
Mode 10



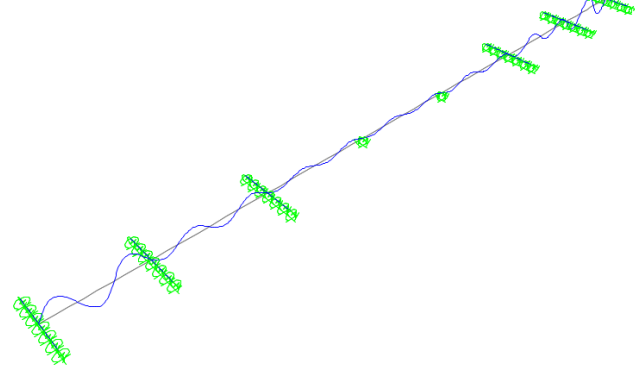
Mode 11



Mode 12

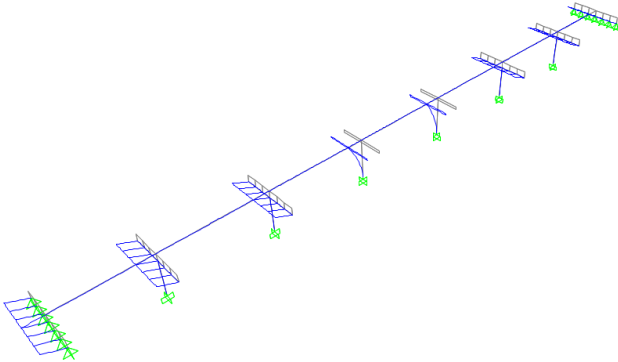


Mode 13

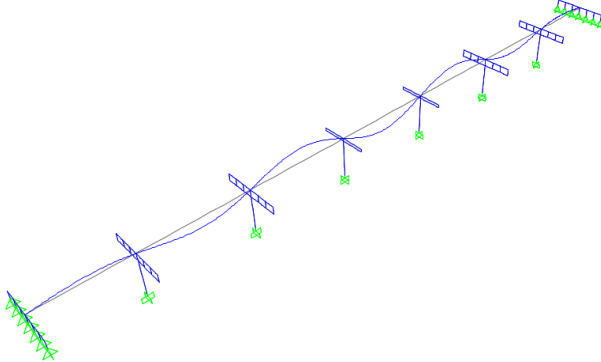


Mode 14

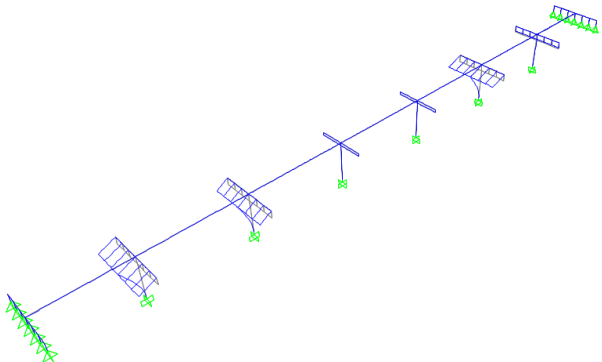
# Model with piers



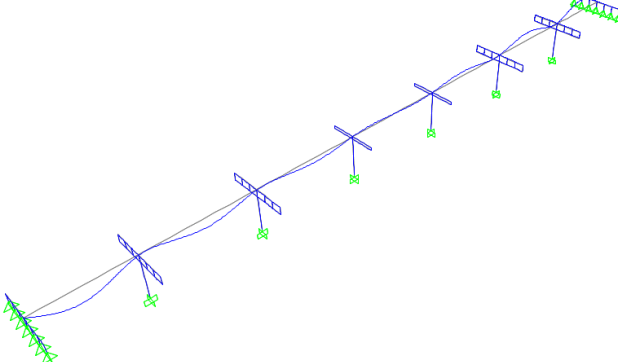
Mode 1



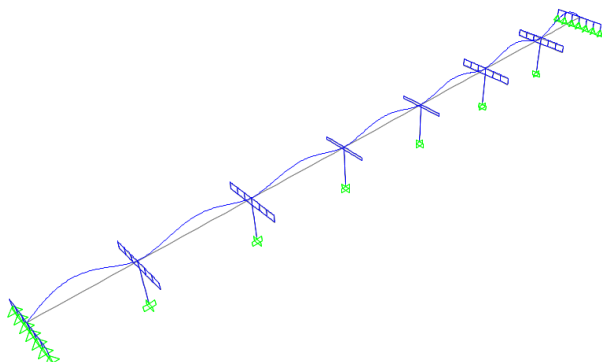
Mode 2



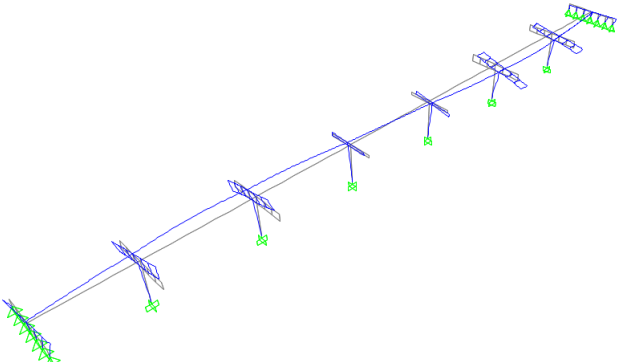
Mode 3



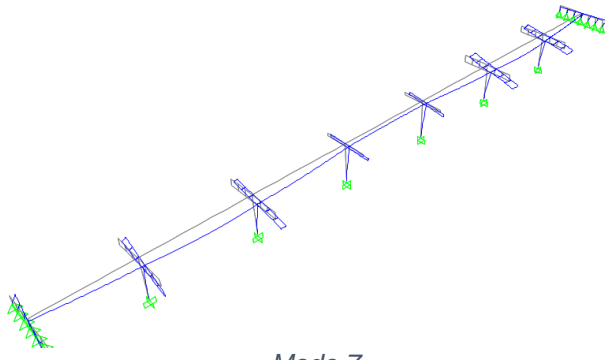
Mode 4



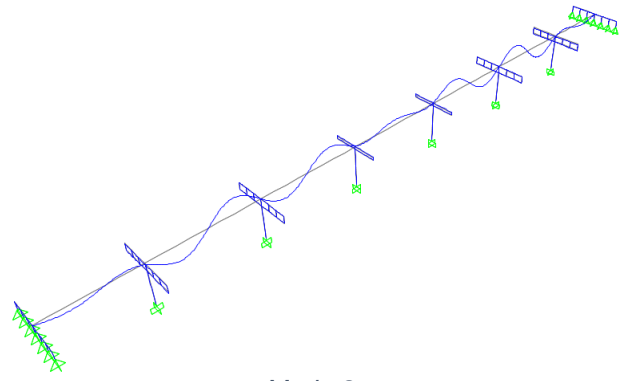
Mode 5



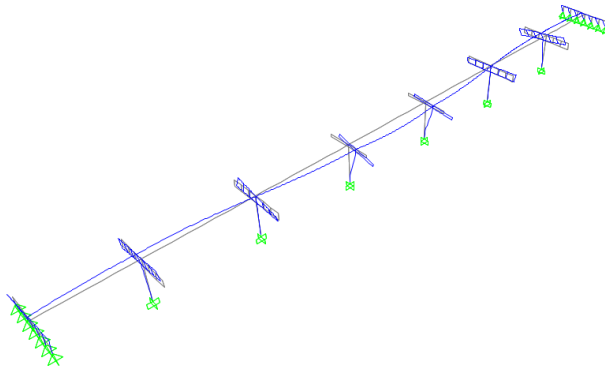
Mode 6



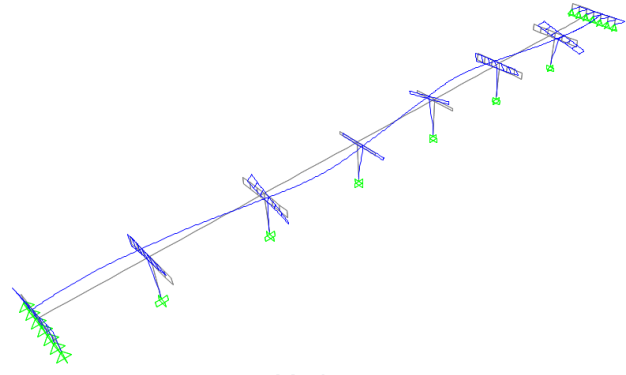
Mode 7



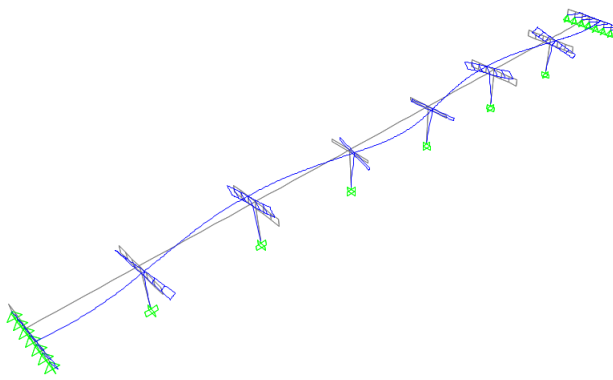
Mode 8



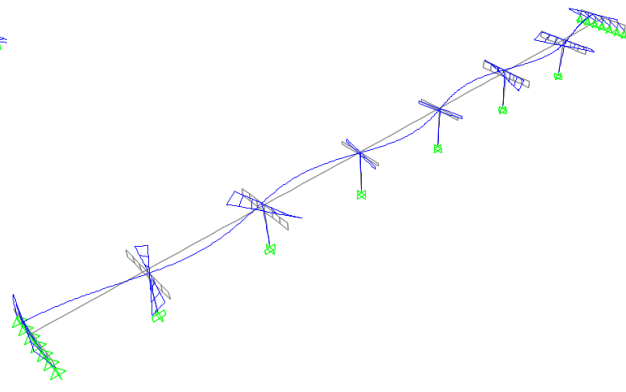
Mode 9



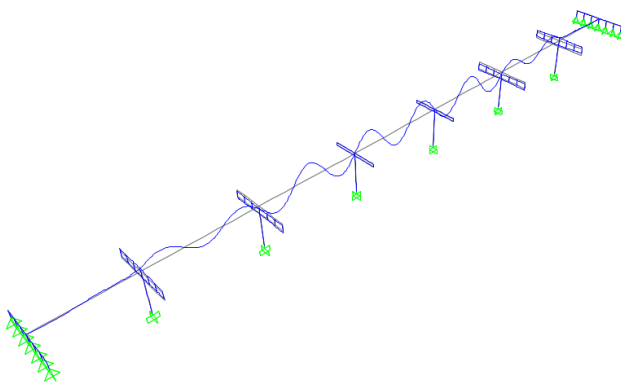
Mode 10



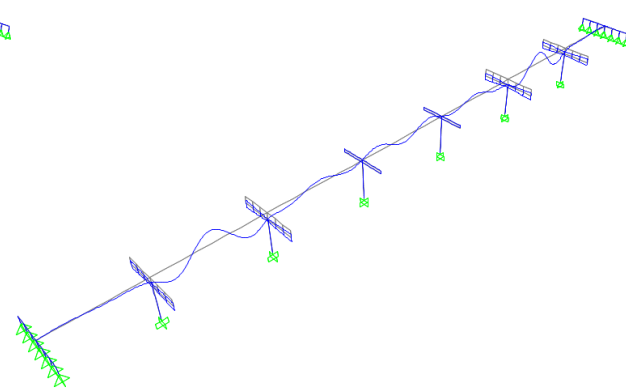
Mode 11



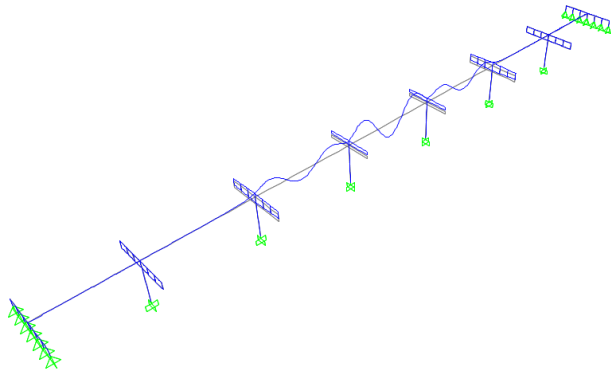
Mode 12



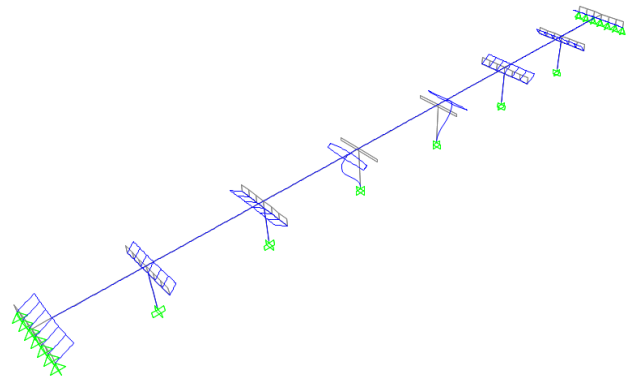
Mode 13



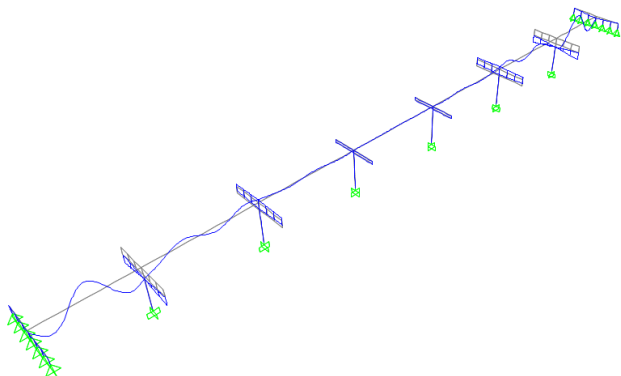
Mode 14



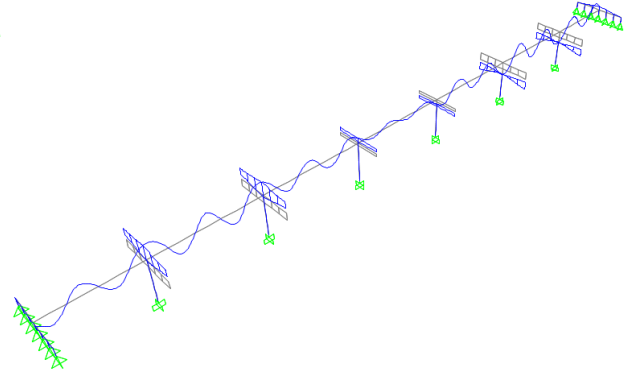
Mode 15



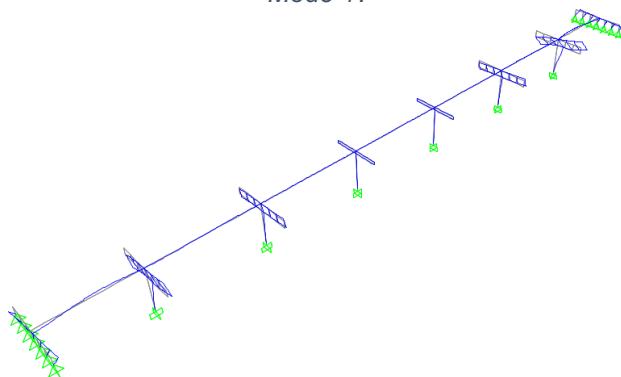
Mode 16



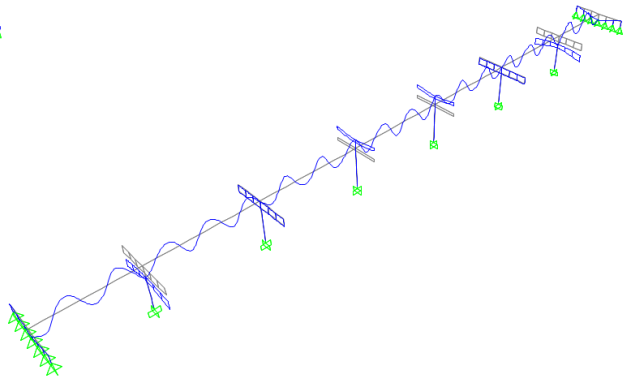
Mode 17



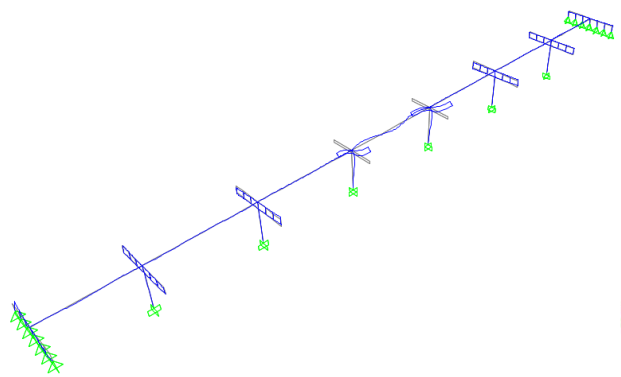
Mode 18



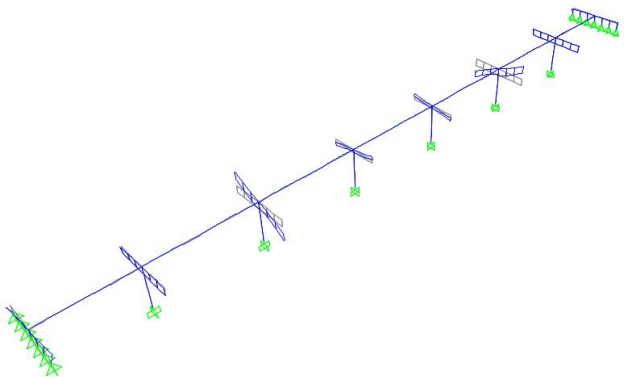
Mode 19



Mode 20



Mode 21



Mode 22



